Corrosion in CO_2 transport pipeline

The effect of dissolved and free water in dense phase CO_2

Bjørn Helge Morland

Thesis for the Master's degree in chemistry

60 ECTS credits

UiO : University of Oslo

March 2015

Corrosion in CO_2 transport pipeline

The effect of dissolved and free water in dense phase CO_2

Chemistry is necessarily an experimental science: its conclusions are drawn from data, and its principles supported by evidence from facts.

Michael Faraday, 1791 to 1867

2015

Corrosion in CO_2 transport pipeline

The effect of dissolved and free water in dense phase CO_2

Bjørn H. Morland

http://www.duo.uio.no/

Print: IFE-trykkeriet, Institute for Energy Technology

Acknowledgement

This thesis is a part of the requirements for the Master of Science degree in Chemistry at the University of Oslo. The experimental work was performed at Institute for Energy Technology (IFE) at Kjeller in collaboration with Solid-State Electrochemistry at the Center for Materials Science and Nanotechnology from August 2013 to March 2015.

I would like to thank my supervisor, Arne Dugstad and my co-supervisor Reidar Haugsrud, for always being there when I needed them and for inspiring me to become a scientist. Thanks to the department of Materials and Corrosion Technology at IFE for being a creative place where nothing is impossible, and to all my colleagues for shearing their skills and knowledge. Special thanks to Malgorzata “Gosia” Halseid and Gaute Svenningsen for guiding me through the world of scientific writing, Tommy Nordby for his services with building and maintenance of the equipment, Tor Blakseth for helping with design and building of the loop, Espen Lorentzen for helping me with molding of the samples, and Adriana Tadesse for eagerly helping me with film weight characterization. I would also like to thank the Department Head, Rolf Nyborg, for facilitating the possibility for me to achieve the Master degree. Thanks a lot to the Kjeller Dense Phase CO_2 Corrosion project and all the participants from Gassnova, Gassco, Total, Statoil, and Shell for making it possible to build the experimental equipment, and for contributed to the project with their knowledge. Especially, I would like to mention Han de Reus who unfortunately passed away during this project. He was an inspiration for us all and will be missed by the corrosion community.

This Master thesis could not be performed without the enormous support from my family, I am thankful to Anni, Terje and my parents not only for being interested in my work, but also for helping me to get the time to study, by child-minding. A special thanks to Morten who did mandatory voluntary work for me a whole weekend so I could write. I must send great thanks to my two boys, Christoffer and Thomas, who patiently waited for me to close the lap-top to join them in short play moments. Finally I would like to thank my wife, Cecilie, for holding the fort, supporting me through hard times, and for helping me with the writing. I would not have made it without you.

Kjeller, March 2015

Bjørn H Morland

Abbreviations

CCS	-	Carbon Capture and Storage
SEM	-	Scanning Electron Microscopy
EDS	-	Energy Dispersive X-ray Spectroscopy
CR	-	Corrosion rate
IPCC	-	The Intergovernmental Panel on Climate Changes
IEA	-	The International Energy Agency
Gton	-	Giga ton
Dense phase CO_2	-	Both liquid and supercritical CO_2
ppmv	-	Parts per million volume, for water in CO_2, 2.44 ppmv = 1 ppmw
ppmw	-	Parts per million weight
LPR	-	Linear Polarization Resistance
B-value	-	The Stern-Geary constant
HSAB concept	-	Hard and Soft (Lewis) Acids and Bases
IFE	-	Institute for Energy Technology
Hastelloy C276	-	Nickel based corrosion resistance alloy, type C276
CRA	-	Corrosion Resistance Alloy
TDLS	-	Tunable Diode Laser Spectroscopy
PEEK	-	PolyEther Ether Ketone
pm	-	Pico meter
nm	-	Nano meter
µm/y	-	Micro meter per year
mm/y	-	Milli meter per year
HPCIL	-	High Pressure CO_2 Impurity Loop

Abstract

The carbon dioxide (CO_2) concentration in the atmosphere has increased dramatically over the last century, and much of this increase is a direct consequence of human activities. Being a greenhouse gas, CO_2 significantly contributes to global warming, and there is an international agreement to reduce emission of CO_2. One method to reduce CO_2 release is carbon dioxide capture and storage (CCS). CCS entails to capture waste CO_2 from large point sources, and transport it to a permanently deposit, usually in geological formations. The transported CO_2 is likely to contain impurities like water, oxygen, nitrogen dioxide, sulfur dioxide and hydrogen sulfide. These impurities are known to cause corrosion, dust and/or solid formations, and may lead to operational difficulties. The present study examined how water as an impurity, both as a free water phase and water dissolved in dense phase CO_2, affects the corrosion of carbon steel.

There are few experimental studies that have examined corrosion in CO_2 transport pipelines, and these few studies have shown different corrosion rates in experiments where the reported amount of dissolved water in the CO_2 was the same. These discrepancies may reflect short-comings in methodology in some of these studies, where formation of free water may have contributed to high corrosion rates. The present study was undertaken to resolve some of the controversy related to corrosion in pure CO_2/water systems. For this study we designed experimental equipment that allowed complete control of the water concentration in CO2, without the risk of droplet formation. This provides realistic results that mimic the situation in the operating pipelines.

Three corrosion experiments were conducted with water dissolved in CO_2 at 25 °C and 95 bar of pressure. Even with water concentrations close to the solubility limit, the general corrosion rates were below 1.5 µm/y and no localized attacks were found. A fourth experiment was conducted at and above the solubility limit of water in CO_2. Even though we could confirm at the end of the experiment that water had accumulated in the loop, the corrosion rate was still at 1.0 µm/y, with no localized attacks. A final experiment was performed at 35 °C and 95 bar of pressure, in which no corrosion was detected. Corrosion products were found on the surface in all experiments, but at low quantities, most likely less than of practical significance.

However, with water levels above the solubility limits, i.e. in the present of free water phase, the corrosion rate increased by 3 to 4 orders of magnitude (2 mm/y to 16 mm/y, pressure depended).

For a CO_2 transport pipeline these results suggest that the corrosion will not be a problem as long as the water is kept below the solubility limit. However, it is extremely important to avoid liquid water ingress as this would dramatically reduce the lifetime of the pipeline.

Table of contents

Acknowledgement V
Abbreviations VII
Abstract IX
Table of contents XI
1. Introduction 1
1.1 Motivation 4
1.2 Background 5
1.2.1 Properties of pure CO_2 5
1.2.2 Capture source 5
1.2.3 Impurities in the captured CO_2 8
1.2.4 Existing CO_2 pipelines 10
1.2.5 Steel types 11
1.2.6 Effects of water on corrosion 12
1.3 Aim of the study 15
2. Corrosion mechanism in water and CO_2 17
2.1 Determine corrosion by Linear Polarization Resistance 19
2.2 Corrosion in CO_2 with dissolved water 22
3. Experimental 27
3.1 HPCIL with water dosing and analyzer 27
3.1.1 High pressure CO_2 impurity loop 27
3.1.2 Water dosing unit 28
3.1.3 Analyzing module 30
3.1.4 Calculated water concentration 36
3.1.5 The lag time 39
3.1.6 Experimental matrix – dissolved water 41
3.1.7 Corrosion coupons, preparation and analysis 43
3.1.8 Calibration 49
3.2 Dense phase loop with instruments 51

3.2.1 Dense phase loop 51
3.2.2 The test section and sample holder 52
3.2.3 Corrosion rate measurements 55
3.2.4 The experimental matrix 57
3.2.5 Sample handling and characterization 58
4. Results 61
4.1 HPCIL with water content below saturation 61
4.1.1 Experiment Solu Blank (Test run) 61
4.1.2 Experiment Solu 02 – different water levels 62
4.1.3 Experiment Solu 03 - high water level and constant temperature 65
4.1.4 Experiment Solu 04 -temperature changes at constant water level 67
4.1.5 Experiment Solu 05 - low temperature and constant water level 70
4.1.6 Experiment Solu 06 - supercritical conditions 72
4.1.7 Reference sample 75
4.1.8 Sample data 77
4.1.9 Film thickness estimation by Monte-Carlo method 80
4.2 Dense Phase Loop and free water saturated with CO_2 83
4.2.1 Iron count versus weight loss 83
4.2.2 Dense phase loop and the first version test section 84
4.2.2.1 Experiment Geo 01 - corrosion test at 100 bar CO_2 84
4.2.2.2 Experiment Geo 02 - corrosion test with ramping pressure 86
4.2.2.3 Glass cell test at 1 bar, Geo 03 89
4.2.3 Dense phase loop and the second version test section 90
4.2.3.1 Experiment Geo 04 - corrosion test with ramping pressure 90
4.2.4 Dense phase loop and the third version 93
4.2.4.1 Experiment Geo 05- corrosion test with ramping pressure 93
4.2.5 B-values from sweep 96
4.2.6 Summary of data, corrosion rates and B-values 97
5. Discussion 101

5.1 Equipment and analyzing techniques 101
5.1.1 Controlling the amount of dissolved water in dense phase CO_2 101
5.1.1.1 Pressure oscillation in the water dosing unit 102
5.1.1.2 Temperature fluctuation 102
5.1.1.3 Heated pressure regulator 104
5.1.1.4 Massflow controllers 104
5.1.2 Water measurements 105
5.1.2.1 Leakage 105
5.1.3 Flow loop with free water phase 106
5.1.3.1 Iron measurement 106
5.1.3.2 Electrochemical setup 107
5.1.3.3 Test section and sample holder 107
5.2 Discussion of results 108
5.2.1 Free water phase with dissolved CO_2 108
5.2.1.1 Corrosion rates 108
5.2.1.2 B-value 109
5.2.1.3 Possible copper contamination 111
5.2.2 Water dissolved in CO_2 112
5.2.2.1 Comparison of water measurements and corrosion rates (Solu 02) 113
5.2.2.2 Water precipitation and adsorption 114
5.2.2.3 Corrosion rates 117
5.2.2.4 Corrosion products 120
5.2.2.5 Effects of O_2 121
6. Conclusion 123
7. Further work 125
References 126
Appendix 131

1. Introduction

The Intergovernmental Panel on Climate Changes (IPCC) concluded that it is extremely likely that human influence has been the dominant cause of the observed climate changes since the mid-20th century [1]. In particular, global warming has increased dramatically over the last 200 years, primarily due to increased amount of greenhouse gases in the atmosphere. Greenhouse gases absorb infrared light emitted from the earth, thereby preventing heat from leaving the atmosphere, leading to an increased earth surface temperature (Figure 1).

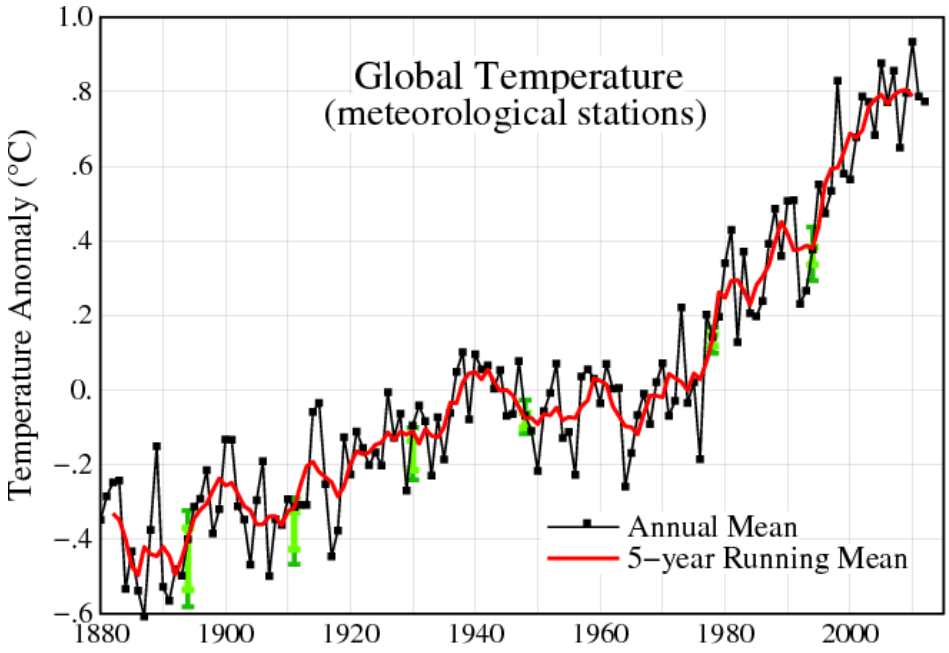

Figure 1 *The instrumental record of global average temperatures as compiled by the NASA´s Goddard institute for Space Studies [2].*

CO_2 is the primary greenhouse gas emitted through human activities, with an annual release of about 30 Gtons [1]. Consequently, the concentration of CO_2 has increased by 40% since pre-industrial times (Figure 2). Today there seems to be broad political agreement that the increase in anthropogenic emission of greenhouse gases must be reversed. Parties of the United Nations Framework Convention on Climate Changes (UNFCCC) have agreed to "stabilize greenhouse gas concentrations in the atmosphere at a level that would prevent dangerous anthropogenic interference with the climate system" [3]. As a consequence, strategies to reduce the release of CO_2 have gained extensive focus over the last years, both politically and as an area of research.

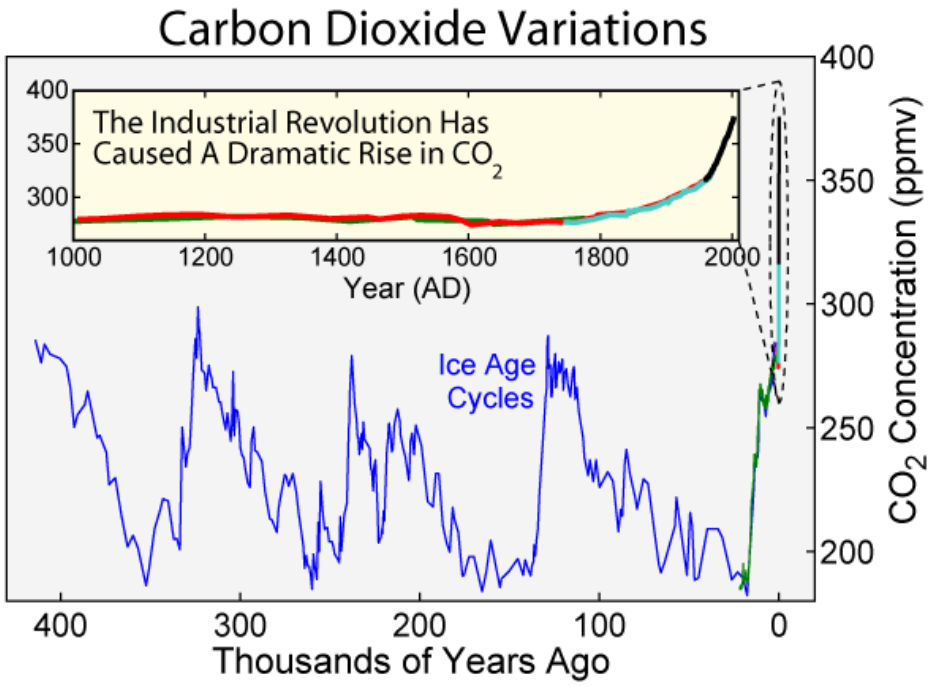

Figure 2 *Variations in atmospheric carbon dioxide levels over the last 400,000 years. Data are from proxy sources (ice cores - blue, red and green lines). The recent data (black line) are from direct measurement at Mauna Loa Observatory. Note the large increase in CO_2 concentration over the last 200 years. Image created by Robert A. Rohde / Global Warming Art.*

One such strategy is to capture waste CO_2 from large point sources, and transport it to a permanent storage site, normally in underground geological formation. This process is referred to as carbon capture and storage (CCS), and the goal is to permanently deposit the CO_2 where it can no longer enter the atmosphere. The International Energy Agency (IEA) has set as a goal referred to as «The Blue Map Scenario» [4] to cut the global energy-related CO_2 emissions by 50% by year 2050 (compared to 2005 levels), with CCS set to deliver one-fifth of the reduction in greenhouse gas emissions. This implies an annual injection of 7.4 Gton of CO_2 into geological formations such as saline formations, oil and gas reservoirs, and deep unmineable coal seams by 2050 [4]. CCS has also been a hot topic in the Norwegian media: in 2007, the Prime Minister of Norway (Jens Stoltenberg) clamed in his New Year speech that a full scale CCS plant within 2018 would be as important for Norway as putting a man on the moon was for the US. In the years to follow, a lot of money was granted to research on CCS, and a test center was built at Mongstad. The idea was to eventually develop this test center into a full scale CCS plant, featuring CO_2 cleaning, transport, and storage. In 2013 the project was cancelled and CCS on Norwegian shelf has not been put into action, but the ambition to develop full scale CCS remains.

In principle, the technology for large scale capture and storage of CO_2 is available. It is in use by the oil and gas industry to reduce the CO_2 content of their commercial gases. There are two fields in Norway which are currently transporting CO_2 back to underground reservoirs, but none of them are faced with all the major challenges related to full scale CCS. CO_2 captured from combustion or oxyfuel, is likely to contain impurities like water, oxygen, nitrogen dioxide, sulfur dioxide and hydrogen sulfide [5, 6]. These impurities can cause corrosion, dust and solid formations which may lead to operational difficulties. However, the safe levels of impurities required to prevent technical failure is not known, and an extensive cleaning process is very costly. Therefore, there is a need for well-founded CO_2 specifications describing the amounts of various impurities and combinations of impurities that can safely be captured, transported and stored with the CO_2.

In CSS, the site of storage is usually quite far from the site of capture, thus transport of the captured CO_2 will be necessary. CO_2 can be transported by ships, pipelines or a combination of both. However, for large volume and short to medium distances, pipeline transport is usually the most cost effective means of transportation. For a number of countries, including Norway, the preferred storage locations will be offshore, necessitating offshore pipelines between the capture and the storage facilities. The USA has routinely transported CO_2 in land based pipeline for over 30 years, giving rise to the assumption that CO_2 transport in CCS will not be a challenge, and therefore no research on this topic is needed [6, 7]. Although some valuable data can be extrapolated from the existing CO_2 transport pipelines, CCS pipelines will deal with different challenges. For instance in response to accident, malfunction or operational errors, water may enter offshore pipelines. This is likely to greatly affect the corrosion rate, and thus the lifetime of the pipeline [8].

Despite the extensive focus on CCS, both politically and scientifically, the attention given to the safe transport of CO_2 in pipelines has been surprisingly low.

1.1 Motivation

The CCS consists of three different technical areas i.e. capture, transport, and storage which all have to harmonize, for the CCS to succeed. The CO_2 from the capture plant must have a composition that does not harm the pipeline or cause reactions forming solids that might plug the reservoir. To be able to define a safe CO_2 specification knowledge on how impurities in the CO_2 may degrade the pipeline materials is required. Insight into those processes is required to prevent unnecessary and expensive cleaning of the CO_2 in the capture plant. Consequently, research into these processes is of great important to ensure safe transport for the CCS industry, while keeping the cost as low as possible.

The aim of the thesis is to study the effect of water on the CCS pipeline integrity and thereby determining the amount of water that can be accepted in the CO_2 for CCS transport.

The possibility for accidental ingress of water has to be considered in order to determine what kind of safety procedure should be considered when designing the pipeline and its integrity management system. Therefore the effect of a free water phase and increasing pressure of CO_2 on corrosion will also be addressed.

New and improved experimental equipment will be designed to rule out experimental errors which could occur when water dissolves in CO_2 and thereby promote high quality results.

1.2 Background

1.2.1 Properties of pure CO_2

CO_2 is a colorless, odorless and non-flammable gas which exists in our atmosphere at a concentration of approximately 0.039 percent by volume. It has a melting point of -56.5°C at 5.1 bar (triple point), and a boiling point of -78.5°C at atmospheric pressure. The phase diagram for pure CO_2 is shown in Figure 3. In theory, CO_2 could be transported as a solid, liquid or gas. However, the most efficient states to transport CO_2 in pipelines are as a liquid or supercritical fluid at 70 to 200 bars in the range 4 to 45°C. CO_2 transport by ships, on the other hand, is usually conducted in the liquid CO_2 phase only as indicated in Figure 3. "Dense phase CO_2" is a term that covers CO_2 in both its liquid or supercritical phase.

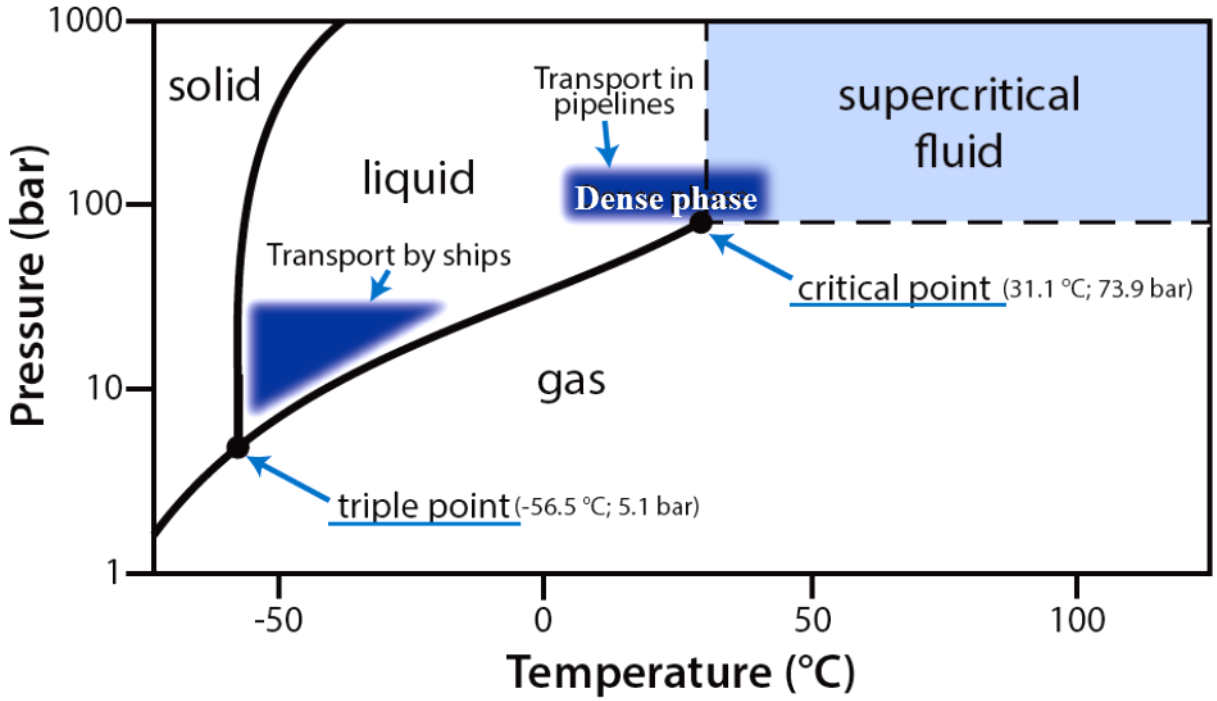

Figure 3 *CO_2 phase diagram. The relevant pressure and temperature ranges for CO_2 transport are indicated.*

1.2.2 Capture source

There are three major capture sources for CO_2 in CCS technology: pre-combustion, oxyfuel and post-combustion. All three are related to energy conversion, and are described in Figure 4. In addition to these, it is possible to capture CO_2 from industrial processes. Although some of these processes uses CO_2 and therefor works as temporary storage sites, they will in the end release CO_2 to the atmospheric pool.

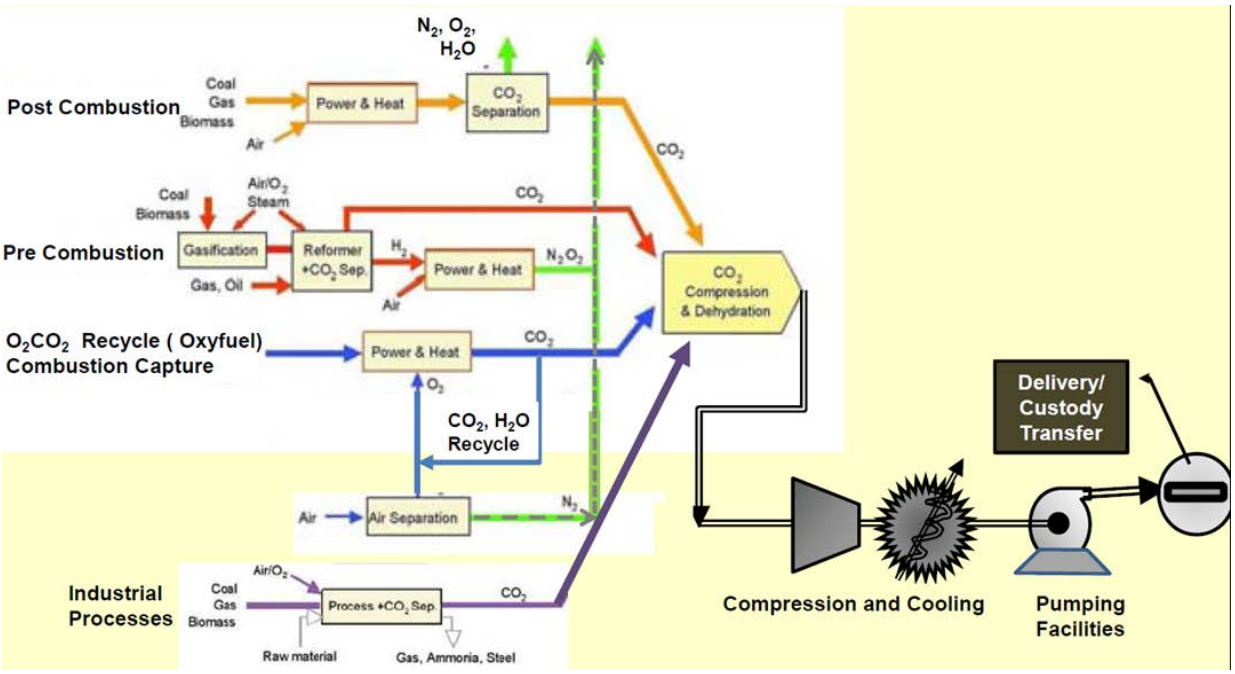

Figure 4 *Carbon dioxide capture technologies [9].*

The easiest and most economical way to transport CO_2 is as liquid or supercritical phase. This implies that all capture technologies will need a compression stage before the CO_2 can be transported.

Pre-combustion

As the name indicates, pre-combustion capture means that the CO_2 is collected before the fuel is burned. Pre-combustion involves partial oxidation, also referred to as gasification, where oxygen is added to pulverized coal and form synthetic gas (see Figure 4 for details). In the first stage, carbon monoxide (CO) and hydrogen (H_2) is produced (Equation 1). In the next stage CO reacts with steam (H_2O) to from CO_2 and H_2 (Equation 2).

$$C_xH_y + (x/2)\ O_2 = xCO + (y/2)\ H_2 \qquad \textbf{Eq 1}$$

$$CO + H_2O = CO_2 + H_2 \qquad \textbf{Eq 2}$$

The CO_2 is then separated out and captured, while H_2 is burned to produce heat and power.

Oxyfuel

In oxyfuel capture, the CO_2 is captured during fuel combustion. The fuel is burned in a mixture of pure oxygen and recycled flue gas. The reason for this is that combustion of fossil fuels in pure O_2 can result in very high temperature, about 3500°C, which is too high to be tolerated by the power plants used today. However, the CO_2 in the recycled gas reduces the combustion

temperature to reasonable ranges, for example 1300 to 1400°C in gas turbines and 1900°C in oxyfuel coal boilers [9].

The recirculation in oxyfuel combustion, gives increased CO_2 concentration in the flue gas compared to conventional flue gasses, making it possible to efficiently remove CO_2 before processing for transportation (Figure 4).

Post-combustion

When CO_2 is captured after the burning of fuel (coal, gas, or petroleum) in air (Figure 4), the process is referred to as post-combustion. The heat from the combustion generates steam, which drives a steam turbine. The turbine generates electricity. The flue gas, a product of the combustion process, is removed from the boiler and filtered. The flue gas is taken through several processes before the CO_2 finally is separated out. Before the CO_2 can be captured, sulphur must be removed from the flue gas, since sulphurous compounds will also bind to the capture sorbent and disturb the CO_2 capture process. The capture of CO_2 from post-combustion has been the focus for extensive research. Two parallel projects are conducted on the test center of Mongstad [10, 11]; Aker Solutions has an amine plant, and Alstom has a chilled ammonia plant there, both of which use the exhaust from the Mongstad refinery as a capture source. The capturing techniques are constantly developing, and what will be the best method for CO_2 capture, remains to be determined. This knowledge is likely to develop over time, when the technologies are put into full scale use and allowed to mature. Of the technologies for CO_2 capture discussed above, the post-combustion CO_2 capture has been the main focus of attention, since it easily can be adapted to existing combustion plants.

1.2.3 Impurities in the captured CO_2

The captured CO_2 will contain impurities that can form separate phases when the impurity concentrations exceed their solubility limits. This is a pressure and temperature depended mechanism, and an example is shown in Figure 4. The impurities can change the phase behavior, the viscosity and the thermodynamic properties of the CO_2. In a normal CCS transport situation, all the impurities should be present at a concentration well below the solubility limit. The different capture techniques give different impurities in the captured CO_2. In this context, everything that end up in the captured gas, other than CO_2, is regarded an impurity. To transport 100 percent clean CO_2 should not cause any problem in terms of flow and corrosion, even in the presence of water under the solubility limit [5].

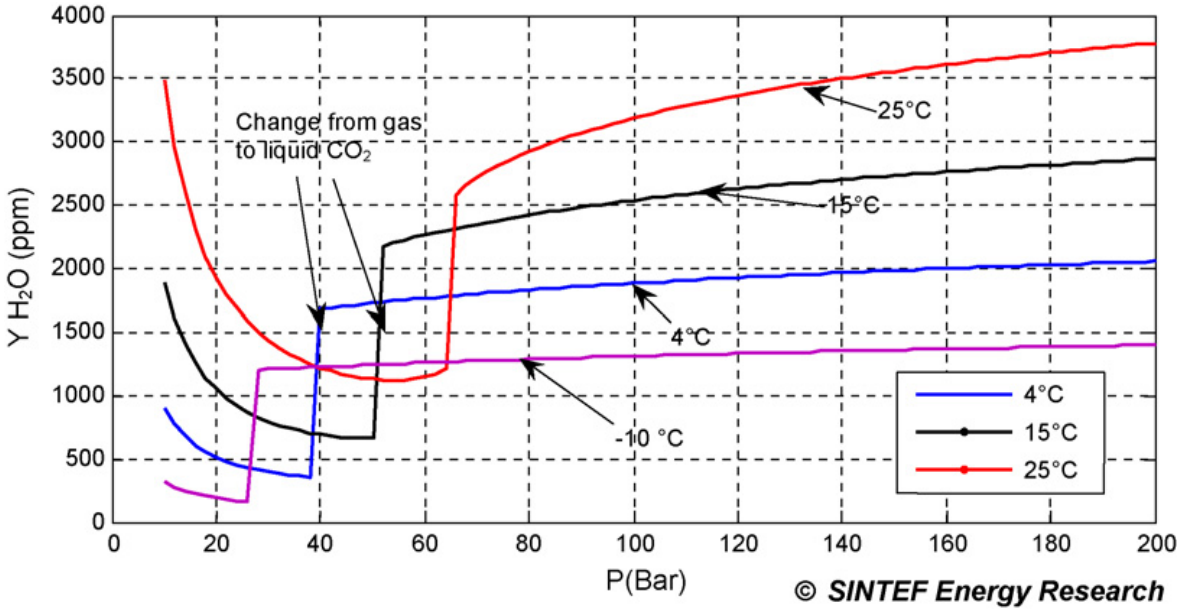

Figure 5 *Solubility of water in pure CO2 as a function of pressure and temperature [6].*

Other impurities might create problems, and the impact of the potential interactions between the impurities are largely unknown [12]. Therefore, knowledge about the types and amounts of impurities to be expected from the different capture technology is important for the safe implementation of full scale CCS. The most likely impurities to be present in the CO_2, along with the expected maximum level of each impurity are given in Table 1. There is an evident lack of published data from real capture plants. Thus, the data given in Table 1 are indicative values that have not been fully proven in the field. Water is not listed as an impurity but expected concentrations are between 50 and 500 ppmv of H_2O [5].

Table 1 *Maximum expected impurity content of the CO_2 for different combustion methods. Note that these are indicative maximum values and not the most likely values [13].*

	Post-combustion	Pre-combustion	Oxy-fuel
	/ ppmv	/ vol.-%	/ vol.-%
CO	20	0,40	0
H_2S	0	3,41	0
H_2	0	0,18	0
O_2	100	0	3,00
NO_2	100	0	0,25
SO_2	100	0	0,25
CH_4	200	0,08	0
Ar	0	0,20	0,25
N_2	1690	0,60	0,75
CO_2	balance	balance	balance

To further complicate the situation, a possible future scenario is that several CO_2 sources will be connected to a pipeline infrastructure, with a main pipeline that carries CO_2 from several different sources to a common reservoir. This makes it very difficult to predict the concentration of impurities in the CO_2 stream, and to make general CO_2 specifications for safe transport. Many other factors must also be taken into consideration, for instance capital costs and energy consumption, whether Enhanced Oil Recovery (EOR) is a goal for the process, and the properties of the end storage target (aquifers or other storage). Despite all these unknown factors, a large fraction of the CCS industry still believes that CO_2 transportation will be non-problematic.

There are numerous unknown factors that might come into play; like interaction between impurities which can lead to corrosion and formation of liquids acids and solids. In the end, the only way to know if CO_2 transport based on the current understanding will be possible from corrosion and safety point of view is to perform well controlled experiments under conditions relevant for transport of CO_2 by pipelines or ships. For corrosion consideration the most challenging impurities are SO_x and NO_x in combination with H_2S, O_2 and H_2O [12]. The interaction between these impurities and their effects on carbon steel are largely unknown, so experiments must be conducted to find out what will give a safe transport of the CO_2.

1.2.4 Existing CO_2 pipelines

More than 5000 km of pipelines are currently used to transport CO_2, and there is over 30 years of experience with large-scale transport of CO_2. The majority of the CO_2 pipelines are located in North America, transporting CO_2 from natural sources to oilfields as part of EOR operations. The longstanding experience with CO_2 transport in USA is often used as an argument that the CO_2 transport will not be a challenge for CCS, since no corrosion attacks has been reported in the pipeline system in the USA. However, the impurities transported in the existing pipelines (Table 2) differ from the impurity compositions expected in CCS (Table 1 vs. Table 2).

Table 2 *Composition of CO_2 transported in existing pipelines. All values are vol% if not stated otherwise. No flue gas impurities like SO_x, NO_x concentrations were reported in the analyses, and for most pipelines the concentration of O_2 is not reported. It is unclear, however, whether this means that these impurities were not measured or whether they were measured but not detected.*

	Canyon Reef Carriers[14]	**Central Basin Pipeline[5]**	**Sheep Mountain[15]**	**Bravo Dome Source[16]**	**Cortez Pipeline[17]**	**Weyburn[17]**	**Jackson Dome, NEJD[5]**
CO_2	85-95	98.5	96.8-97.4	99.7	95	96	98.7-99.4
CH_4	2-15 (C6H14)	0.2	1.7	-	1-5	0.7	Trace
N_2	<0.5	1.3	0.6-0.9	0.3	4	<300 ppm	Trace
H_2S	<200 ppm	<20 ppm	-	-	0.002	0.9	Trace
C2+	-	-	0.3-0.6	-	Trace	2.3	-
CO	-	-	-	-	-	0.1	-
O_2	-	<10 ppmw	-	-	-	<50ppmw	-
NOx	-	-	-	-	-		-
SOx	-	-	-	-	-		-
H_2	-	-	-	-	-	Trace?	-
Ar	-	-	-	-	-		-
H_2O	50 ppmw	257 ppmw	129 ppmw	-	257 ppmw	20ppmv (8 ppmw)	-
Source	Anthropogenic	Natural	Natural		Natural	Anthropogenic	

1.2.5 Steel types

The transport of CO_2 in CCS will be conducted in pipelines alone or in pipelines combined with ships. Even in situations where ships will be the main transport carrier, the CO_2 needs to go through a pipeline before ship transportation and during injection in the storage. The IEA has set as a goal that CCS should account for a 7.4 Gtons reduction of the annual CO_2 emission by the end of 2050 [4]. Obviously a lot of pipelines will be needed for this goal to be achieved. A rough estimate, based on a flow rate of 1.5 m/s of dense phase CO_2, indicates that about 2000 individual pipelines (12" outer diameter) will be needed to transport the CO_2. The Weyburn pipeline is about 330 km long, and has a wall thickness of 10 mm, and an outer diameter of 12". Based on these measures, the amount of steel to make that pipeline can be estimated to about 24 kton. Assuming that this represents the average dimensions of a pipeline, about 48 Mton of steel would be required to build the necessary pipelines to meet the goal for CO_2 removal. So, the cost of steel is an important factor when calculating the profitability of a pipeline.

Steel is an alloy of iron and carbon, containing less than 2% carbon and less than 1% manganese together with small amounts of silicon, phosphorus, sulphur and oxygen. There are many different types of steel; in fact more than 3500 different grades of steel are available. These vary in price as well as physical, chemical and environmental properties [18, 19]. However, in reality, carbon steel would be the primary choice for CO_2 pipelines, since other grades of steel are much more expensive. Carbon steel is divided into three main groups: low-carbon steel (0.05-0.30 wt% carbon), medium-carbon steel (0.3-0.6 wt% carbon) and high-carbon steel (0.6-1.5 wt% carbon). Low-carbon steel, also called mild steel, is the most common steel type used in pipelines. Small changes in composition separate the steel grades from each other. The compositions of some typical mild steels are shown in Table 3.

Table 3 *Composition of some typical mild steel grades.All values are in gram/100 gramm (%wt). Iron as balance.*

Grade	C	Si	Mn	Ni	P	S	Cr	Mo	V	N	Nb	Ti	Al	Cu	-
L290NB (1.0484)	max 0.17	max 0.4	max 1.2	max 0.3	max 0.025	max 0.02	max 0.3	max 0.1	max 0.05	max 0.012	max 0.05	max 0.04	0.015 - 0.06	max 0.25	CEV < 0.42
L360NB (1.0582)	max 0.2	max 0.45	max 1.6	max 0.3	max 0.025	max 0.02	max 0.3	max 0.1	max 0.15	max 0.012	max 0.05	max 0.04	0.015 - 0.06	max 0.25	V+Nb+Ti < 0.15, CEV < 0.45
X65/L450MB (1.8975)	max 0.16	max 0.45	max 1.6	max 0.3	max 0.025	max 0.2	max 0.3	max 0.1	max 0.1	max 0.012	max 0.05	max 0.06	0.015 - 0.06	max 0.25	V+Nb+Ti <0.15, CEV < 0.43
C75/38Mn6 (1.1127)	0.34 - 0.42	0.15 - 0.45	1.4 - 1.65	max 0.4	max 0.035	max 0.035	max 0.4	max 0.1							Cr+Mo+Ni <0.63

Experiments with X65 and C75 steel [20], showed that X65 steel corroded 30 to 70% faster than C75 steel, highlighting the fact that small compositional changes can have large effects on the corrosion rate. Two types of carbon steel were used in the present study: X65 from the Ormen Lange pipeline and foils of a carbon steel referred to as S355J2. This steel is equivalent to St52-3N, a type of mild steel.

1.2.6 Effects of water on corrosion

The chemical composition of the transported CO_2, i.e. the types and concentrations of impurities present, is expected to be different in CCS than in present forms of CO_2 transport. The impurity composition of the CO_2 might have major effects on the chemical stability of the pipeline in which the CO_2 is transported. The typically impurities expected to be present in CCS CO_2 transport is shown in Table 1, but not all of these impurities are likely to influence the corrosion rate or solid formation. The impurities that most likely have a corrosive effect are: water, hydrogen sulfide, oxygen, sulfur dioxide, and nitrogen dioxide [21, 22]. In addition to the impurities originating from the captured gas, there might be some carry over from the capture plant, such as amines (used to capture CO_2) and glycol (used for dehydration of the CO_2 before compression). Small amounts of these compounds might end up in the CO_2. Some reports suggest that the presence of glycols such as mono ethylene glycol (MEG) can reduce the corrosion rate [23-25] in a free water phase. The same effect could be expected for amines. However, it is also possible that glycols may increase the corrosion risk by extracting the water vapor from the bulk phase and form an aqueous phase locally.

Free water phase

It is very important to distinguish between water present as a separate aqueous phase and water dissolved in the CO_2. It is well known that a free water phase in the high CO_2 pressures expected in CCS pipelines will result in unacceptably high corrosion rates [8, 20, 23, 24, 26-31]; the corrosion rate can vary between 0.2 to 50 mm/y depending on pressure, temperature and flow rate (Table 2). A free water phase can occur by accidental ingress of water or by water condensation in systems with inadequate drying of CO_2.

Only a limited number of corrosion experiments have been carried out with dense phase CO_2 and free water. Table 4 summarizes the test conditions and corrosion rates for experiments where the samples were exposed to a circulating aqueous phase. There is a wide spread of corrosion rates. Temperature, flow and pressure could influence the corrosion rates. Zhang [30] tested different temperatures in static conditions with 95 bar of CO_2. The corrosion rates (2-5 mm/y) increased with an increase in temperature from 50 °C to 80 °C and decreased from 80 °C to 130 °C. Nor et al. [32] showed that the corrosion rate increases with increasing flow and they concluded that an increase in temperature seems to increase the flow sensitivity of the CO_2 corrosion. The literature shows [23] that the corrosion rate increases with increasing CO_2 partial pressure until 40 bar, where it starts to decrease.

This study will investigate the pressure dependency of CO_2 corrosion at high CO_2 pressures relevant for CCS.

Table 4 *Summary of experiments with free aqueous phase from ife database [33].*

Exp. no	Temp °C	Pressure bar	Water phase	Duration days	Flow/ mixing	CR mm/y	ref
F1	12	100	Pure	1-3	1 m/s	6.3	[21]
F2	13	100	Pure	1-3	1 m/s	3.2	[21]
F3	13	100	Pure	1-3	3 m/s	6.2	[21]
F4	25	58	1% NaCl	6	Slow circ.	2.4	[23, 34]
F5	25	64	1% NaCl	6	Slow circ.	3.6	[23, 34]
F6	25	80	1% NaCl		1m/s	7.5	[32]
F7	25	80	1% NaCl		1.5 m/s	12	[32]
F8	40	40	1% NaCl	6-12	Slow circ.	4.9	[23, 34]
F9	40	58	1% NaCl	6-12	Slow circ.	4.4	[23, 34]
F10	40	85	1% NaCl	6-12	Slow circ.	1.7	[23, 34]
F11	40	95	1% NaCl	6-12	Slow circ.	0.6	[23, 34]
F12	50	80	1% NaCl	6	Slow circ.	4.6	[23, 34]
F13	50	40	1% NaCl	6	Slow circ.	6.9	[23, 34]
F14	50	20	1% NaCl	6	Slow circ.	4.3	[23, 34]
F15	50	60	1% NaCl	6	Slow circ.	2.3	[23, 34]
F16	50	100	Pure	1-3	1 m/s	33	[21]
F17	50	100	Pure	1-3	3 m/s	38.3	[21]
F18	50	150	Pure	1-3	3 m/s	41.7	[21]
F19	50	95	Pure	4	rot.cage	5.9	[20, 35]
F20	50	95	Pure	4	rot.cage	8.9	[20, 35]
F21	80	135	Pure	4	rot.cage	11	[20, 35]
F22	80	135	Pure	4	rot.cage	14.3	[20, 35]
F23	80	80	1% NaCl		1m/s	25	[32]
F24	80	80	1% NaCl		1.5 m/s	240	[32]

Dissolved water in CO_2

Table 5 summarizes the corrosion rates found in the literature for dissolved water in CO_2 experiments and the test conditions. The S in experiment number indicates stagnant condition, while F means some circulation over the sample.

Table 5 *Summary of experiments with dissolved water in CO_2 from IFE's database[33].*

Exp. no.	H_2O ppmv	Pressure bar	Temp °C	Exposed days	CR mm/y	Ref.
F01	488	100	25	14	no	[36]
F02	1220	100	25	18	<0.01	[21, 36]
F03	1800	82	35	5	0.026	[37]
F04	1800	82	35	5	0.032	[37]
S01	100	79	31		1.1	[38]
S02	240	80	40	7	0.08	[39]
S03	244	76	40		1.2	[40]
S04	300	80	35	2	0.003	[41]
S05	490	80	40	7	0.07	[39]
S06	610	63	22	42	No	[42]
S07	700	80	35	2	0.004	[41]
S08	730	80	40	7	0.06	[39]
S09	980	80	40	7	0.08	[39]
S10	998	63	22	21	slight	[42]
S11	1000	79	31		2.5	[38]
S12	1220	100	20	30	No	[8]
S13	1200	80	35	2	0.01	[41]
S14	1200	80	40	7	0.07	[39]
S15	1770	80	35	2	0.03	[41]
S16	2440	76	40		2.3	[40]
S17	2650	80	50	2	0.014	[41]
S18	2800	80	35	2	0.07	[41]
S19	3670	80	40	7	0.08	[39]
S20	4880	76	40		2.5	[40]
S21	4880	130	40		3.5	[40]
S22	Sat	80	35	0.6	0.11	[41]
S23	Sat	80	35	1	0.11	[41]
S24	Sat	80	35	2	0.10	[41]
S25	Sat	80	40	7	0.11	[39]
S26	Sat	80	40	7	0.17	[39]
S27	Sat	80	40	7	0.11	[39]
S28	Sat	80	50	0.6	0.09	[41]
S29	Sat	80	50	1	0.03	[41]
S30	Sat	80	50	2	0.02	[41]
S31	Sat	80	50	1	0.4	[27]
S32	sat	150	80	28	0.1	[43]

When the water concentration is below the solubility limit (Figure 5), most labs find the corrosion rate to be insignificant for pure CO_2-H_2O systems [8, 29, 42, 44-49]. However, other researchers have reported higher corrosion rates, even above 3 mm/y in lab experiments [38, 40, 50]. Localized attacks up to 1.4 mm/y have also been reported [41, 51]. In summary it seems like the effect of water on the corrosion rate is an important parameter that is not well agreed upon.

1.3 Aim of the study

The present study will carry out research on the effect of water as an impurity in CO_2 at CCS transport conditions. A test system will be made to mimic such conditions experimentally. It will also require methodology development. More specifically the aims of this work are:

Aims:

1) Design and build a test loop which realistically mimics the key features of CCS transport. The loop needs to allow continuous monitoring of pressure, flow and temperature as well as on-line measurements of impurities. Furthermore, the setup should allow change of any parameter independently at any time during the course of the experiment.

2) To test the stability, precision and repeatability of the system prior to experiments.

3) Perform experiment to determine how different concentrations of water dissolved in CO_2 affects the corrosion rate of carbon steel.

4) Perform experiments to determine the corrosion rate of carbon steel in high pressure CO_2 in the presence of a free water phase.

2. Corrosion mechanism in water and CO_2

The corrosion process including precipitation of corrosion products is summarized visually in Figure 6.

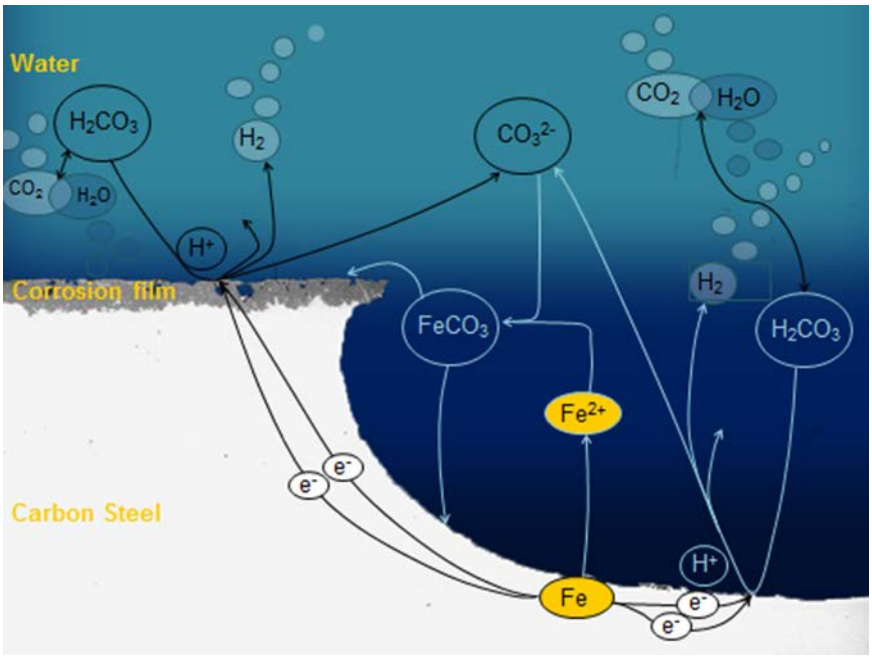

Figure 6 *Corrosion in liquid water containing dissolved CO_2.*

When CO_2 dissolves in water it becomes partly hydrated and forms carbonic acid:

$$CO_2 + H_2O \leftrightarrow H_2CO_3 \qquad \textbf{Eq 3}$$

Carbonic acid is diprotic and dissociates in two steps:

$$H_2CO_3 \leftrightarrow H^+ + HCO_3^- \qquad \textbf{Eq 4}$$

$$HCO_3^- \leftrightarrow H^+ + CO_3^{2-} \qquad \textbf{Eq 5}$$

The resulting pH is a function of the CO_2 partial pressure as illustrated in Figure 76. When carbon steel is exposed to this acidic water it is not a question of whether the steel will corrode, but rather a question of how quickly. The overall corrosion reaction for iron (steel) in this environment can be written:

$$Fe + 2H_2CO_3 \rightarrow Fe^{2+} + H_2 + 2HCO_3^- \qquad \textbf{Eq 6}$$

Bicarbonate (HCO_3^-) is formed in Equation 6, and the pH in the solution will therefore increase until the concentrations of dissolved Fe^{2+} and HCO_3^- become higher than the solubility and form $FeCO_3$.

$$Fe^{2+} + CO_3^{2-} \rightarrow FeCO_3(s) \qquad \textbf{Eq 7}$$

The $FeCO_3$ can deposit on the steel and form a protective layer (often referred to as corrosion film in the CO_2 corrosion literature) that can reduce the corrosion rate up to 3 orders of magnitude. When this corrosion film is damaged locally, pitting or localized attack develop as indicated in Figure 6.

The corrosion of iron (carbon steel) is an electrochemical process involving anodic (dissolution of iron) and cathodic (evolution of hydrogen) reactions. These reactions have been discussed in a number of papers that have been reviewed by Nesic [52-54] and Dugstad [55, 56]:

Anodic reaction

The overall anodic dissolution of iron is:

$$Fe \rightarrow Fe^{2+} + 2e^- \qquad \textbf{Eq 8}$$

Several multi-step mechanisms have been suggested in the literature. Bockris [57] suggested a pH dependent mechanism more than 50 years ago:

$$Fe + H_2O \leftrightarrow FeOH + H^+ + e^- \qquad \textbf{Eq 9}$$

$$FeOH \xrightarrow{\boldsymbol{rds}} FeOH^+ + e^- \qquad \textbf{Eq 10}$$

$$FeOH^+ + H^+ \leftrightarrow Fe^{2+} + H_2O \qquad \textbf{Eq 11}$$

This mechanism that was suggested to be valid for strongly acidic media was for many years also assumed to apply for corrosion in CO2 environment where the pH can vary from 3.5 to 7. As pointed out by Nesic [53], it was overlooked that Bockris experimental data indicated that the pH dependency decreased rapidly with increasing pH. The reaction order with respect to OH^- was 2 at low pH, but decreased towards 1 and 0 for pH>4.

Several mechanisms have been proposed to account for the dependency of pH of Fe, e.g. by Nesic et al. [53, 54], but the actual pH dependency is still debated [56].

It should be noted that the pH for the free water phase experiments in this project is expected to be about or lower than 4 and therefore might follow the Bockris mechanism.

Cathodic reactions

It is referred to two main cathodic reactions in the literature:

$$H^+ + e^- \rightarrow \frac{1}{2} H_2 \qquad \textbf{Eq 12}$$

$$H_2CO_3 + e^- \rightarrow \frac{1}{2} H_2 + HCO_3^- \qquad \textbf{Eq 13}$$

Equations 12 and 13 are the overall reaction routes and do not reveal the detailed mechanisms of the proton reduction. In fully dissociated strong acids corrosion and H_2 production occur according to Equation 12. The rate controlling mechanism is transport of H^+ to the steel surface (mass transfer limit). Its contribution to the corrosion rate is small above pH 5, a typical pH in many CO_2-water systems. When the water contains CO_2, dissociation of H_2CO_3 will act as a source for H^+ and increase the corrosion rate. The concentration of H_2CO_3 depends on the CO_2 partial pressure (Henry's law) and is almost independent on pH. That means that H_2CO_3 as an H^+ source becomes more and more dominating when the pH increases.

It has been suggested that direct reduction of H_2CO_3, may take place (Equation 13) and thus increase the corrosion rate beyond the mass transfer limited reduction rate of H^+. This mechanism has been generally accepted since first proposed by de Waard in 1975 [58], but has been questioned in recent reviews [55, 56].

2.1 Determine corrosion by Linear Polarization Resistance

The corrosion rate can be calculated from the corrosion current by assuming an electrolytic dissolution reaction of the sample:

$$S \rightarrow S^{n+} + ne^- \qquad \textbf{Eq 14}$$

The current can be related to mass with Faraday's law:

$$Q = nFM \qquad \textbf{Eq 15}$$

where Q is the charge in coulomb from the reaction, n is the number of electrons transferred in the reaction per atom, F is the faraday's constant equal 96486.7 coulomb/mole, and M is the number of moles reacting. M is the reacted species (mass, m) divided by atomic weight (AW) of the species (M = m/AW). By introducing equivalent weight (EW) which is the mass of the species that will be oxidized by one Faraday of electric charge, EW = AW/n, by substituting this into Equation 15 we get:

$$m = \frac{EW \cdot Q}{F} \qquad \textbf{Eq 16}$$

The corrosion rate (CR) can be calculated if the density and the area of the sample is known, and using the relation that charge (Q) equals current (I) multiplied by time (t) :

$$CR = \frac{I_{cor} \cdot K \cdot EW}{\rho \cdot A} \qquad \textbf{Eq 17}$$

where CR is the corrosion rate in mm per year, K is unit defining (for corrosion rate in mm/y) constant, 3270 mm g A^{-1} cm^{-1} $year^{-1}$, I_{cor} is the average current in ampers (A), EW is a dimensionless equivalent weight of the sample material, ρ is the density of the metal, g/cm^3, and A is the exposed area of the sample, cm^2. The only part of the equation we have to determine is the average corrosion current. This current cannot be measured directly. By changing the potential close to the open circuit potential in the range –5 to +5 mV and measuring the current a straight line is obtained in a current versus voltage plot (Figure 7) where the slope is the polarization resistance.

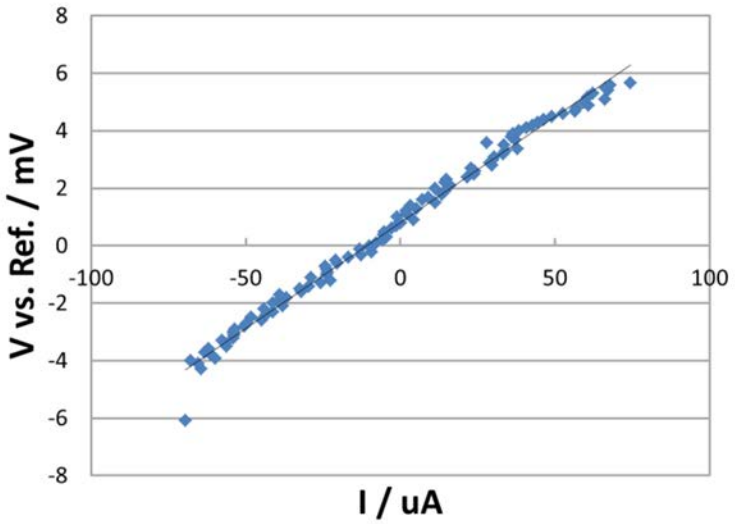

Figure 7 *The current verus the potential around the open circuit voltage, the slope of the line is the polarization resistance.*

The average corrosion current density is calculated as:

$$i_{cor} = \frac{I_{cor}}{A} = \frac{B}{R_P} \qquad \textbf{Eq 18}$$

where i_{cor} is corrosion current density, A/cm^2, R_P is the polarization resistance, ohms cm^2, and B is the Stern-Geary constant (B-value), volts. The Stern-Geary constant is used to convert LPR measurements to corrosion rates, and can be calculated from Tafel slopes where both cathodic and anodic reactions are activation controlled (standard ASTM G102). Tafel plot is log (current) versus potential see Figure 8. The equation is as followed:

$$B = \frac{b_a \cdot b_c}{2.303\,(b_a + b_c)} \qquad \textbf{Eq 19}$$

where:

B is the Stern-Geary, called B-value, in volts,
ba is the slope of the anodic Tafel reaction in volts/decade, and
bc is the slope of the cathodic Tafel reaction in volts/decade.

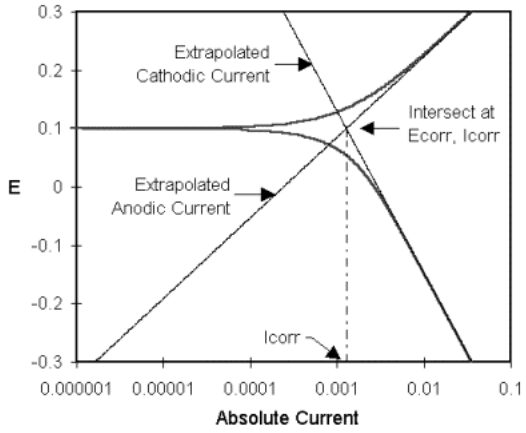

Figure 8 *A Tafel plot [59].*

A numerical fit of the Butler-Volmer equation (Equation 20) by adjusting the values of E_{cor}, I_{cor}, b_a, and b_c enables determine of the Stern-Geary constant from anodic and cathodic sweeps. This curve fit does not require a fully developed linear portion of the measured data [59]:

$$I = I_a + I_c = I_{cor} \cdot \left(e^{\frac{2.3 \cdot (E - E_{cor})}{b_a}} - e^{\frac{-2.3 \cdot (E - E_{cor})}{b_c}}\right) \qquad \textbf{Eq 20}$$

Where I is the measured current A, E is the electrode potential in volt, and E_{cor} is the corrosion potential in volt.

The polarization resistance will be determined by LPR measurements, while the Stern-Geary constant (B-value) will be estimated by fitting the CR(LPR) to the CR(Iron count). Normally the Stern-Geary constant is calibrated against the weight loss in the end of the experiment. In this study the corrosive environment changes during the experiments, different corrosion rates will occur and the weight loss will represent an average of the whole experiment.

A combination of Equation 17 and Equation 18 was used to fit the CR(LPR) to the CR(iron count) to find the B-value:

$$B = \frac{CR(\text{iron count}) \cdot \rho \cdot A \cdot R_P}{K \cdot EW} \qquad \textbf{Eq 21}$$

where $CR_{(iron\ count)}$ is the corrosion rate from iron measurement, mm/y, ρ is the density of iron, 7.86 g/cm^3, A is the area of the carbon steel sample, ~9 cm^2, RP is the measured LPR value, K is unit defining constant, 3270 mm g A^{-1} cm^{-1} year^{-1} , and EW is a dimensionless equivalent weight of iron, 27.92. Solving the equation, the B-value (V) can be expressed as:

$$B = 7.75 \times 10^{-4} \cdot CR(\text{iron count}) \cdot R_P \qquad \textbf{Eq 22}$$

2.2 Corrosion in CO_2 with dissolved water

It is generally accepted that there is no corrosion in pure CO_2. The corrosion detected when water is dissolved in CO_2 must therefore occur in an aqueous layer on the metal surface. As known to the author no papers has so far been published on the mechanism of corrosion in CO2 with dissolved water, but in atmospheric corrosion this process has been studied extensively and mechanisms have been proposed. The theory discussed in this chapter is inspired by the understanding of atmospheric corrosion.

Formation of a aqueous layer

Water may bond to the metal surface in different ways, either through the oxygen atom in the water molecule or as a dissociated species. Water adsorption leads to a surface covered by hydroxyl, atomic oxygen and atomic hydrogen [60]. The first monolayer seems to be adsorbed in a highly immobile manner on the hydroxylated surface, while the second and third monolayers of water are more mobile and randomly orientated [61]. The numbers of monolayers adsorbed to the surface increase with the relative humidity and time, approximated numbers of monolayers versus relative humidity are presented in Table 6.

Table 6 *Water monolayers versus relative humidity at 25 °C [61].*

Relative humidity (%)	Number of monolayers
20	1
40	1.5 - 2
60	2 - 5
80	5 - 10

The water bonds to the hydroxylated surface with a strength similar to the hydrogen bonding between water molecules in a liquid phase which increases the possibility for water clusters to form on the surface. Kinks or steps on un-defined surfaces are highly reactive sites which promote water clustering and the probability of anode-cathode area formation. When there are more than three monolayers of water on the surface the properties approach those of bulk water [62].

Deposition of CO_2

There are two types of deposition into the aqueous layers, wet and dry deposition. The wet deposition requires mist or dew, whereas dry deposition requires that there are no water droplets in the gas phase. Wet deposition could happen when the dissolved water in CO_2 increases beyond the solubility limit and precipitates, a situation where water droplet formation and CO_2 solubility in the water droplets becomes important. Dry deposition might be the dominating process as long as the water is below the solubility limits. Figure 9 illustrate the different processes involved in dry deposition of CO_2 into an aqueous layer on the steel surface.

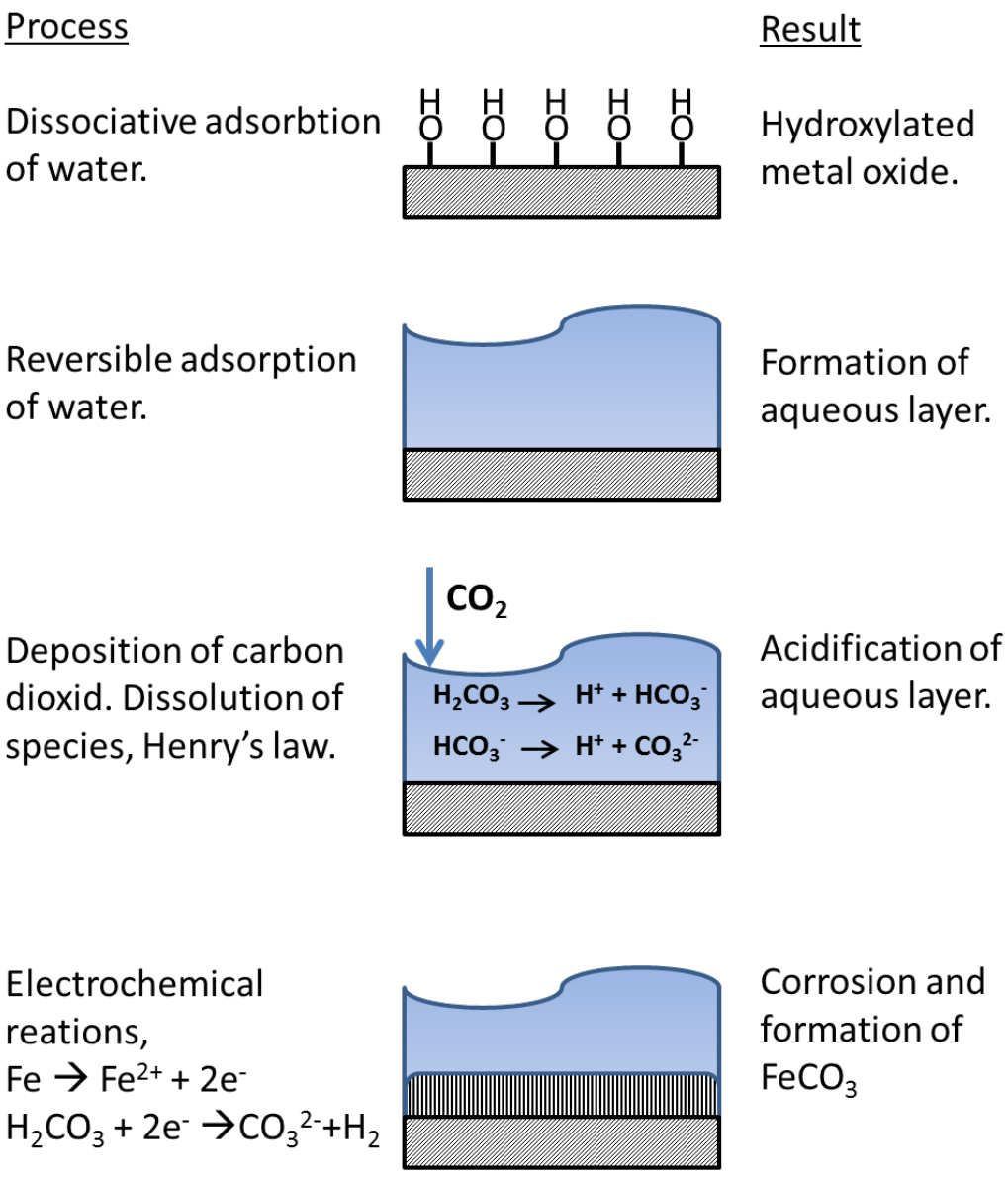

Figure 9 *Adsorption of water on the metal surface and dry deposition of CO_2 (modified from [61])*

Formation of corrosion products

The corrosion rate can be influenced by many parameters, e.g., the solubility of Fe^{2+}, the deposition rate of corrosion products, the hydration rate of CO_2 forming carbonic acid, and formation of protective products/film on the surface. Figure 10 illustrates the process occurring in or at the solid phase (the corrosion product). The growth of the film can be a sequence of consecutive steps of the mention parameters, where also the HSAB concept (Pearson acid base concept) could be important [61]. It was found that products of crystalline state are more corrosion resistant than amorphous ones [63]. The transition from an amorphous to a crystalline state is determined by aging or slow growth of amorphous phases through dissolution-reprecipitation processes [61].

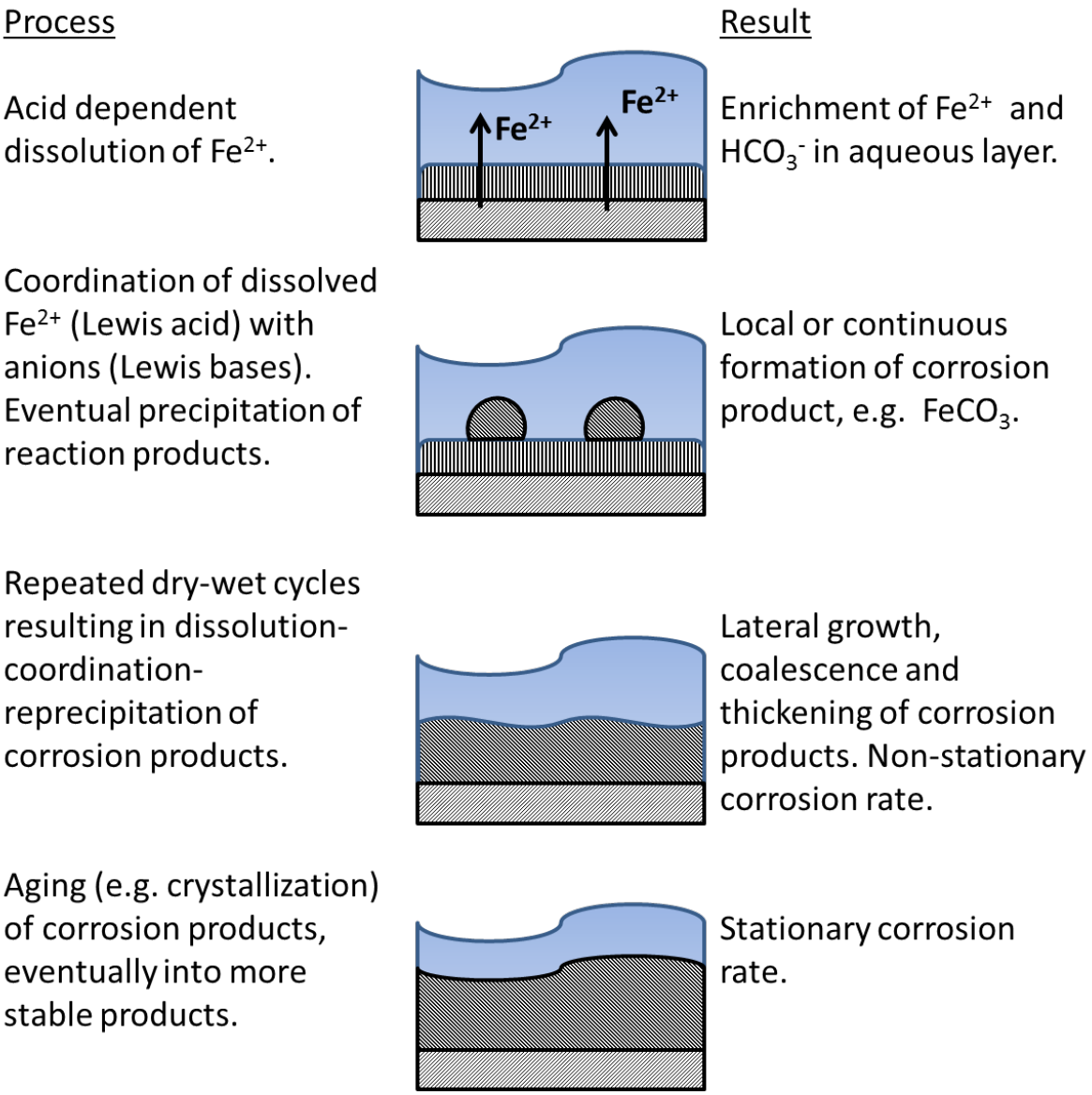

Figure 10 *Formation of corrosion products at the surface(modified from [61]) .*

Calculation corrosion rates from water consumption

One mole of water is consumed per one mole of iron (Equation 3 to 7), by knowing the consumption of water the corrosion rate of the sample can be calculated from a combination of the following equations:

$$C_{H2O} = \frac{n_{H2O}}{n_{CO2}} \cdot 1000000 \qquad \textbf{Eq 23}$$

$$n_{CO2} = \frac{V_{CO2} \cdot \rho_{CO2}}{MW_{CO2}} \cdot 1000 \qquad \textbf{Eq 24}$$

$$n_{H2O} = n_{Fe} = \frac{A_{Fe} \cdot CR \cdot \rho_{Fe}}{10 \cdot MW_{Fe}} \qquad \textbf{Eq 25}$$

Where C_{H2O} is the consumed water in ppmv/y, n_{H2O} is the amount of consumed water in mol/y, n_{CO2} is the amount of CO_2 in the loop in mol.

In Equation 24, V_{CO2} is the volume of dense phase CO_2 in the loop in liters, ρ_{CO2} is the density of CO_2 at a given temperature and pressure in g/cm^3, MW_{CO2} is the molecule weight of CO_2 in g/mol.

And for Equation 25, A_{Fe} is the area of the carbon steel sample in cm^2, CR is the corrosion rate of the carbon steel sample in mm/y, ρ_{Fe} is the density of iron in g/cm^3, and MW_{Fe} is the molecule weight of iron in g/mol.

The corrosion rate equation (mm/y) will then be given by:

$$CR = \frac{C_{H2O} \cdot V_{CO2} \cdot \rho_{CO2} \cdot MW_{Fe}}{A_{Fe} \cdot \rho_{Fe} \cdot MW_{CO2} \cdot 100} \qquad \textbf{Eq 26}$$

3. Experimental

Two loops were used in this work. One loop was used for corrosion studies in dense phase CO_2 containing a known amount of water (High Pressure CO_2 Impurity Loop, HPCIL) and the other loop was used for corrosion studies in water saturated with CO_2, called Dense Phase Loop.

3.1 HPCIL with water dosing and analyzer

The equipment for testing corrosion on carbon steel under dense phase conditions was a dedicated flow loop built at IFE. There are only few testing rigs reported for this purpose in the world and no data has been published from corrosion studies with full control of water concentration in dense phase CO_2.

3.1.1 High pressure CO_2 impurity loop

The HPCIL was built in Hastelloy C276, a corrosion resistant material. The loop was designed for a pressure up to 500 bars and is placed in a cabin for HSE reasons (see Figure 11). A cooling unit and heating clamps controlled the temperature of the loop in the range 0°C and 60°C. The volume of the loop was 2.15 liters. There was one inlet for the CO_2 pre-mixed with water and an outlet to analyze the water concentration. The loop could be considered as a reaction chamber with mixing (ideal mixing volume) and changes in the water levels will follow a normal dilution situation as long as no corrosion reactions or adsorption occurs. To avoid pressure fluctuations, the outlet had the same mass flow as the inlet. The temperature should be kept constant since fluctuations as low as 0.1°C could result in pressure changes up to 1 bar. The temperature, pressure, and flow were logged for all experiments. Before a new experiment started, the loop was ventilated with CO_2 to make sure that no oxygen was present. The carbon steel sample was placed in the test section and the whole loop was filled with dry CO_2 until the pressure reached 95 bar using a booster pump. The test section was closed until the required water level was measured in the loop (bypass is opened so we have circulation). The circulation pump makes sure that the fluid is circulated around in the loop and can be adjusted to the required flow rate.

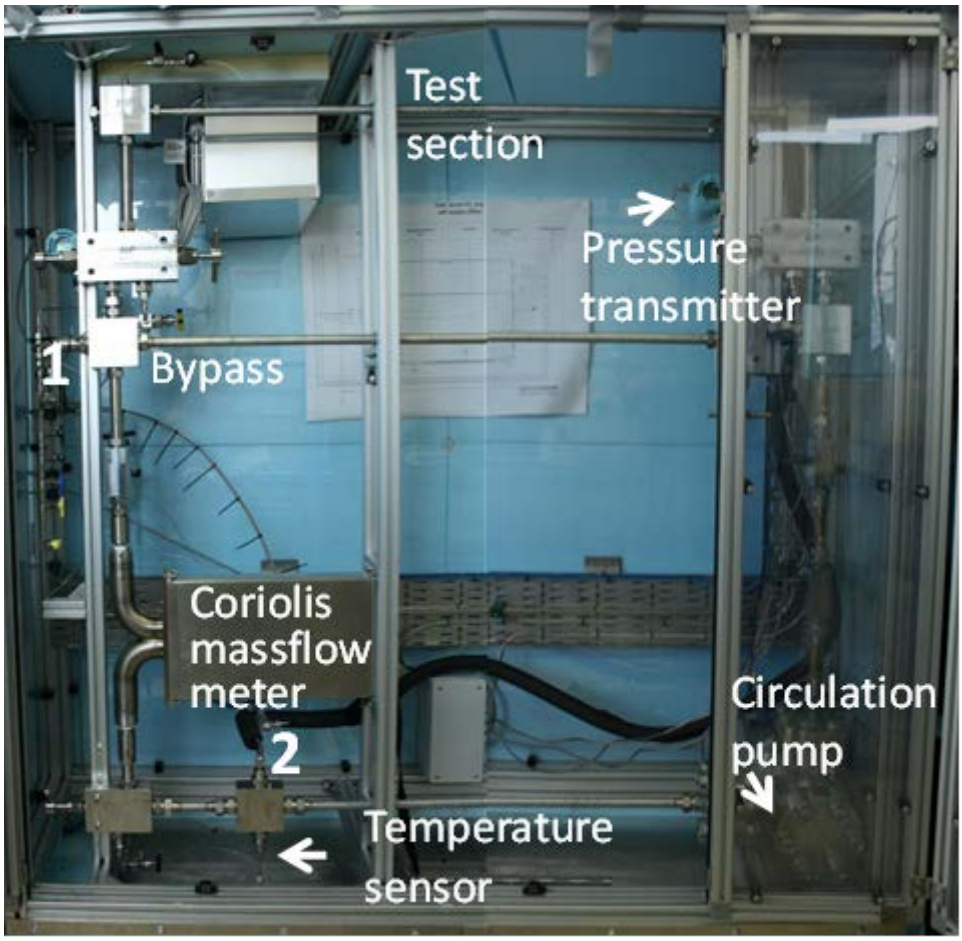

Figure 11 *The high pressure CO_2 impurity loop. The test section is on the top where the carbon steel sample can be placed. Bypass of the test section is in the middle, Temperature sensor, two pressure transmitters, and a coriolis massflow meter are placed as indicated on the figure. The inlet for the CO_2 with pre-mixed levels of water is indicated with "1", and the outlet from where CO_2 can be sent to the analyzer for the determination of water concentration in CO_2 is indicated with "2".*

3.1.2 Water dosing unit

The water dosing unit was designed and built at IFE. This unit was important for two reasons: it delivered a steady and adjustable water concentration in the CO_2 flow, and it adjusted and maintained the pressure of the whole system.

The water dosing unit was based on moisturizing of the gases. When a gas is bobbled through water, the gas is saturated with water. Thus the amount of water can be adjusted by varying the temperature of the water, and mixing the moist gas with a dry gas at various ratios makes it possible to adjust the water levels over a wide range. In the experiment, dense phase CO_2 passed through the water instead of gas. The dense phase was CO_2 saturated with water at a controlled temperature, in this case 20°C. The temperature was controlled by a Huber

thermostatic bath. The water saturation of CO_2 at 20°C is about 2900 ppmv (see Figure 5). Since the system is continuously dosed, and therefore not in complete equilibrium, the water level could be lower. Figure 12 shows an image of the water dosing unit with pressure controller.

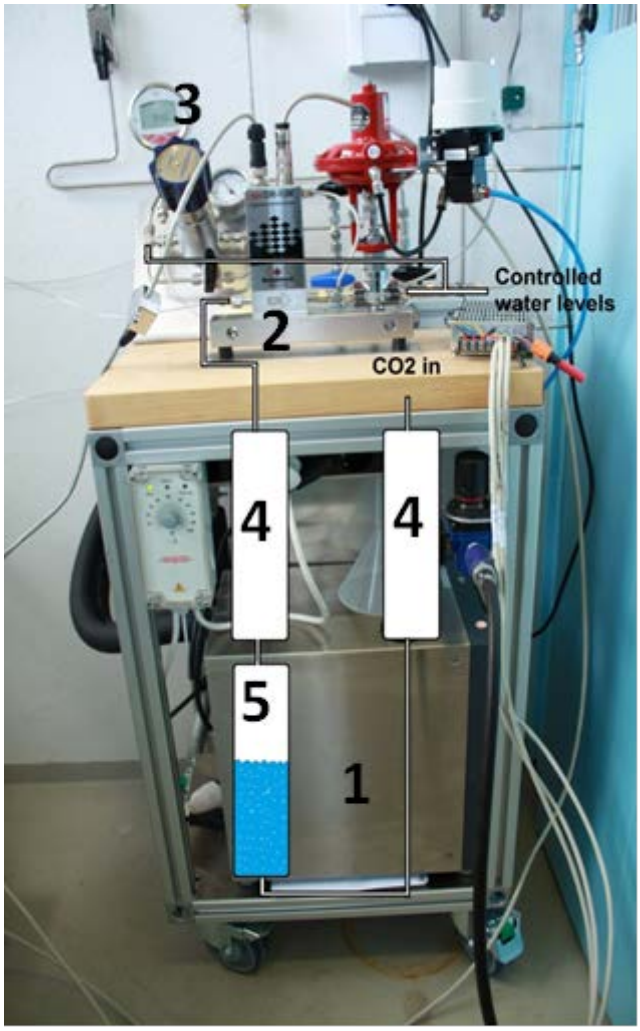

Figure 12 *The water dosing unit consists of a thermostatic bath from Huber (1), mini-coriolis mass flow controller from Bronkhorst (2), liquid pressure regulator (3), CO_2 expansion tanks (4), and humidifier tank from Swagelok (5). The dense phase CO_2 enters the first expansion tank before it gets wetted in the humidifier, then the CO_2 enters the second expansion tank so water droplets can fall out. All tanks are temperature controlled. The wetted CO_2 is then dosed in by the mass flow controller and mixed with 95 bars of dry CO_2 from the liquid pressure regulator before it enters the CO_2 loop.*

To ensure that the wetted CO_2 only flowed in one direction, the pressure before the mass flow controller was set to 10 bars above the pressure of dry CO_2 from the liquid pressure regulator. The total volume of the expansions tank and the humidifier was 900 ml, and about 150 ml of water was added to the humidifier. It took 6 to 60 hours (depending on the dosing rate) to move CO_2 through the humidifier and the second expansion tank before it reached the mass flow controller. The CO_2 used for the experiments was delivered from a 50 liters bottle with riser. The CO_2 is liquid at about 57 bars pressure at room temperature. The booster pump was an air driven pump (HI 5L-SD-120) from Lewa, 1 bar of air gave 120 bar of pressure for the fluid.

The outlet pressure from this pump was set to 105 bars of CO_2 both to the liquid pressure regulator and the humidifier. The liquid pressure regulator reduced the system pressure to 95 bars, which gave the humidifier 10 bars overpressure to push the wetted CO_2 into the dry CO_2. The critical part to maintain the wanted water level was the ventilation rate at the analyzer, because that rate eventually determined how much dry CO_2 the liquid pressure regulator would send through to keep the pressure fixed at 95 bars. The coriolis mass flow controller was always set to a fix number according to the wanted water level, so if the ventilation rate changed during the experiment the water level would also change. Higher ventilation rate gave lower water level and lower ventilation rate gave higher water level.

Mini-coriolis mass flow controller

A mini CORI-FLOW from Bronkhorst was used for controlling the mass flow. The instrument operates according to the Coriolis principle. When a fluid flows through a vibrating tube, the Coriolis forces will bend or twist the tube (Figure 13). The tubes will always vibrate at their natural frequency, which is a function of the tube geometry, tube material properties, and the mass of the fluid inside the tubes. The small displacements of the tube are detected by sensors and evaluated electronically.

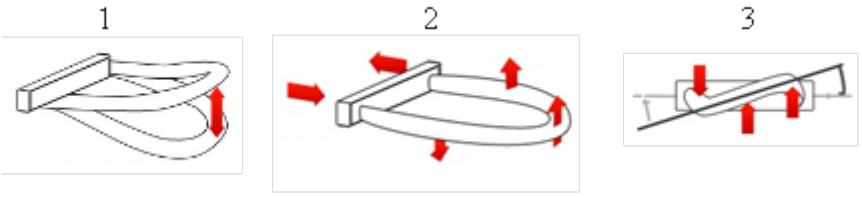

Figure 13 *The figure shows the coriolis force: The flow tube is vibrating without any mass flow (1). When flow is added the fluid force acts to the vibration of the flow tube (2), resulting in twisting of the tube (3) which can be detected and the mass flow calculated.*

3.1.3 Analyzing module

There are several techniques for measuring water concentration in gases, but due to the high pressure it was not possible to find any technique that could measure the water concentration in dense phase CO_2 directly. Therefore the CO_2 pressure had to be reduced from 95 bars to 2 bars. This means that the CO_2 will move from liquid phase to gas phase (crossing phase boundary, see Figure 3), and this is an analytical challenge. The depressurization will cause a temperature decrease, possibly as low as -78.5 °C at which CO_2 will become solid (dry ice). This temperature decrease will lower the solubility of water in the CO_2 and the excess of water will form a separate liquid or solid phase. The water measurements become unstable and incorrect if this situation occurs, as illustrated by the example in Figure 14. A heated gas regulator was

used to prevent condensation of water due to cold spots while pressure was reduced, and the temperature in the phase transition area was about 100°C.

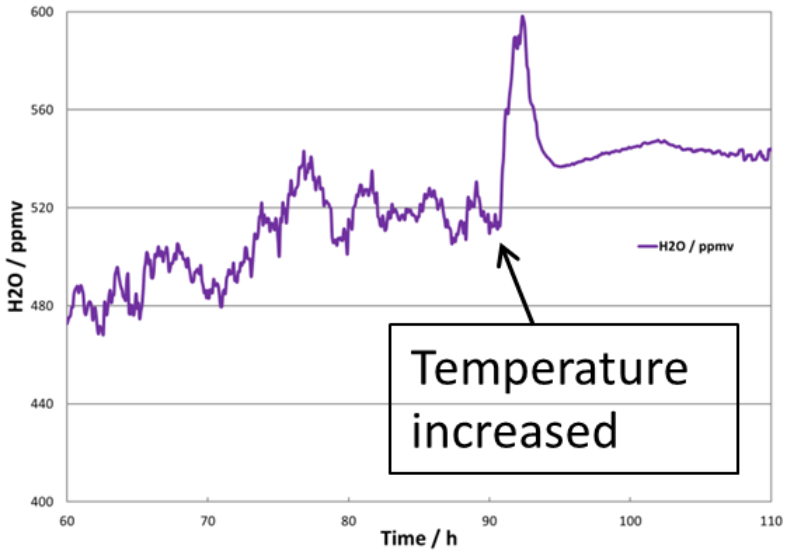

Figure 14 *Graph showing the results of water measurement of 95 bar dense phase CO_2 with a heated gas regulator which reduces the pressure down to 2 bars.*

At low water contents the measurements were fairly stable, but when the concentration got higher the measurements started to fluctuate (Figure 14). This was attributed to water condensation in the regulator. When the temperature in the gas regulator was increased after about 90 hours, the measurement became stable again. A peak can be observed when the temperature is increased which indicates that the heated gas regulator is drying up before it stabilizes at the correct water level. After the pressure was decreased to 2 bars the CO_2 entered the analyzing module as gas phase. This module consisted of different analyzers, but only water and oxygen analyzer was used in the present work. Figure 15 shows a picture of the analyzing module. The flow of CO_2 gas going through the analyzers is controlled by a mass flow controller (Bronkhorst). The flow was set to 500 ml/min which equals approximately 1.1 g/min of liquid CO_2 at 20°C, and it was kept constant in all the experiments.

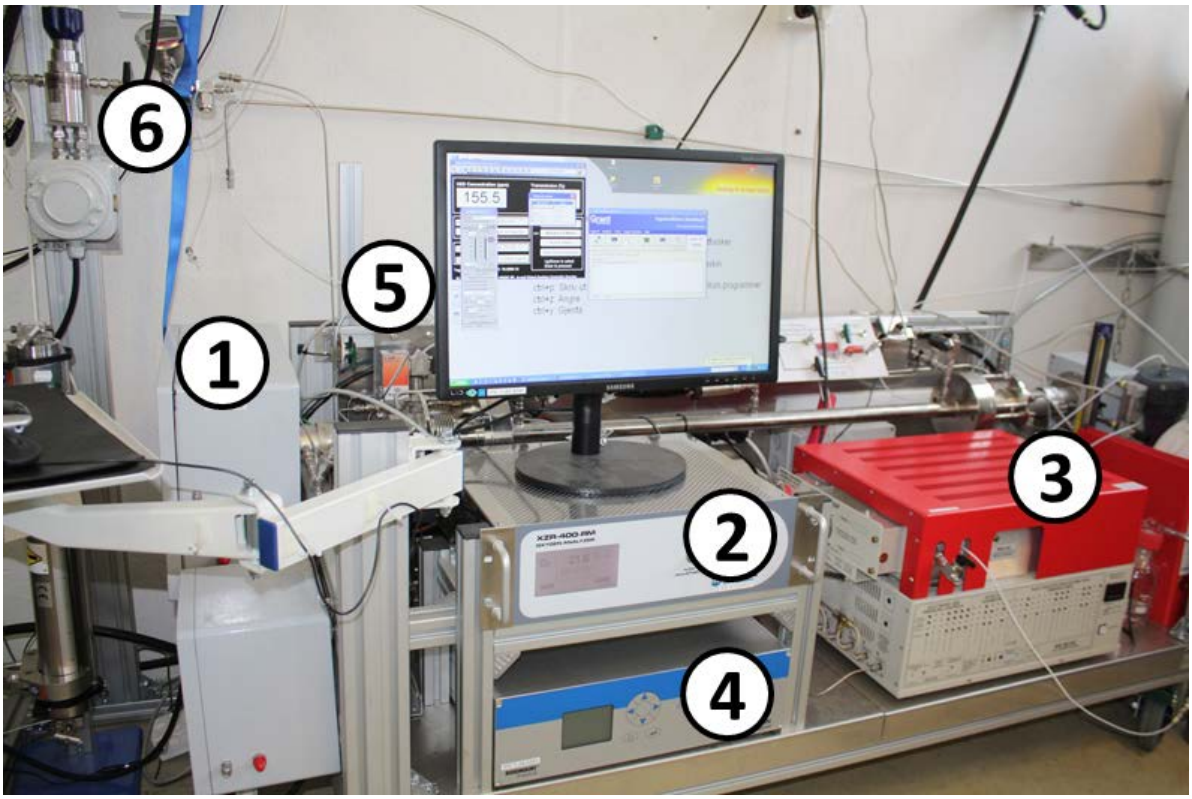

Figure 15 *The analyzing module consists of a Tunable Diode Laser Spectroscopy,TDLS200 from Yokogawa (1), a zirconia oxygen analyzer, XZR400TS from Michell (2), an industrial gas chromatograph from SRI GC (3), a UV/IR photometer called X-stream from Emerson (4), and a squirrel data logger from Grant. Tubing and valveswere made of stainless steel (SS316) delivered by Swagelok. After the heated gas regulator (6), a mass flow meter from Bronkhorst (5) controls the ventilation rate out of the loop and into the analyzers. The CO_2 enters first the TDLS for measuring the water concentration and then the XZR400TS to check the oxygen concentration. After that the CO_2 is ventilated to the atmosphere.*

Water measurements

A tunable diode laser spectroscope (TDLS) was used for water analysis. The analyzing principle was based on absorption spectroscopy in which the amount of light that is adsorbed when it travels through the sample is measured. The absorption is proportional with the concentration and follows the Beer-Lambert law:

$$A = \text{Log}_{10}\, I_o/I = ebc \qquad \textbf{Eq 27}$$

Where: I_0 is the intensity of the reference light
I is the intensity of the light passing through the sample
e is the molar absorptivity (L mol^{-1} cm^{-1})
b is the path length of the sample (cm)
c is the concentration of the compound in the gas (mol L^{-1})

Stretching and bending of the bonds within molecules occur at a frequency that is specific to that particular bond. If the vibration causes a change in dipole of the molecule then light at a particular frequency in the infrared band will be absorbed. A known problem in absorption spectroscopy is interference of other components. This is related to the resolution of the spectroscopic method, and for CO_2 and H_2O that would be a problem for normal spectroscopy with low resolution. However, the TDLS instrument had a resolution as low as $4x10^{-14}$ meters (0.04 pm) since the diode laser had a very narrow wavelength emission. This made it possible to acquire 100 – 1000 data points across the peak [64], which gives the possibility to choose peaks that do not overlap or interfere with each other, as illustrated in Figure 16.

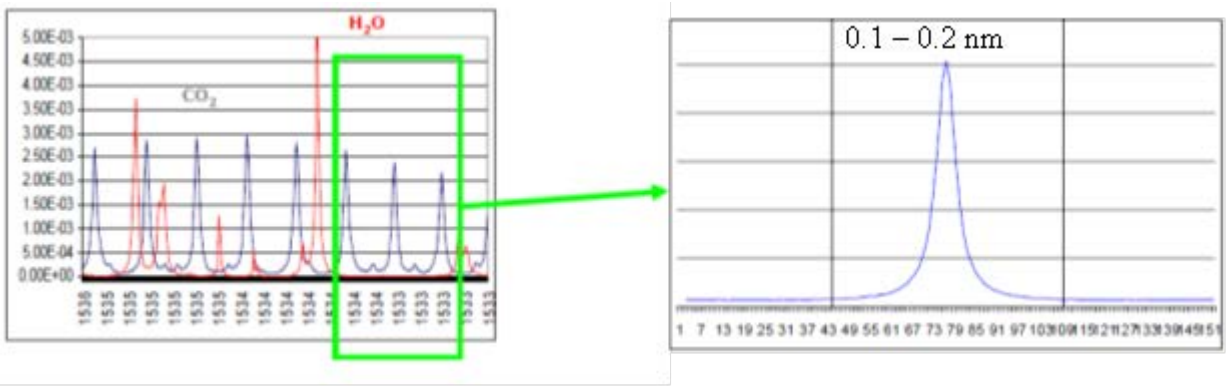

Figure 16 *Choosing the right peaks that do not interfere with each other [64].*

An overview of the TDLS200 is given in Figure 17. The electronic box (1) includes the central processing unit which controls the system parameters, software for signal processing, and logging system. The laser module (2) consists of laser, collating lens, laser mount, and a validation chamber which can be used for running calibration gases through. The detector module (3) holds the detector, focusing lens, and the detector mount. The detector electronics (4) is situated at the end. It is possible to mount the TDLS200 on any application as long as the pressure is lower than 20 bar. An Inconel tube (1.2 meters long and an inner diameter of 25 mm) was used as sample chamber for the water measurements.

The TDLS analyzes continuously and the logging rate was one point every 5 minutes.

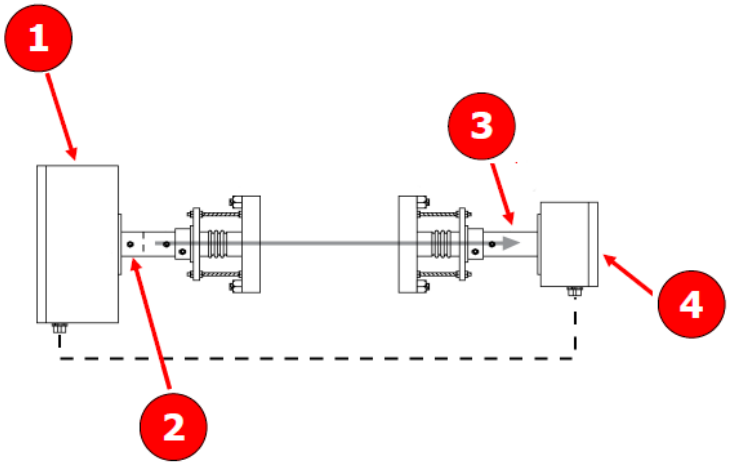

Figure 17 *An overview of the TDLS200 which consists of electronic box (1), laser module (2), detector module (3), and detector electronics [64].*

Oxygen measurements

The oxygen analyzer (XZR400TS) was placed downstream the TLDS analyzer. The measuring was performed with a zirconia (zirconium oxide) sensor which could detect oxygen at trace levels. The zirconia sensor uses a solid state electrolyte and is stabilized with yttrium oxide. The sensor electrode is platinum which is plated on opposing sides of the zirconia probe and at high temperature the zirconia lattice becomes porous, allowing the movement of oxygen ions. The driving force is the partial pressure of oxygen and the movement of oxygen ions across the zirconia produces a differential voltage between the two electrodes, which can be linked to the partial pressure difference between the reference and the sample gas [65]. This principle is based on Nernst equation, see Figure 18 and Equation 28.

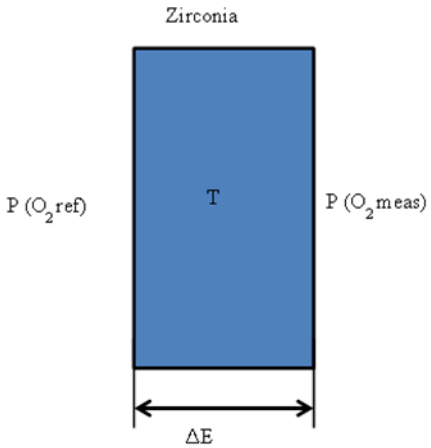

Figure 18 *Zirconia sensor operating principle.*

$$\Delta E = \frac{R \cdot T}{4 \cdot F} \cdot \ln\left(\frac{p_{O_2 meas}}{p_{O_2\ ref}}\right) \qquad \textbf{Eq 28}$$

Where:

ΔE is the potential difference (volts)
R is the gas constant (8.314 J mol^{-1} K^{-1})
T is the absolute temperature (K)
F is the Faraday constant (96484 coulomb mol^{-1})
P (O_2 meas) is the partial pressure of measured sample
P (O_2 ref) is the partial pressure of the reference oxygen, often 21%

The conductivity of zirconia increases exponentially with temperature and is optimized at temperatures above 600°C.

The experiments were supposed to be run under oxygen free conditions and the oxygen measurements were done to control that no oxygen entered the system during the experiments. Since analytical grade CO_2 (5.0) was used, the maximum expected level of oxygen was less than 10 ppmv. During the experiments, 1 to 4 ppmv of oxygen was measured.

Performance testing of dosing unit and analyzing module

The loop can be bypassed such that the dosing unit can feed CO_2 directly to the analyzing module. Different dosing rates were tested and the water concentration was measured by the TDLS. The results are shown in Figure 19. The purple line shows the water concentration measured in the CO_2, while the green line shows the dosing rate of wet CO_2. The total flow of CO_2 through the analyzer was 64 g/h so the difference between the total flow and the dosing rate of wet CO_2 is equal the dry CO_2 from the liquid pressure regulator. If a water level of 500 ppmv is requested then the dosing rate of wet CO_2 would be 12 g/h and 54 g/h of dry CO_2. The new water levels are reached fairly quickly since it is only the volume of the tubing from the dosing unit to the analyzer which needs to be diluted. There are a measuring lag of about 36 minutes between setting a new dosing rate and the water measurement changes. The time to equilibrium will increase when the loop volume is added to the system.

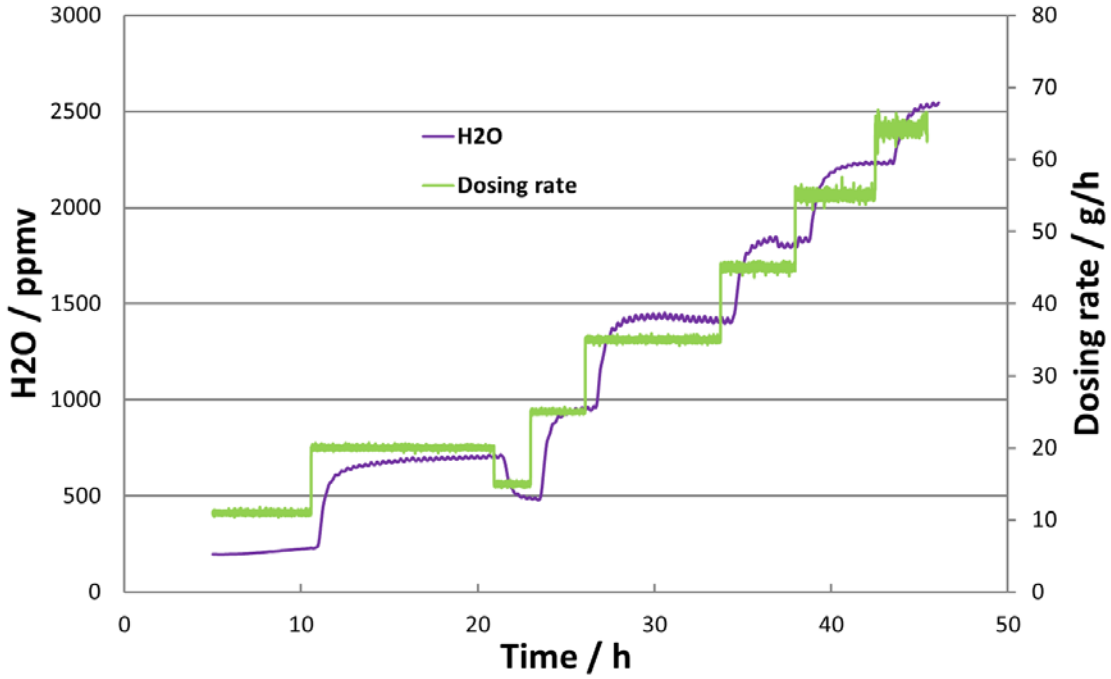

Figure 19 *Graph comparing the injected and analysed level of water.*

3.1.4 Calculated water concentration

Mixing in a first-order system

A calculated water concentration based on what was dosed to the loop is needed for comparison with the measured water concentration in order to see deviations of water signal due to corrosion or adsorption. Some of the experiments were performed with ramping of water concentration and a comparison with ideal water concentrations calculated from a first order differential equation (Figure 20) is therefore needed. The same equation is used to determine the time or volume needed for an ideal mixing volume to be completely mixed. The industry standard is that it should be three times the volume of the chamber purged through in order to get good mixing [66]. Mixing in a volume with purging in new fluid will never reach complete equilibrium but rather move asymptotically towards the equilibrium as the injected volume approaches infinity (Figure 20). For the industry this is too much volume of fluid or time so they settle often with 95 percent correct blend which equals three times purging of the mixing volume. If 99 percent correct blend is wanted the purging of the mixing volume will be five times the volume. To find these numbers we need to look at the step response of a first-order system like the one below:

$$Tx^{\bullet} + x = f(t) \qquad \textbf{Eq 29}$$

where T is the time constant, x is output value, $\dot{x}$ is the time rate of change of output value, and f(t) is the input, a step function. By solving the equation we end up with:

$$y(t) = k(1-e^{-t/T}) \qquad \textbf{Eq 30}$$

where y(t) is the gain or response, it tells us how far we are from the finale value, k is the finale value and in our case it will be the new concentration, t is the time and must be $t \geq 0$, and T is the time constant which will be in our case the time it takes to change the volume or the mass unit (see Figure 20).

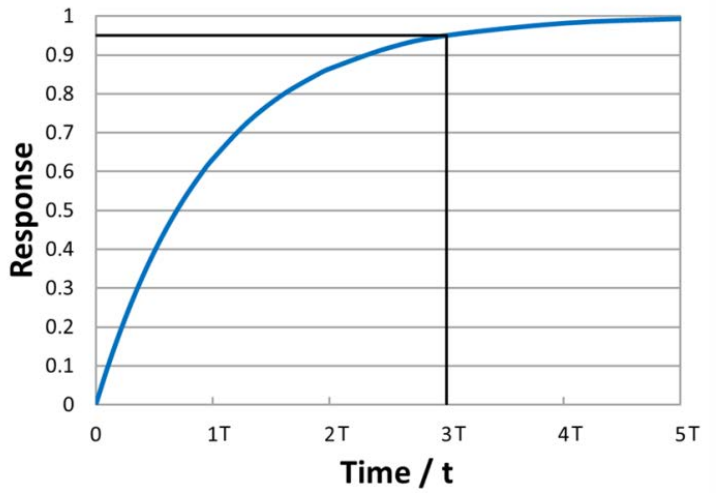

Figure 20 *A first-order system (Eq 30) where the response is plotted as a function of time (T). The finale value, k, is set to 1.*

The plot shows that after 3T, 0.95k or 95 percent of k, the finale value, is reached. By defining T as *the time it takes to change the CO_2 loop volume were 1T is one volume*, it will take three times the volume to get to 95 percent of the final concentration. The plot also tells that the finale value will be reached when time or volume goes toward infinity. The equation that could be used for calculating the theoretical water concentration will in the end be as Equation 30 below.

$$C_{H2O}(t) = C_{H2O,\,final}\cdot(1 - e^{-t/T}) \qquad \textbf{Eq 31}$$

Where T (time constant) is the time it takes to change the mass of CO_2 in the loop. By solving this equation it was found that it takes 80 hours to change three times the mass of the CO_2 in the loop (the total mass of CO_2 in the loop at 25°C is 1736 g and flow rate was 65 g/h). This corresponds with the observation of the result presented in Figure 14. Figure 21 shows a comparison of the theoretical and analysed data.

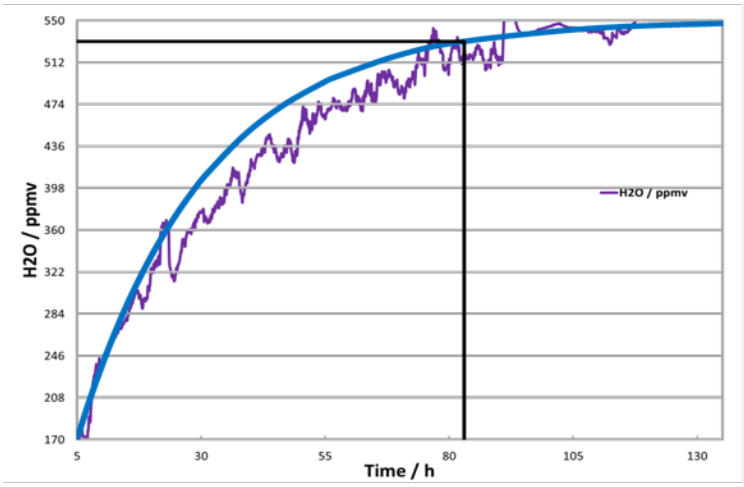

Figure 21 *Comparison of the calculated first-order system lag and of the measured water concentration in the solu blank experiment.*

Diluting equation

The calculated water concentration was added to the diagram to verify that both dosed and measured concentration followed a first order system, often call first-order lag. To simplify the calculation a dilution equation was used (Equation 32), since the volume or mass of the loop was constant, and the water concentration in the CO_2 to the loop was higher or lower than the concentration from the dosing unit. A dilution scenario is defined by the mass of the CO_2 in the loop, the water concentration in the loop, the water concentration in the CO_2 feed and the mass flow in and out of the loop:

$$C_{meas} \cdot m_{tot} = m_0 \cdot C_0 + m_1 \cdot C_1 \qquad \textbf{Eq 32}$$

Where C_{meas} is the measured concentration after dilution, m_{tot} is the total mass of CO_2 in the loop, m_0 is the mass of CO_2 in the loop subtracted from the mass coming in with concentration C_0, at that time, while m_1 is the incoming mass with the new concentration C_1. The incoming mass and the analyzed mass is the same, what goes out will be replaced by new mass since the main gas regulator is set to a fixed pressure of 95 bar at all time. The mass flow through the loop was fixed at 65 g/h, so the mass change was only depending on the time. So the smaller the mass change is the more accurate this equation will be and it fits very well with the first order differential equation.

To save time overdosing is necessary, and the concentration from the dosing unit was set to about 500 ppmv H_2O over the finale concentration (C_{final} + 500 ppmv). When the final concentration was reached the set point was changed to flatten the curve. This can be seen in Figure 34 (second part of diagram). So instead of running the first order to 95 percent steady state we ran it to about 50 percent and then changed the set point.

3.1.5 The lag time

The measurement lag (observed in Figure 19) is not so important for the measurements of corrosion rates in the experiments, but it is important for fitting of the theoretical water concentrations. The total lag time for a system is the sum of all delays in the system, like measurement delay, in-process delay, conditioning delay and transport delay. The lag time from the transport delay will be the volume of all pipes, valves, fittings, and the heated gas regulator combined with the flow rate in the different parts. The measurement delay for the TDLS would be the time it takes to get an ideal mixing in the sampling tube, since the TDLS measures continuously and the measuring response is very quick. The in-process delay could be poor mixing in the reaction chamber and dead legs in the process piping which should be treated as a mixing volume, three times the volume for good mixing [66]. The sample conditioning delay in the test set up could be caused by adsorption of water on tube walls and/or liquid-side delay in sample vaporization. Many of these delays have been removed by optimizing the design of the dosing unit and the analyzing module, but two remained; the transport delay of dense phase CO_2 to the heated gas regulator and the adsorption of water on the tube wall. The sampling line and sampling point have been designed to minimize dead legs and mixing volume. Transport delay can be determined by calculating the volume of the dense phase CO_2 on the high pressure side and the gaseous CO_2 on the low pressure side of the heated gas regulator and dividing it by the flow rates. The adsorption of water on the tubing walls is more difficult to calculate and therefore it is better to test it in pipes with known sizes. To reduce this lag time it would be best to use electro polished tubing or tubing with silica coating [66]. IFE used commercial grade stainless steel 1/16 – inch tubing (lower the volume) in order to keep the transport delay low Electro polished tubing in that size is hard to come by.

The transport delay is shown in Table 7. Comparing these values with the observed values in Figure 19 some deviation can be seen which can be explained by adsorption of water on the stainless steel wall.

Table 7 *Calculation of transport delay from water dosing unit to the analyzer.*

Tubing	**Inner dia (mm)**	**Length (mm)**	**Volume (ml)**	**phase**	**Density (g/ml)**	**Flowrate**	**Lag time (min)**
1/16-inch	0.8675	8450	5.0	Liquid	0.83	65 g/h	3.8
1/8-inch	1.755	720	1.74	Liquid	0.83	65 g/h	1.3
6 mm	4	430	5.40	Liquid	0.83	65 g/h	4.1
Gas regulator			15	Liquid	0.83	65 g/h	11.5
6 mm	4	600	7.54	Gas		500 ml/min	0.02
31 mm	25	1200	589	Gas		500 ml/min	1.2
						Sum	21.9

The largest contribution for the transport delay came from the dense phase side, and was about 22 minutes. This was lower than the observed delay in Figure 19, chapter 3.1.3, which was about 36 minutes. So the other types of delays contributed with 14 minutes delay, for which adsorption of water on the tubing wall probably was the largest. When the calculated lag time for dosing CO_2 to the loop was about 31 minutes, the observed value in the experiment Solu Blank was 100 minutes. This can probably be explained by large surface of the loop so the adsorption delay increases. If we only look at the delay from closing and opening the sampling line from the loop to the analyzer we are down to a calculated lag time of 16 minutes while the observed lag time is 20 minutes. This line has much lower exposed surface and therefore the adsorption delay is lower.

3.1.6 Experimental matrix – dissolved water

Six experiments where preformed in the High Pressure CO_2 Impurity Loop and they are listed in Table 8, together with the experimental parameters.

Table 8 *Overview of all the experiments preformed in the HPCIL.*

Experiment name	Pressure (Bar)	Temperature, Loop (°C)	Water conc. (ppmv)	Flow (m/s)	Run time (h)	Sample surface area (cm^2)
Solu Blank	95	25	150 – 2360*	1.0	362	N/A
Solu 02	95	25	570 – 2380*	0.4	422	1246
Solu 03	95	27 → 20**	2500	0.4	267	1258
Solu 04	95	27 → 12***	2500	0.4	189	1252
Solu 05	95	8 ↑↓ 14***	2500	0.4	551	1254
Solu 06	95	35	2500	0.4	334	232.8

* Ramping of concentration to five different water levels.

** Supposed to be ramping of temperature, but due to cooling failure only two different temperatures were tested.

*** Temperature ramping, constant water levels

Solu blank experiment

Experiment Solu Blank was performed without corrosion coupons in the test section to test the dosing and analyzing system and to confirm that measured and theoretical water concentration was comparable. The results where compared with Solu 02 to see if there is any deviation when carbon steel is exposed in the experiment.

The experiment Solu Blank was performed at 25°C, 95 bars of CO_2 and 1.0 m/s flow rate. The water concentration was first ramped up to the highest concentration achievable. It should be noted that there was no heating on the wetting chamber for the CO_2 in this experiment. The wetting chamber held a temperature about 17°C and this gives a lower solubility of water in CO_2 than the 20°C which the other experiments had. The dosing rate is changed during the experiments to reach new water levels in the CO_2, and in the end only dry CO_2 was added.

Solu 02 experiment

Experiment Solu 02 was performed under similar conditions as experiment Solu Blank (95 bars and 25°C) but with two carbon steel corrosion coupons present in the test section. The first sample was a carbon steel foil with a total area of 248 cm^2 (103.3 cm long and 1.2 cm wide, both sides were exposed). The second sample was shavings from a steel rod packed in a steel mesh cylinder with an estimated surface area of 998 cm^2. The total carbon steel surface area exposed in this experiment was 1246 cm^2. The same mesh cylinder sample was exposed in the experiments Solu 02 to 05. The reason for applying so large surface area was to pick up quicker

changes in the measured water concentration if corrosion occurs. The mesh cylinder gave a large pressure drop over the test section and only 0.4 m/s flow rate could be achieved.

When the material is corroding, one mole H_2O is consumed per one mole of iron. If the corrosion rate of carbon steel is 1 mm/year, the water consumption should be 56 ppmv per hour for this system with 1.883 liters of CO_2 and 1246 cm² of carbon steel (Equation 26). It was difficult to observe such small changes in water concentration. Therefore the flow loop was stopped for a known period of time to allow the carbon steel samples to corrode. During closed periods the dosing unit and analyzer were fed from the bypass line instead and the water concentration from the dosing unit was measured. After the experiment the carbon steel foil was taken out, put in a heated cabinet for preservation and thereafter being characterized with SEM, EDS.

Solu 03 experiment

This experiment was performed with a fixed high water concentration of 2500 ppmv. Saturation level at this condition is 3200 ppmv. A carbon steel foil with an area of 260 cm^2 (Length 103.3 cm and 1.26 cm wide, exposed on both sides) was placed in the test section together with the mesh cylinder, this gave an exposed carbon steel surface of 1258 cm^2. The flow rate was set to 0.4 m/s and the pressure was 95 bar. The experiment was started at a temperature 25°C which was later adjusted to 20°C. Due to a failure with the cooling system, the temperature couldn't be decreased further as planned. After 267 hours the experiment was stopped and the carbon steel sample was taken out and analyzed.

Solu 04 experiment

During this experiment the concentration of water was 2500 ppmv. A carbon steel foil with an area of 255 cm^2 (length, 103.5 cm and width, 1.23 cm, exposed on both sides) was placed in the test section together with the cylinder described before. This gave an exposed carbon steel surface area of 1252 cm^2. After the water concentration was adjusted to 2500 ppmv in the CO_2 loop, the temperature was lowered in several steps. This was done to bring the CO_2/water system in the loop closer to the solubility limit of water in CO_2 i.e. increase the relative humidity in the CO_2 in order to see if a significant drop in water measurement occurs. At a temperature of 25°C the solubility of water is 3200 ppmv. In the presented experiment 2500 ppmv of water is dosed to the system. This means that a relative humidity (relative to the solubility limit) equals 78.1 percent. If the temperature is decreased to 15°C the relative humidity is close to 100 percent (Figure 5) and further decreases will lead to an oversaturation of water which can cause formation of a free water phase. If corrosion, adsorption or hydrates formation takes place while the temperature decreases, changes in water concentration should be observed. The experiment was ended after 189 hours and six different temperature steps. The sample was preserved in a heating cabinet for analyzing.

Solu 05 experiment

Experiment Solu 05 was performed at low temperature, between 8 and 14 °C and the pressure was 95 bar. The dosing concentration of water was set to 2500 ppmv. A carbon steel foil with an area of 256.2 cm^2 (length 103.3 cm and width 1.24 cm, exposed on both sides) was placed in the test section together with the mesh cylinder, which gave a total exposed carbon steel surface area of 1254 cm^2. The temperature was 10°C from the start and was ramped up and down around this temperature. The motivation for this was to see whether the corrosion rate increases suddenly when the solubility limit for water in CO_2 is exceeded as well as if the water concentration decreases when the temperature is below the hydrate point i.e. 9°C at 95 bars. The relative humidity is over 100 percent throughout the entire experiment so water should precipitate inside the CO_2 loop. By increasing the temperature, and thereby increasing the water solubility it is expected an increase in the measured water concentration due to dry up of previously precipitated water. Therefore the temperature was increased to 25°C. In the end of the experiment only dry CO_2 was dosed to the CO_2 loop to enhance the dry up rate. This dry up period can be compared with the same situation in Solu Blank and the calculated dilution rate of the water concentration. The experiment was ended after 551 hours and nine temperature levels. The sample was preserved in a heating cabinet for analyzing.

Solu 06 experiment

The aim of the experiment Solu 06 was to see if higher temperature would affect the corrosion rate and the water measurements. The temperature was set to 35°C and the water level to about 2500 ppmv. The pressure was 95 bar and the flow rate 0.4 m/s. A carbon steel foil with an area of 232.8 cm^2 (length 95.4 cm and width 1.22 cm, exposed on both sides) was placed in the test section. Mesh cylinder was not present this time. At this pressure and temperature CO_2 is in its supercritical state. The experiment was stopped after 334 hours and the sample was preserved in a heating cabinet before it was analyzed.

3.1.7 Corrosion coupons, preparation and analysis

The corrosion coupons used in the experiments in the high pressure impurity CO_2 loop was carbon steel foils cut to fit inside the test section. The steel was S355J2 (equivalent to St52-3N), a type of mild steel. The chemical composition is shown in Table 9.

Table 9 *The chemical composition (wt. %) of the carbon steel grade S355J2.*

	C	Mn	Si	P	S	Cu	Fe
S355J2	≤0.2	≤1.6	≤0.55	≤0.030	≤0.030	≤0.55	Balance

Sample preparation

The foil samples were cut to about 100 cm x 1.2 cm, the thickness was 0.20 mm. A reference sample was made and prepared.

The samples were first washed in acetone and then in isopropanol, wiped with a lint free tissue and ground by hand with a 600 grit abrasive paper (Carbimet, P600, SiC from Buehler). Finally the samples were washed again in acetone and isopropanol and dried in a heating chamber at about 50°C. The actual length and width was measured with a slide caliper (Vernier) and the samples were weighted using an analytical grade scale (Precisa, XT620M, d = 0.001g, Precisa Instruments Ltd.).

Sample mounting

Since the mesh cylinder occupied some of the test section, the carbon steel foil had to be folded. The folded sample was mounted on a holder made of polyether ether ketone (PEEK) and placed inside the test section, as shown in Figure 22.

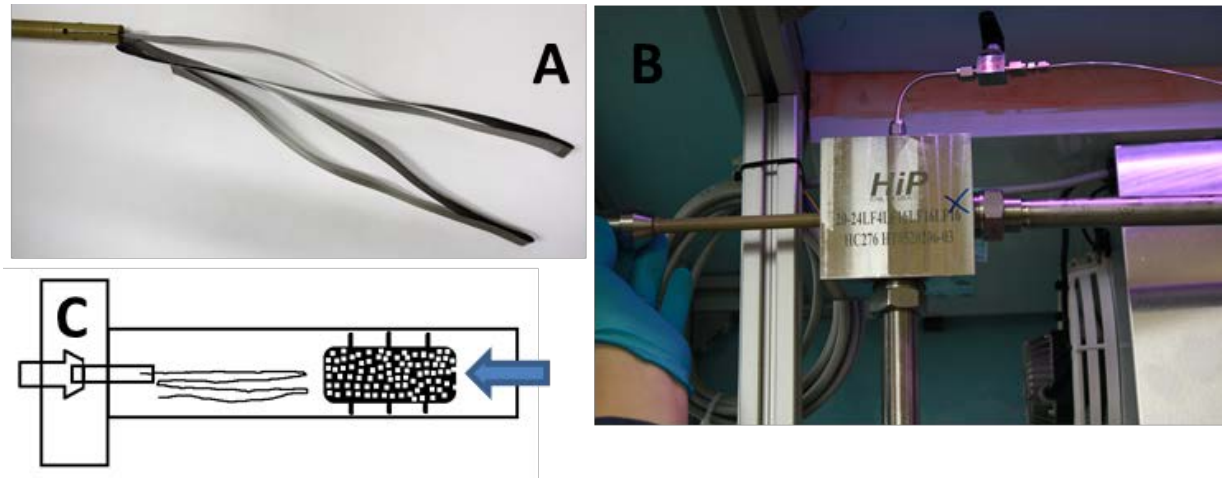

Figure 22 *The sample, a carbon steel foil, was mounted on a peek holder (A). The sample is folded so we can place it inside the test section (B). After the sample and the mesh cylinder was mounted inside the test section (C) we opened the valves to the loop and CO_2 (blue arrow in picture C) could circulate through the mesh cylinder and over the folded sample.*

This setup was used for experiments Solu 02 to 05. In the last experiment, Solu 06 only the carbon steel foil had been used and folding was therefore not necessary.

Stripping and weight loss

After the experiments the carbon steel foil was weighted and photographed. Then the sample was cut in smaller pieces used for SEM analyzes and chemical removal (stripping) of the corrosion product film that covered the steel surface. An average film thickness was calculated from the weight loss data. The scale used for this was Mettler Toledo, NewClassic, MS204S.

The stripping liquid was an inert (for the metal) solution made of 1 l 36% hydrochloric acid, 50 grams of tin(II)chloride ($SnCl_2$) and 30 grams of antimony trichloride ($SbCl_3$), commonly known as Clark's solution. The sample was placed in the stripping solution for one minute, scrubbed with a soft plastic brush under flowing water and the procedure was repeated one more time. At the end, the sample was cleaned with distilled water and isopropanol, dried and weighted. The difference between as-exposed and stripped sample is the weight of the products (corrosion film) on the carbon steel surface. As the area of the sample is known, the average film weight can be calculated. Assuming that iron carbonate is the only possible corrosion product with density 3.8 g/cm^3 the average film thickness could be estimated. Five reference samples were given the same treatment so the metal loss caused by the stripping could be subtracted. The weight loss was found to be 0.04 percent of the total weight of the reference sample. To verify if there was a significant difference between the film weights in the experiment, a statistical analysis was performed. The analysis used was one-way ANOVA, Tukey pairwise comparison with the program Mini Tab. Knowing the weight of the foil sample before and after the experiment, and the film weight it is then possible to calculate the total mass loss of the sample by using Equation 33.

$$m_{ML} = m_{MAE} - m_{MBE} - m_{FW} \qquad \textbf{Eq 33}$$

where m_{ML} is the total mass loss, m_{MAE} is the mass of the sample after the experiment, m_{MBE} is the mass of the sample before the experiment, and m_{FW} is the total film weight . Corrosion rate (CR) in mm/y can be calculated by Equation 8.

$$CR = \frac{m_{ML}}{\rho \cdot A \cdot t} \cdot 10 \qquad \textbf{Eq 34}$$

Where m_{ML} is the total mass loss (g), ρ is the density of iron (7.86 g/cm^2), A is the area of the sample (cm^2), t is the duration of the experiment (years) and the factor 10 is for conversion from cm to mm.

Sample characterization

The as-exposed samples were characterized by photos and SEM. The stripped samples were characterized by photos, optical microscopy and 3D profiling (Axioskop 2 MAT equipped with an Alicona ALC13 camera). The 3D data was processed using Mountains Professional 3D software v/7.1.7204 from Digital Surf.

SEM is used for taking picture of the morphology and topography of a sample. It is also possible to look at crystallography, like orientation of grains. In addition the SEM be used for determination of the composition of the sample. The sample is scanned with a focused beam of electrons, which will either be reflected or enters the surface to emit other electrons. The electrons are picked up by detectors and the main part of these is called secondary electrons

(SE) and back scattered electrons (BSE), and they may be utilized to form a picture of the sample which is examined. The SE do not penetrate deep into the sample and are mostly used for surface information and topography, while BSE have much higher energy and can be used for topography, crystallography and identifying elements together with the X-ray's which are also emitted. The electron microscope used in this project was a Hitachi S4800 field emission SEM. The sample was mounted on an aluminum sample holder (Figure 23) and inserted into the SEM through a lock-chamber.

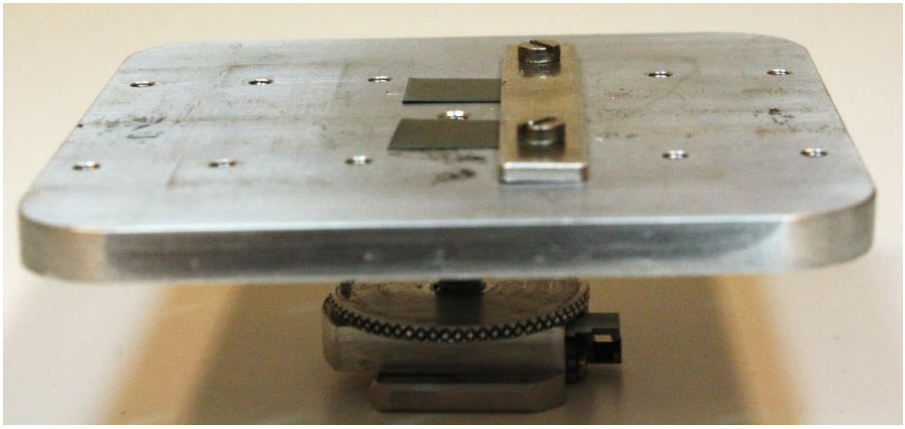

Figure 23 *The aluminum sample holder for the SEM. Two samples mounted on the holder ready for analysis.*

Pictures with magnification of 1000x and 10000x were taken at places which were considered representative for each investigated sample. Moreover, Electron Dispersive X-ray Spectroscopy (EDS) was performed on places representative for the respective samples. EDS is a chemical characterization method where the elements in the sample are identified by analyzing the X-ray emission spectrum. The relaxation of the inner shell electrons in an excited atom sends out a photon and the X-ray energy is the difference of the energy levels in which the relaxation occurs. We can calculate the energy difference for iron and predict were the peaks will occur in the EDS spectra by using the energy levels of the different shells see Equation 35.

$$E_{photon} = E_1 - E_2 \qquad \textbf{Eq 35}$$

We start with calculating K_α for iron, which will be the energy difference from L-shell to K-shell.

$Fe_{L\rightarrow K}$: $E_{K\alpha} = E_K - E_L = 7.112\ KeV - 0.708\ keV = 6.404\ KeV$

And the K_β from M-shell to K-shell will look like this.

$Fe_{M\rightarrow K}$: $E_{K\beta} = E_K - E_M = 7.112\ KeV - 0.054\ KeV = 7.058\ KeV$

The L_α from M-shell to L-shell for iron would be like this.

$Fe_{M \rightarrow L}$: $E_{L\alpha} = E_L - E_M = 0.708\ KeV - 0.003\ KeV = 0.705\ KeV$

At the energy calculated above, peaks characteristic for iron should appear in EDS analysis. It should be noted that there are different energy levels within the different shell and we have to pick the right level to calculate the energy of the relaxation ([67] energy values). More details can be found in reference.

The calculated values can be compared with the values found in an EDS spectrum (Figure 24) of the carbon steel foil. Three distinguished peaks can be seen at 0.7 KeV (L_α), 6.4 KeV (K_α), and 7.0 KeV (K_β), corresponding well with values presented above.

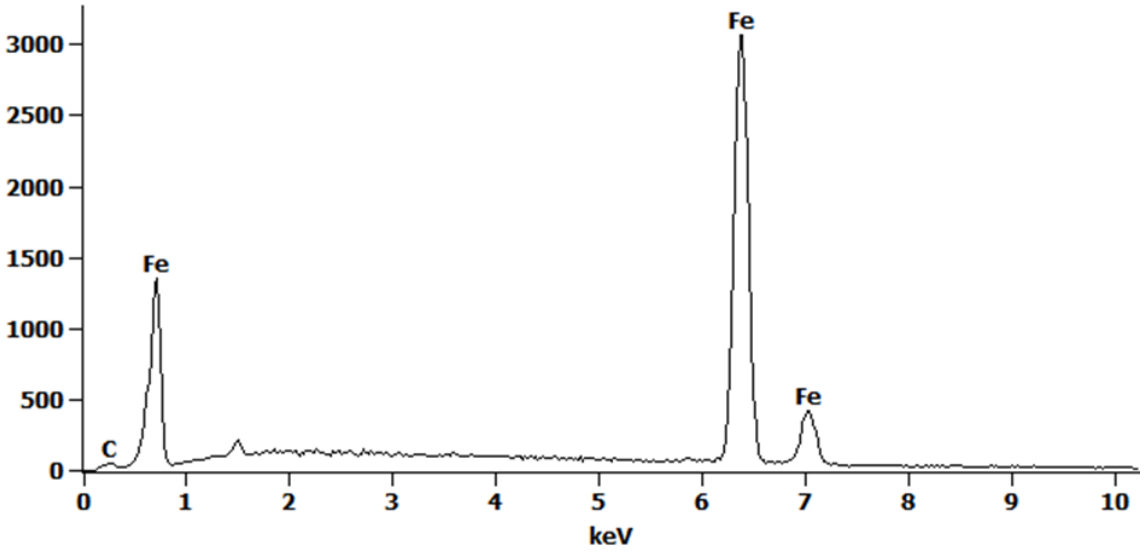

Figure 24 *EDS analysis of an unexposed carbon steel sample at 15 KeV.*

An EDS analysis gives us the elements of the products on the surface, but it was hard to get an accurate ratio between the elements for conclusion on what the product is since the products layer are too thin or porous. The three elements we suspected to be present was iron, carbon, and oxygen. Iron is the main elements in the sample and expected to be found in all analysis. Carbon can be a challenge in EDS analysis, it is very close to the limit of what element can be detected and it can be present in the SEM as a contamination. Typical carbon sources could be the vacuum oil, fingerprints on sample holder, leftover carbon from sample coating, isopropyl alcohol or acetone from sample preparation, and so on. The tendency for the electron beam to attract the carbon is shown in Figure 25.

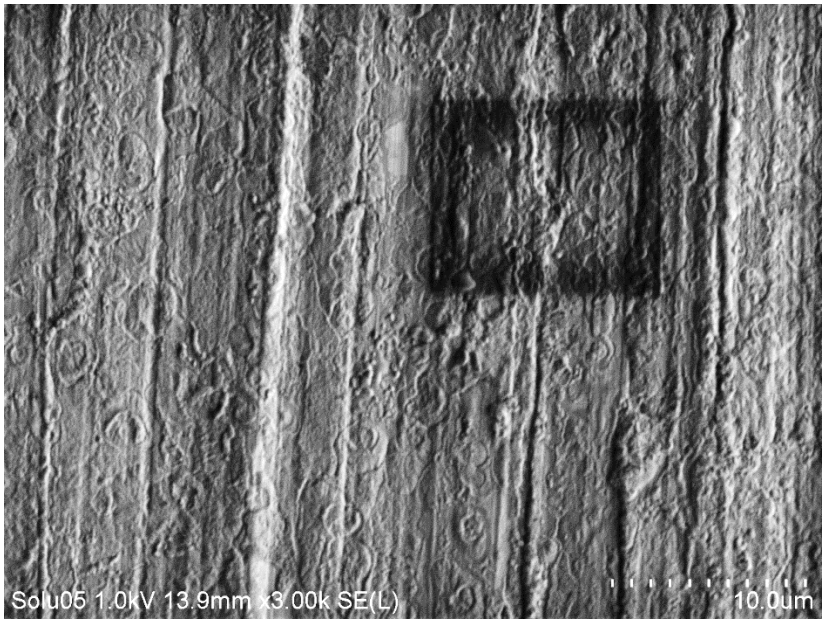

Figure 25 *SEM picture shows carbon deposit on Solu 05 after an EDS analysis.*

The attracting is clearer at lower accelerating voltage since the analyzing time is longer and this will influence the result given by the EDS. Therefor it would be a tradeoff when analyzing a thin layer on top of an iron sample, either use high accelerating voltage so the analyzing time is shorter but then the possibility to shot the electron beam through the layer and into the sample underneath. Or use lower voltage and accept the carbon accumulating around the beam. The best result is somewhere in-between, and always sees the result with some criticism. It is also normal to find aluminum from the sample holder and the EDS detector is a bulk silicon semiconductor crystal which sometimes can give a peak in the analysis spectrum.

An Axioskop 2 MAT was used with an Alicona ALC13 camera for an optical inspection and some profiles were also analyzed for localized attacks (pitting). This is a nice way to measure the depth of the pits, and with user friendly software the profile was analyzed in a good manner. The grinding strips on the reference sample were very clear and could be used as a verification of this method.

Using Monte-Carlo simulation to estimate film thickness

Monte-Carlo simulations were used to simulate the surface film thickness. The program CASINO is based on (CASINO derives from the words “monte CArlo SImulation of electroN trajectory in sOlids”). The program was made by the research team of Raynald Gauvin, professor at Université de Sherbrooke, Québec, Canada [68]. The program can simulate a large amount of electron trajectories in a solid and intend to represent the actual interaction conditions in SEM.

Iron carbonate was used as the substrate, and penetration depth at different acceleration voltages was studied. When the iron carbonate atomic ratio; FeCO3, 1:1:3 is moved towards an increasing level of iron in the EDS analysis, we can assume that the accelerating voltage is so high that it goes through the iron carbonate layer and into the carbon steel matrix underneath. Figure 26 below shows a simulation of electron trajectories in iron carbonate.

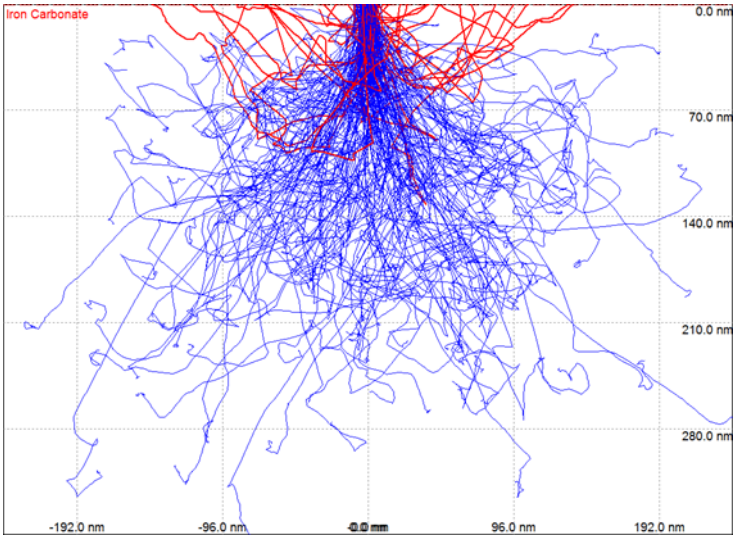

Figure 26 *The blue lines show penetration depth of the electron trajectories and the red lines shows the penetration depth in the sample of electron trajectories that will escape the sample surface, back scattered electrons. The vertical scale shows the depth of the electrons trajectories in nm and the horizontal scale is the width in nm of the electrons trajectories. The simulation was performed on iron carbonate with 5 keV accelerating voltage.*

3.1.8 Calibration

The instruments and analyzers were calibrated before use. For pressure and temperature a Druck calibrator called unomat model TRX-II was used. The temperature sensor was placed in Jofra temperature calibrator, model 202S, and different temperatures was tested together with a reference temperature sensor connected to the TRX-II. The pressure sensor was mounted on a pneumatic / hydraulic hand pump, Druck PV411, and a pressure transmitter (PDCR 960-2036) connected to the TRX-II measured the reference pressure. Different pressures were tested here as well. As for the Mini-Cori flow controller in the dosing unit and the coriolis meter in the loop, the calibration certificates applied, but a zero calibration was performed in addition.

The Yokogawas TDLS200 was calibrated with a chilled mirror, Michell S8000, and a moisture generator (MG-101). The moisture generator can produce different levels of water dissolved in nitrogen and this wetted nitrogen is purged through both the TDLS200 and the chilled mirror. The chilled mirror is a highly accurate dew meter which does exactly what it is called, namely chills a mirror and detects when moisture occur on the mirror. Then it measures the

temperature and gives the dew point of the wet gas. This dew point can be converted to ppmv and compared with the values from the TDLS200. The S8000 has an accuracy of 0.1°C of the measured dew point.

3.2 Dense phase loop with instruments

3.2.1 Dense phase loop

The corrosion experiments with the free water phase saturated with CO_2 was carried out in a special made flow loop made of Hastelloy C276 (Figure 27). The loop was designed for a pressure up to 200 bars and a temperature range from 0°C to 100°C. The loop volume was 0.3 liters plus a reservoir volume of 6.0 liters, totally 6.3 liters. The temperature, pressure, and flow were logged in all experiments.

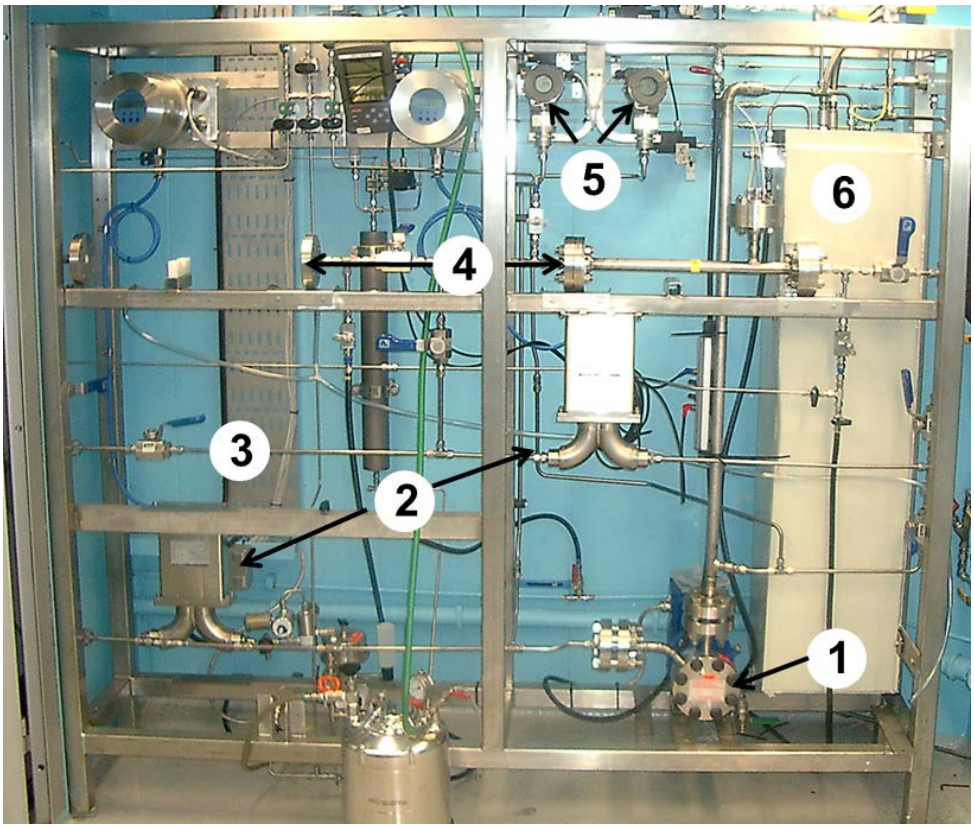

Figure 27 *The figure shows the Dense phase loop, the circulation pump (1) circulate the liquid from the reservoir tank (6) through the Rheonik coriolis massflow meter (2) which measure and controls the flow. Then the liquid can go either over the bypass (3) or into the test sections (4). The liquid returns to the reservoir tank after it passed the test sections. The pressure is measure by Smar pressure transmitter (5).*

Operational procedure

The loop was flushed with CO_2 before each experiment to remove any traces of oxygen from the loop. The loop was then filled with 4.5 liter of the deoxygenated test solutions (osmotic water containing 1 wt.% of sodium chloride). CO_2 from a bottle was used to pressurize the loop. The CO_2 was analytical grad (quality 5.0). A booster pump was used to obtain higher pressures. The test section was closed while the experimental parameters stabilizes in the loop (bypass is

opened so there is circulation). Final oxygen could be removed by bobbling CO_2 through the liquid inside the loop. When the experiment was ready to start the sample was inserted in the test section, the test section was mounted in the loop and flushed through with CO_2. Then the test section was opened and the bypass closed. All the liquid with dissolved CO_2 is circulated over the test section. The reservoir was submerged in a thermostatic bath and it was controlled together with the flow by a control system from ABB system.

3.2.2 The test section and sample holder

The test sections (Figure 28) were made of Hastelloy pipes with Hastelloy C flanges welded at the ends. The test sections were electrically isolated from the rest of the loop by polyether ether ketone (PEEK) spacers mounted between the test section flanges and the loop flanges. The sample holder was also made of PEEK. Two samples (corrosion coupons) can be mounted in the PEEK holder. One sample was used as a working electrode and the other was used as a pseudo reference electrode in the electrochemical measurements. The samples were connected to a Gamry potentiostat via a wire to each sample. The connection points should preferably be dry to avoid galvanic effects. During the project wet connection points were detected so the sample holder was modified twice to reduce this problem.

Sample holder v 1

Figure 28 shows the test section with the sample holder. In the first version of the sample holder the metal casing of the test section served as a counter electrode. The test section is a pipe with welded flanges so that it can be easily mounted into the loop. The sample holder goes inside the test section and the samples are not in electrical contact with the test section. On the sides of the sample holder a position milling is made on the end piece to be sure that the samples are located in the middle of the pipe. The end piece is also perforated to allow the liquid to flow freely.

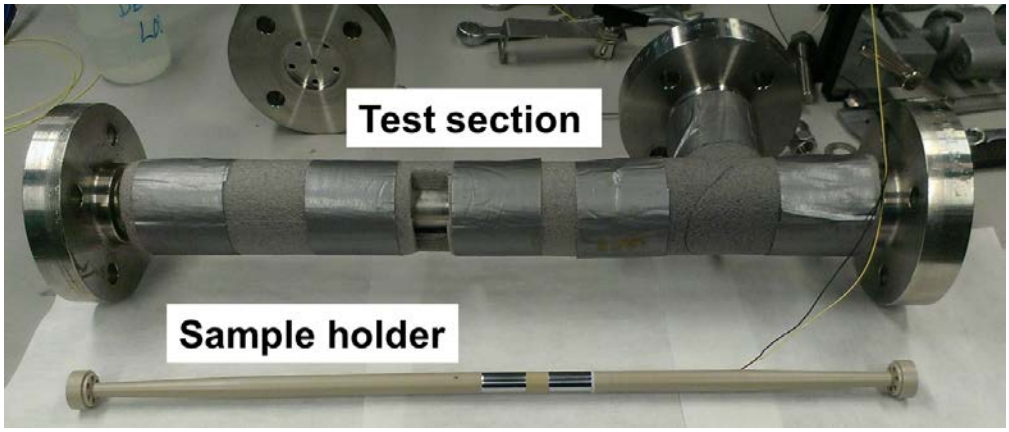

Figure 28 *Test section and sample holder.*

The samples have an outer diameter of 12 mm and the diameter of the PEEK rod decreases gradually from 12 mm in the middle to 8 mm at the ends. This is done to ensure laminar flow over the samples. The wires go inside the PEEK rod and are connected to the sample from underneath. The wire is pinched between the sample and the PEEK rod when sliding the sample on the holder. The wire in all experiments was a single core wire with Teflon as an isolator and copper with silver plating on as the conductive material. A Teflon disk is placed between the sample and the rod to ensure that no liquid goes between the rod and the sample in order to keep the connection points dry. The sample holder has to be divided in two when putting that in the test section since the end parts are larger than the inner diameter (15.6 cm) of the test section. The sample holder is inserted in two parts from each side of the test section and then screwed together.

Sample holder v 2

As the connection point between sample and wire became wetted dry in the first experiments, and in addition a larger connection area was required, a new version of the center piece of the sample holder was made. This time O-rings were used in between the sample and the PEEK rod to prevent liquid to enter the connection area. The wire in the connection area was made as a spiral in order to increase the contact area between the connecting wire and the sample. This should assure that the electric contact was not lost during the experiment. Other practical changes were also made to make assembling of the sample holder and removal of the samples after the experiment easier. Figure 29 shows the new sample holder. The mounting of the sample holder inside the test section was the same as before.

Figure 29 *The second version of the sample holder with O-rings as sealing and large connection area under the sample.*

Sample holder v 3

Since the results of the electrochemical measurements were still not satisfactory, the third sample holder design was tested. The sample holder had good contact and the connection points were dry. Instead of using the test section as counter electrode a PEEK cylinder with platinum wire on the inside wall was machined (Figure 30). This cylinder will now be the outside walls of the sample holder. The platinum wire insulated with Teflon tubing to ensuring no electrical contact with the loop. Figure 31 shows the sample holder and the test section ready to be mounted in the loop.

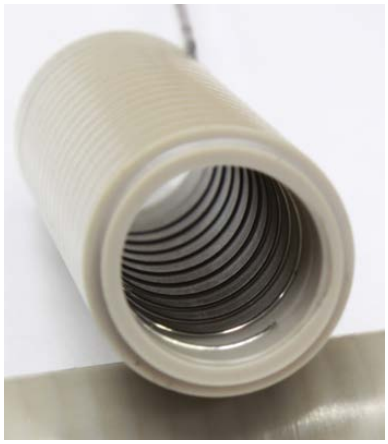

Figure 30 *The counter electrode as a platinum wire placed inside the PEEK cylinder.*

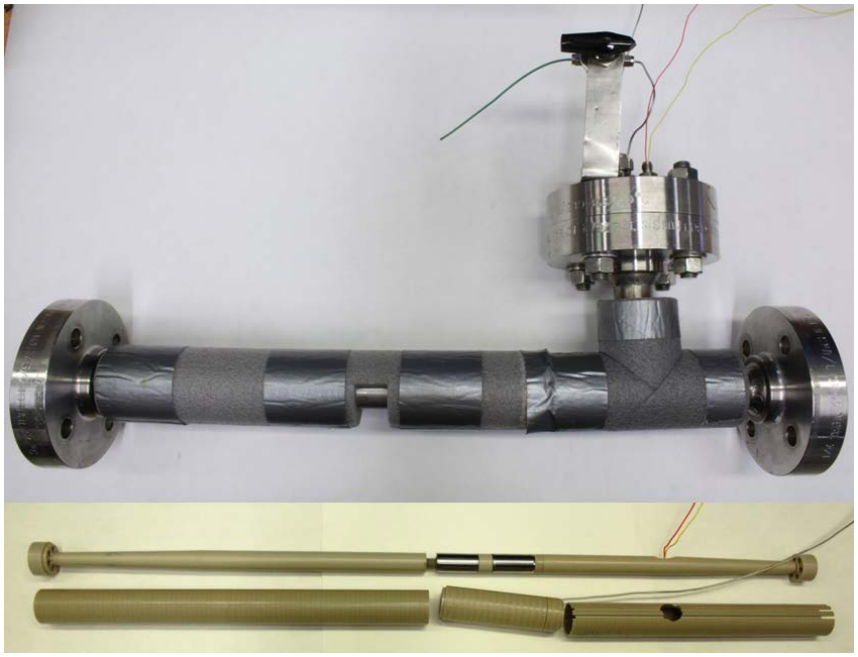

Figure 31 *The lower picture shows the sample holder before it is mounted inside the PEEK cylinder. The center piece of the PEEK cylinder includes the counter electrode.The upper picture shows the test section ready for mounting in the loop. Wires for the connection with sample, reference and the counter electrode is isolated from the test section. A valve with 1/16-inch tubing is mounted as the liquid sampling outlet.*

Geo 3, sample holder v 1, glass cell experiment

The glass cell experiment was a test of the sample holder and measurements. Therefore the samples were taken in and out during the experiment. They were also put in hydro chloric acid to trigger the corrosion rate and for that reason no weight loss are given for those samples. Figure 32 shows the schematics of the glass cell experiment. The electrochemical measurements in the loop was not as expected, to verify these measurement and compared them with the literature a glass cell test was necessary.

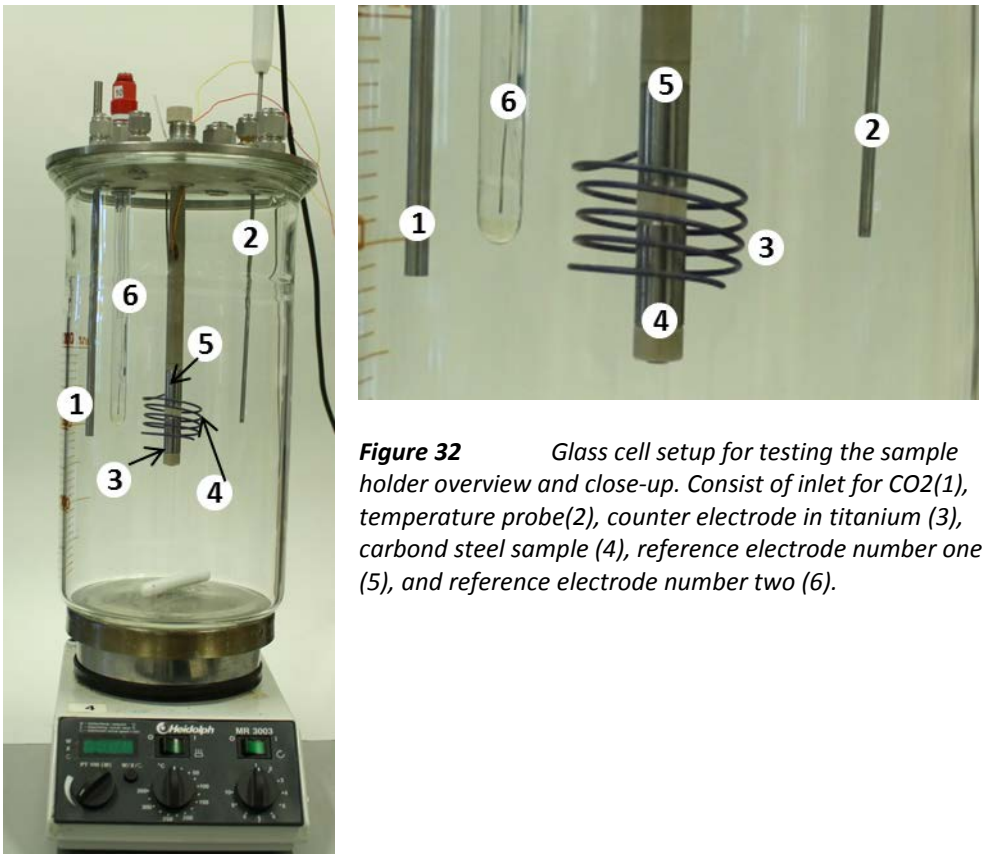

Figure 32 *Glass cell setup for testing the sample holder overview and close-up. Consist of inlet for CO2(1), temperature probe(2), counter electrode in titanium (3), carbond steel sample (4), reference electrode number one (5), and reference electrode number two (6).*

The glass cell was filled with the experimental liquid and bobbled with CO_2 for 4 hours before the sample was introduced. Continuous LPR measurements were performed and liquid samples were taken regularly for iron analysis.

3.2.3 Corrosion rate measurements

Two methods were used to determine the corrosion rates of the carbon steel: one was based on iron measurements in the liquid and the other was based on linear polarization resistance (LPR).

Iron measurement

As the carbon steel corrodes, iron ions (Fe^{2+}) are released to the liquid. The increase of iron ions during an experiment can be used to calculate the corrosion rate if the liquid volume of the system and surface area of the samples are known. Liquid was sampled regularly during the experiments and analyzed for Fe^{2+} using a photo spectrometer: The sample liquid was mixed with a developer solution which makes an orange color complex with Fe^{2+}. Then the

absorbance is measured at 508 nm by a photo spectrometer (Helios Delta UV). The amount of Fe^{2+} ions in the liquid could be determined based on a calibration curve. This is also referred as the iron count.

The developer solution is made of 2.2 g of 1,10-phenanthroline monohydrate, 6 g acetic acid, 4.0 g hydroxylamine hydrochloride and 8.2 g of sodium acetate dissolved in 2 liters of distilled water. It is the compound Fe(II)-phenanthroline complex (see Figure 33) which gives the orange color. The concentration, c, can be found according to the Beer-Lambert's law:

$$A = \varepsilon bc \qquad \textbf{Eq 36}$$

where A is the absorbance measured at 508 nm, ε is the molar absorptivity (L mol^{-1} cm^{-1}), b is the path length of the sample (cm), and c is the concentration of the sample (mol L^{-1}).

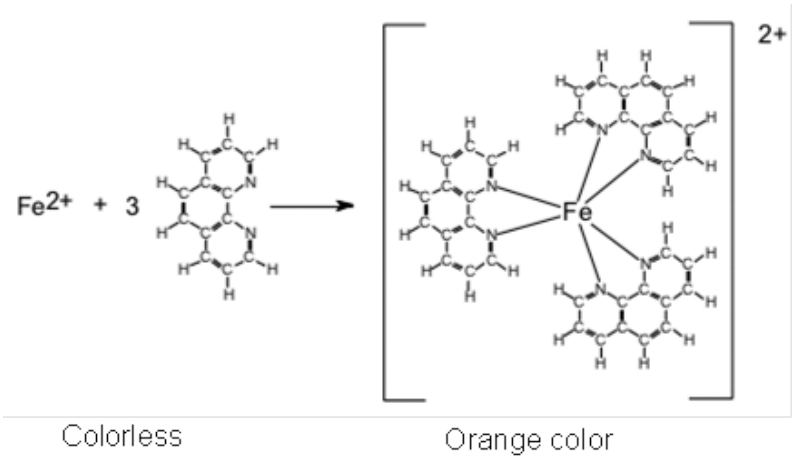

Figure 33 *Iron ions reacting with phenanthroline to create Fe(II)-phenanthroline complex.*

The calibration curve was made of two points, 0 ppmv and 300 ppmv Fe^{2+} -standard. To make the 300 ppmv Fe^{2+} -standard, 1.0533 g ammonium iron(II) sulfate hexahydrate and 10 ml of acetic acid is dissolved in 0.5 liters of distilled water. 20 ml of this solution is added to 1000 ml of the developer solution. Several tests have been done and the linearity of the calibration curve is undisputed.

During measurements of the iron concentration the known amount of developer is first placed in a beaker, then a liquid sample is taken out from the ongoing experiment and immediately added to the beaker and weighed (total weight minus developer weight). As the sample is diluted when it is added to the developer, the value we get from the UV-spectrometer has to be adjusted:

$$C_{sample} \cdot m_{sample} = C_{abs} \cdot m_{total} \qquad \textbf{Eq 37}$$

where C_{sample} is the concentration of iron in the solution from the experiment, m_{sample} is the weight of the sample added to the developer, C_{abs} is the measured concentration by the spectrometer and m_{total} is the mass of the sample and the developer. Since the calibration curve is made from 20 ml of 300 ppmv Fe^{2+} standard added to 1000 ml of developer, the equation had to be adjusted:

$$C_{sample} = \frac{C_{abs} \cdot m_{total} \cdot 20}{m_{sample} \cdot 1020} \qquad \textbf{Eq 38}$$

The calculated concentration is given in ppmv. In order to use this number to calculate the corrosion rate, we have to keep track of the mass of the liquid inside the loop at all time. By weighing the liquid at the beginning and weighing all samples taken out we can follow the mass of the liquid. The following equation is need for calculating the corrosion:

$$CR = \frac{m_{loop} \cdot C_{ppmv}}{\rho_{1\%\ NaCl} \cdot 1000000 \cdot A \cdot \rho_{Fe} \cdot 0.1 \cdot t} \qquad \textbf{Eq 39}$$

where CR is corrosion rate in mm/y, m_{loop} is the mass of the liquid present in the loop at the time iron is measured, in gram, C_{ppmv} is the measured Fe^{2+} concentration, $\rho_{1\%\ NaCl}$ is the density of the liquid in the loop in g/cm^3, A is the area of the carbon steel samples in cm^2, ρ_{Fe} is the density of iron, 7.86 g/cm^3, t is the time when the iron is measured in years. If liquid samples are taken often enough very accurate values of the corrosion rates can be calculated until the precipitation of iron carbonate ($FeCO_3$) starts.

Linear polarization resistance and the Stern-Geary constant

Electrochemical measurements could be performed on both samples in the test section. Linear polarization resistance (LPR) measurements were carried out using a regular 3-electrode electrochemical setup. The carbon steel samples (cylindrical samples, ~25 mm long and 12 mm outer diameter) were used as working electrodes and as pseudo reference electrodes for each other. The test section walls were used as counter electrode (see description of modifications in chapter 3.2.2). The instrument used for the LPR measurements was a Gamry PC3/750 potentiostat with ECM8 multiplexer. LPR measurements were carried out with a 0.05 mV/s potentiodynamic scan rate in the range –5 to +5 mV vs. the open circuit potential.

3.2.4 The experimental matrix

One of the objectives was to determine the corrosion rates at different CO_2 pressure and determine the Stern-Geary constant. Four different loop experiments and one glass cell

experiment were performed. The table below (Table 10) shows the parameters for different experiments.

Table 10 *The experimental parameters for experiments performed in water saturated with CO_2.*

Experiment name	Pressure Bar	Temperature °C	Flow m/s	Duration h	Counter electrode	Sample-holder
Geo 01	100	25	0.65	120	Hastelloy	1.version
Geo 02	1 to 30	25	0.65	213	Hastelloy	1.version
Geo 03	1	25	--	360	Titanium	1.version
Geo 04	1 to 20	25	0.65	90	Hastelloy	2.version
Geo 05	1 to 40	25	0.65	192	Platinum	3.version

All experiments were performed with osmotic water with 1 wt% NaCl.

Calculation of pH and CO_2 solubility

The pH depends on how much CO_2 can be solved in the aqueous phase and the solubility of CO_2 depends on pressure, temperature, and composition of the aqueous phase. The chemical equilibrium calculations of CO_2 dissolved in water with 1 wt % of NaCl were carried out with the MultiScale software (version 8.1 with MEGScale plugin), a computer program used for prediction of mineral deposition in oil and gas operation. The Norwegian University of Science and Technology (NTNU) has developed the present version in a project supported by Statoil and Norsk Hydro. MultiScale is commercially available from the company Expro [69]. The electrolyte model in MultiScale is a "Pitzer model" for dissolved species in addition to a complete PVT model. The model has been specially developed to handle hydrocarbon, CO_2 and H_2S distribution between gas-, oil- and aqueous phases. Complete chemical equilibrium was assumed for all calculations.

3.2.5 Sample handling and characterization

The sample material used in the experiments in the dense phase loop was carbon steel, X-65, cut from the 30" Ormen Lange pipeline. The chemical composition is shown in Table 11.

Table 11 *The chemical composition of the carbon steel grade X-65, iron is the balance, and the maximum allowed weight % within this grade is given in the table.*

	C (wt%)	Mn (wt%)	Si (wt%)	P (wt%)	S (wt%)	Cr (wt%)	Cu (wt%)
X-65	≤ 0.16	≤ 1.6	≤ 0.5	≤ 0.015	≤ 0.005	≤ 0.5	≤ 0.20

There are also other elements which are not listed here.

Sample preparation

The samples were cut and machined to be about 2.5 cm long, the outer diameter was 1.2 cm, and the inner diameter 0.7 cm. The samples were first washed in acetone in an ultrasonic bath and then flushed with isopropanol (Carbimet, P1000, SiC from Buehler). After grinding the samples were washed in acetone and ultrasonic bath again and then flushed with isopropanol before they were dried in a heating chamber. Before use the length and diameter was measured with a slide caliper (vernier) and in the end the samples was weighted (Mettler Toledo, NewClassic, MS204S, d = 0.1 mg).

Sample mounting

The samples were mounted on the sample holder (see Figure 28). After the sample holder was mounted inside the test section the contact between the wire and the sample was checked and made sure that there was no contact between the two samples or the wall of the test section. The test section was mounted in the loop and flushed with CO_2 before the valves were opened and the experimental fluid entered the test section.

Sample post treatment

After the experiment the sample was taken out from the holder. At this stage some of the film fell off as it did not adhere well to the carbon steel surface. The sample was carefully put in isopropanol before they were dried in a heating cabinet. The samples were weighted after they were dry. SEM analysis was performed before the corrosion products on the sample was stripped off as described in chapter 3.1.7.

4. Results

The results will be presented in two main chapters, first the results obtained in experiments with water dissolved in CO_2 are presented and in the second half the results from experiment with CO_2 dissolved in water be presented.

4.1 HPCIL with water content below saturation

The results obtained by experiments in water dissolved in dense phase CO_2 are summarized in Table 12.

Table 12 *Weight loss and corrosion rates for sample used in experiments preformed with water dissolved in CO_2.*

Experiment	Width	Length	Area	Weight before	Weight after	Weight loss*	Corrosion rate
name	**cm**	**cm**	**cm2**	**g**	**g**	**mg**	**μm/y****
Solu 02	1.20	103.30	247.9	20.052	20.051	7.2	0. 8
Solu 03	1.26	103.30	260.3	20.284	20.287	N/A	N/A
Solu 04	1.23	103.50	254.6	20.435	20.434	5.8	1.4
Solu 05	1.24	103.30	256.2	20.233	20.230	12.2	1.0
Solu 06	1.22	95.40	232.8	18.459	18.463	N/A	N/A

* Weight loss is calculated by using the film weight per area in tables above combined with weight before and after experiment.

** Corrosion rate in mm/year is calculated by Equation 34, also using the exposure time in Table 19.

4.1.1 Experiment Solu Blank (Test run)

To verify that water can be dosed in to the loop in a controlled manner, a baseline experiment without corrosion coupons were carried out with stepwise increasing water content up to the solubility limit of water in CO_2.

The test was performed at 25 °C, 95 bar, and with a flow of 1 m/s. Wet CO_2 from the moisturizer was mixed with dry CO_2 in different ratios to obtain different water concentration in the dense phase CO_2. A comparison between injected and analyzed water content is presented in Figure 34. At the beginning, the dosing level of water was set to be 530 ppmv, and after 120h the measured water level (purple line) reached the set point. The set point was increased stepwise, keeping inter-step intervals sufficiently long to allow the measured water concentration to stabilize.

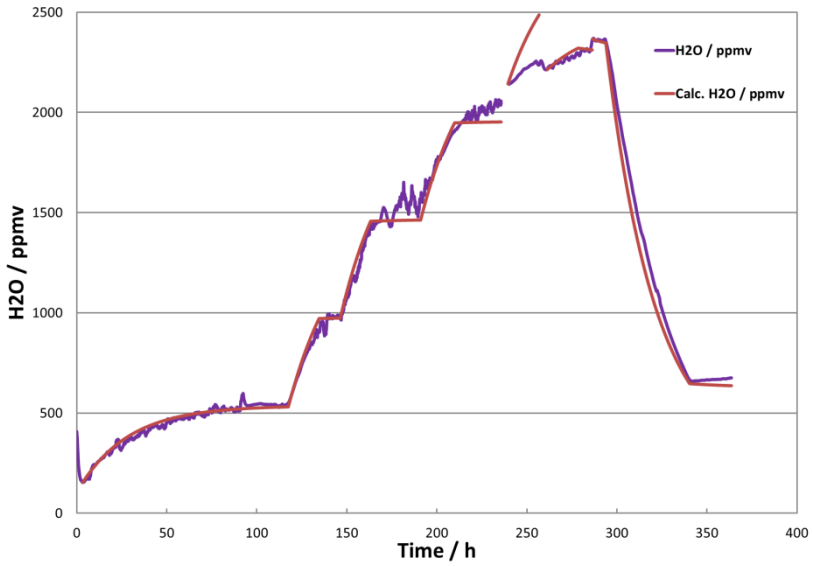

Figure 34 *Measured water levels from test run without corrosion coupons. The test conditions were temperature 25°C, pressure 95 bars and flow 1.0 m/s.*

The measured values follow the calculated water concentration (red line) and confirm that both dosing and measurements relates. The lag time i.e. the time it took from the water concentration was changed in the dosing unit it was measured in the H_2O analyzer, was about 100 minutes. It took approximately 80 hours until the water concentration was stable at the set point level (120 h for the first step). The change in concentration follows an exponential curve of a first order differential equation, as discussed in chapter 3.1.4.

The instability of the water measurements above 1500 ppmv are caused by fluctuation of pressure in the heated gas regulator, resulting in uneven flow rates of gas to analyzing module.

4.1.2 Experiment Solu 02 – different water levels

Water measurements

When a carbon steel sample was placed in the test section, we saw in contrast to Solu Blank (Figure 34) a deviation between the measured and calculated water levels (Figure 35). In the beginning of the experiment, the measured values and the calculated line show good correspondence, but when reaching 1500 ppmv of water there is some deviation observed. The same change is seen at the 2000 ppmv level. With water level set to 2800 ppmv, the measured water concentration never exceeded 2400 ppmv.

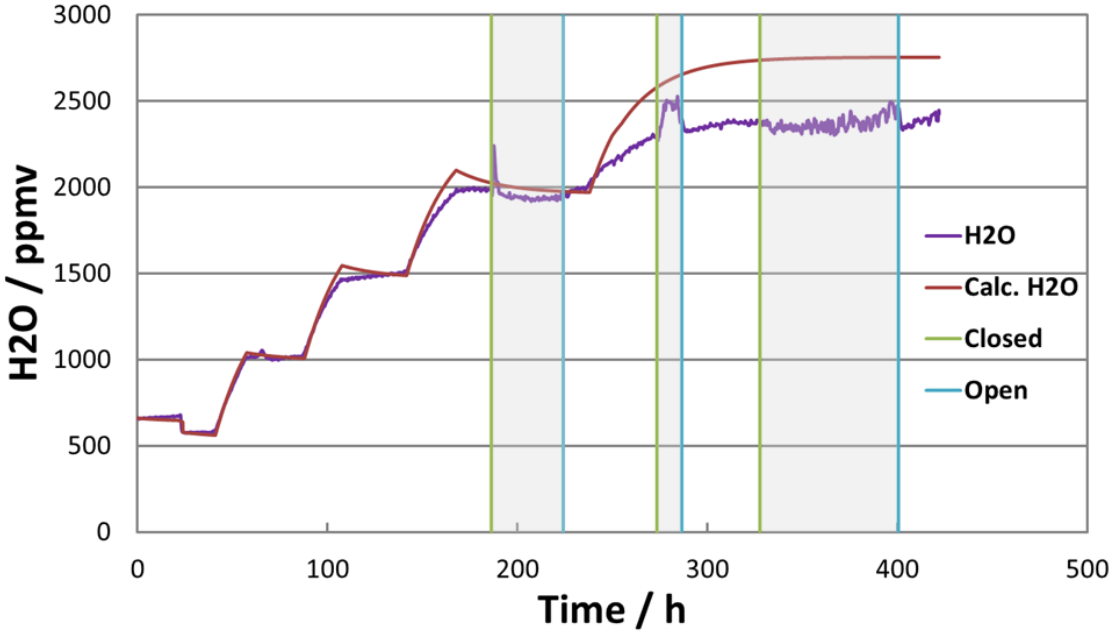

Figure 35 *The Solu 02 experiment was performed at 25°C, 95 bars 0.4 m/s flow. The measured water level (purple line) is plotted as a function of time and compared with therotical curve (brown line).*

A drop in water concentration was seen after 22.5 hours when the test section that was filled with dry CO_2 was opened. The CO_2 feeding to the loop was stopped for certain periods of time (grey area between green and blue line in Figure 35) and the H_2O concentration measured in these periods is the concentration in the CO_2 that was bypassed the loop and routed directly to the analyzer.

No large changes detected in the water concentration in the loop before and after these periods, but after the last period the water concentration had dropped by about 40 ppmv. This is equal to a corrosion rate 0.01 mm/year (as calculated by Equation 26) if all the water is used in the corrosion process of the carbon steel sample.

Visual examination and SEM analysis of the sample surface

By visual examination of the sample it was clear that the surface had a slightly more grayish color (Figure 36A) than before the exposure. SEM analysis of showed traces of corrosion product (Figure 36B and C) compared to the reference (Figure 51). The solid formation on the surface is more visible at higher magnification (picture C).

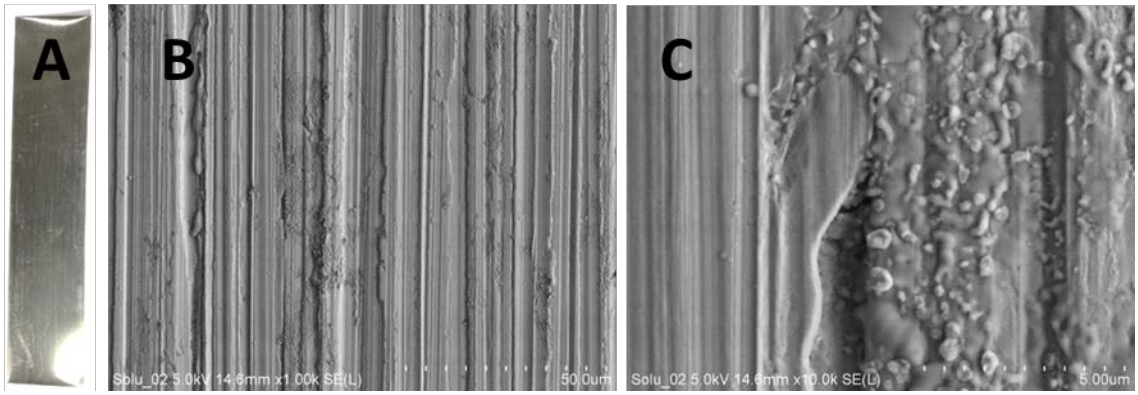

Figure 36 *Image of the carbon steel sample exposed in experiment Solu 02 (A) reveled a slight change in color of the surface. SEM images taken at 1.000X (B) and 10.000X (C) magnification. The stripes were caused by the sample preparation with grinding paper.*

EDS analysis of the corrosion product

EDS analyses (Figure 37) confirm the present of iron (Fe), carbon (C), and oxygen (O) in a ratio suggestive of iron carbonate ($FeCO_3$), but there was some variance in the measurement which might be caused by too high accelerating voltage versus thin layer of products. See chapter 4.1.9.

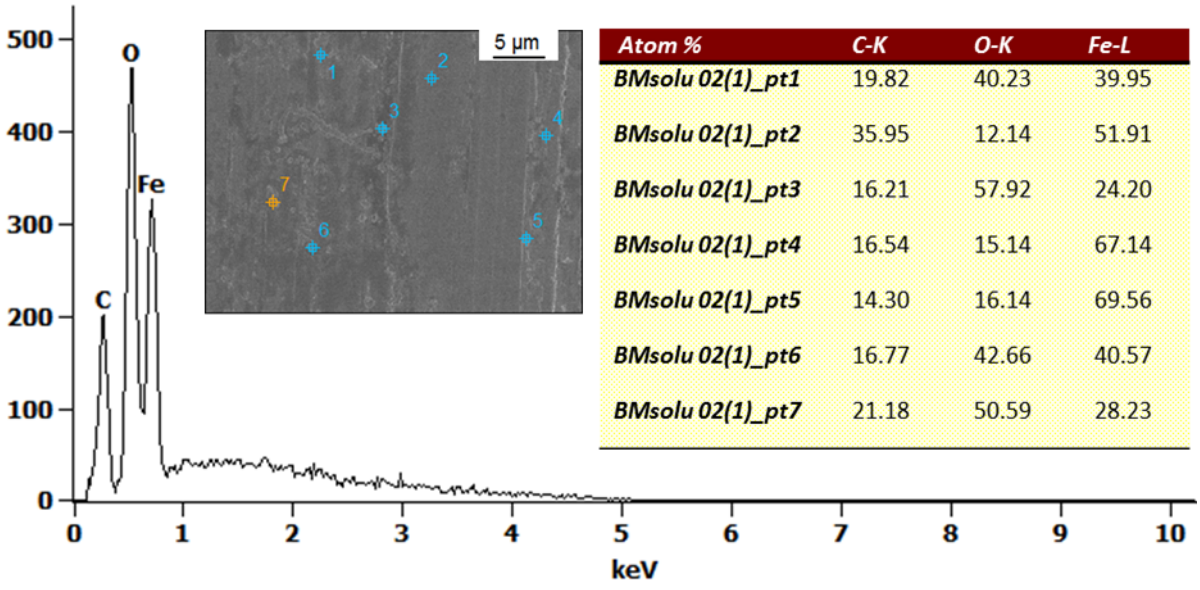

Atom %	C-K	O-K	Fe-L
BMsolu 02(1)_pt1	19.82	40.23	39.95
BMsolu 02(1)_pt2	35.95	12.14	51.91
BMsolu 02(1)_pt3	16.21	57.92	24.20
BMsolu 02(1)_pt4	16.54	15.14	67.14
BMsolu 02(1)_pt5	14.30	16.14	69.56
BMsolu 02(1)_pt6	16.77	42.66	40.57
BMsolu 02(1)_pt7	21.18	50.59	28.23

Figure 37 *An EDS analysis taken at 5.0 KeV on the surface of a carbon steel sample exposed in the loop experiment, solu 02. The table shows a seven point analysis on the surface and are given in atomic percent.*

Weight loss

The weight loss of the sample was measured to be 29 ± 11 μg/cm^2 and film weight was 25 ± 11 μg/cm^2 (average ± SD; n = 5 samples) after the reference weight loss is withdrawn (the raw data for all experiments are summarized in Table 13). This corresponds to an average corrosion rate of 0.8 μm/y and an average film thickness of about 80 nm.

4.1.3 Experiment Solu 03 - high water level and constant temperature

Water measurements

The water concentration was kept at about 2500 ppmv as shown in Figure 38, and the temperature kept around 25°C.

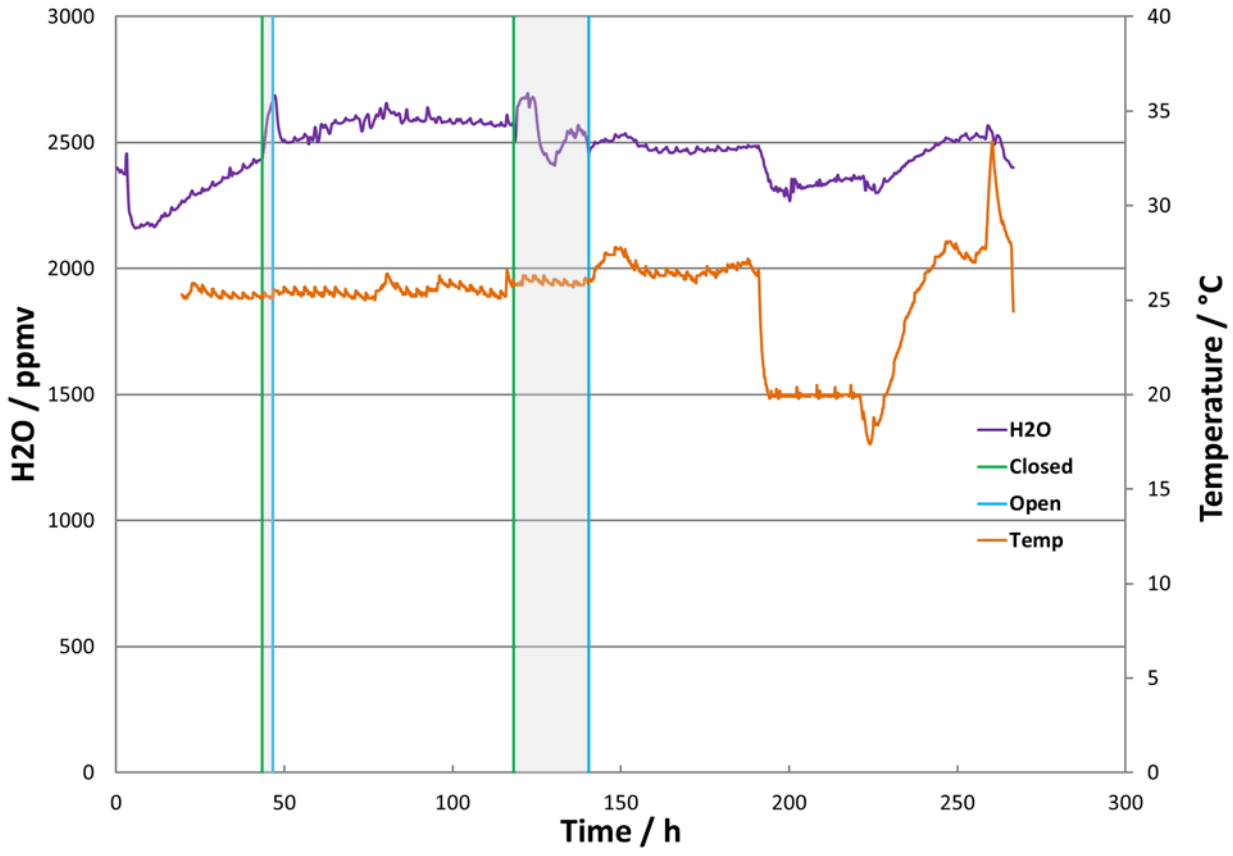

Figure 38 *The Solu 03 experiment was performed at the temperature 25°C, 95 bars of pressure, and a flow of 0.4 m/s. The measured water level (purple line) and the temperature (orange line) are plotted as a function of time.*

In the beginning of the experiment there is a characteristic drop in the water level due to the opening of the test section, and then the water concentration gradually increases to the set water level. As described in previous chapter the grey area between green and blue line indicates closed loop, no dosing or analysis of the loop in this period. At the second closed period the water dosing rate was adjusted to 2500 ppmv and after the closed period the water level had dropped about 60 ppmv, which would correspond to a corrosion rate around 0.05 mm/year (as calculated by Equation 26). When the temperature was lowered to 20°C, the water level also decreased. The cooling unit failed and the experiment was therefore stopped after 263 hours.

Visual examination and SEM analysis of the sample surface

Visual inspection of the carbon steel sample revealed no sign of corrosion, whereas a closer look using the SEM showed some products on the surface (Figure 39) compared to the reference (Figure 51).

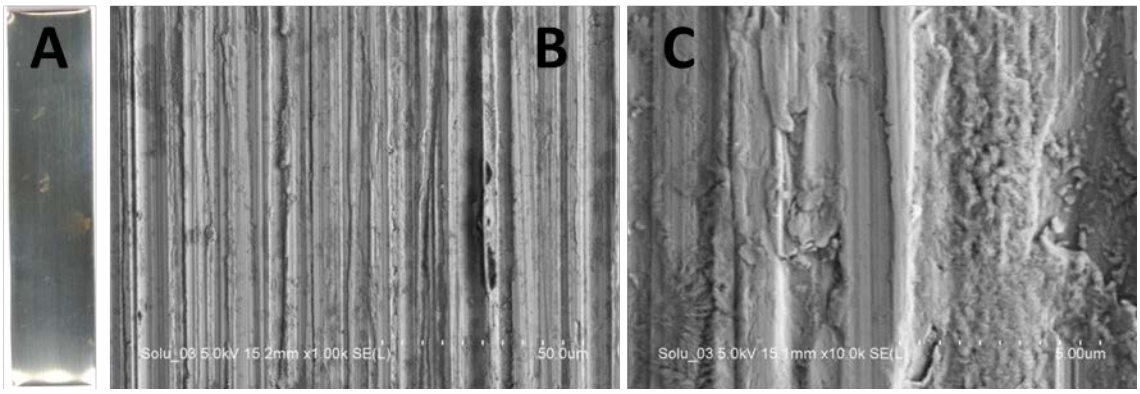

Figure 39 *Optical camera picture(A) and SEM(B&C) of carbon steel sample exposed in experiment Solu 03 at two different magnifications, 1000 times(B) and 10000 times(C) magnification. The stripes seen in the background of the sample comes from sample preparation with grinding paper.*

There are diverged products at the surface, seen as a bit darker spots in picture B.

EDS analysis of the corrosion product

EDS analysis (Figure 40) on the surface showed the present of Fe, C, and O, but not necessary in the ratio characteristic for the expected $FeCO_3$.

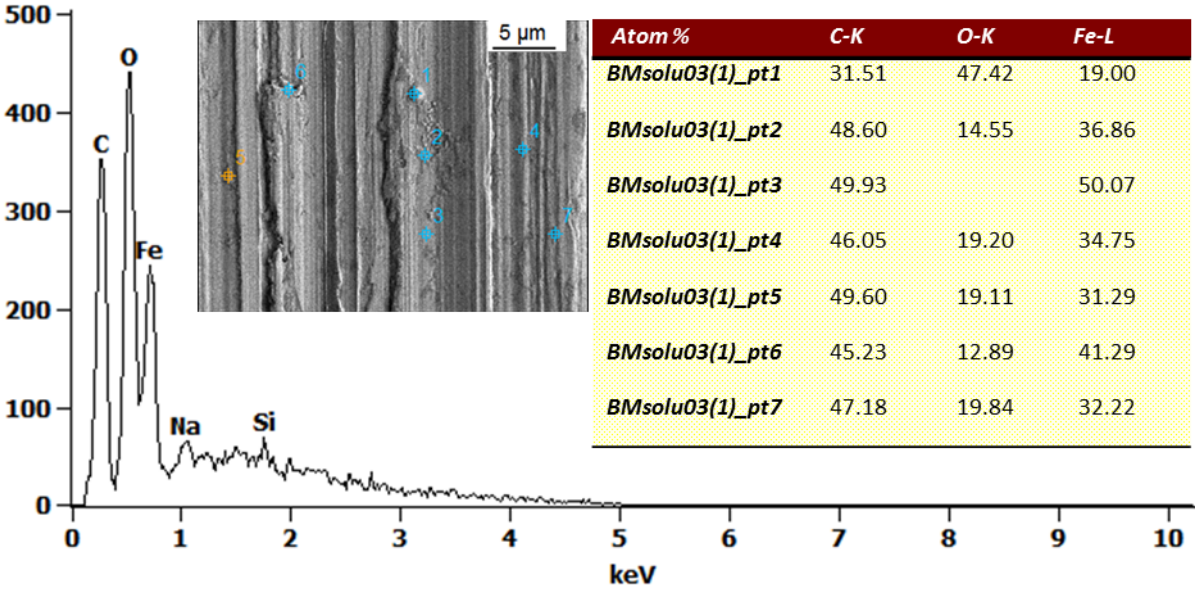

Atom %	C-K	O-K	Fe-L
BMsolu03(1)_pt1	31.51	47.42	19.00
BMsolu03(1)_pt2	48.60	14.55	36.86
BMsolu03(1)_pt3	49.93		50.07
BMsolu03(1)_pt4	46.05	19.20	34.75
BMsolu03(1)_pt5	49.60	19.11	31.29
BMsolu03(1)_pt6	45.23	12.89	41.29
BMsolu03(1)_pt7	47.18	19.84	32.22

Figure 40 *EDS analysis taken at 5.0 KeV on the surface of a carbon steel sample exposed in the loop experiment, solu 03. The table shows a seven point analysis place on the surface and are given in atomic percent.*

Weight loss

The weight of the sample had increased but the film weight was less than the reference weight loss during stripping of the film (the raw data for all experiments is summarized in Table 14). This might come from errors during sample handling. So no number on weight loss and film weight can be given.

4.1.4 Experiment Solu 04 -temperature changes at constant water level

Water measurements

Figure 41 shows the temperature and water concentration changes during the experiment. The saw-toothed shape of both temperature and water curve is more visible when the temperature gets lower. The reason for this is the defrost function on the cooling unit, every third hour it heats up the cooling ducts to prevent icing. During the period between 120 to 140 hours the time interval for defrosting was increased. It ended with blocking of the cooling ducts and poorer cooling effect. This is merely an observation and will not affect the experiment in a significant degree.

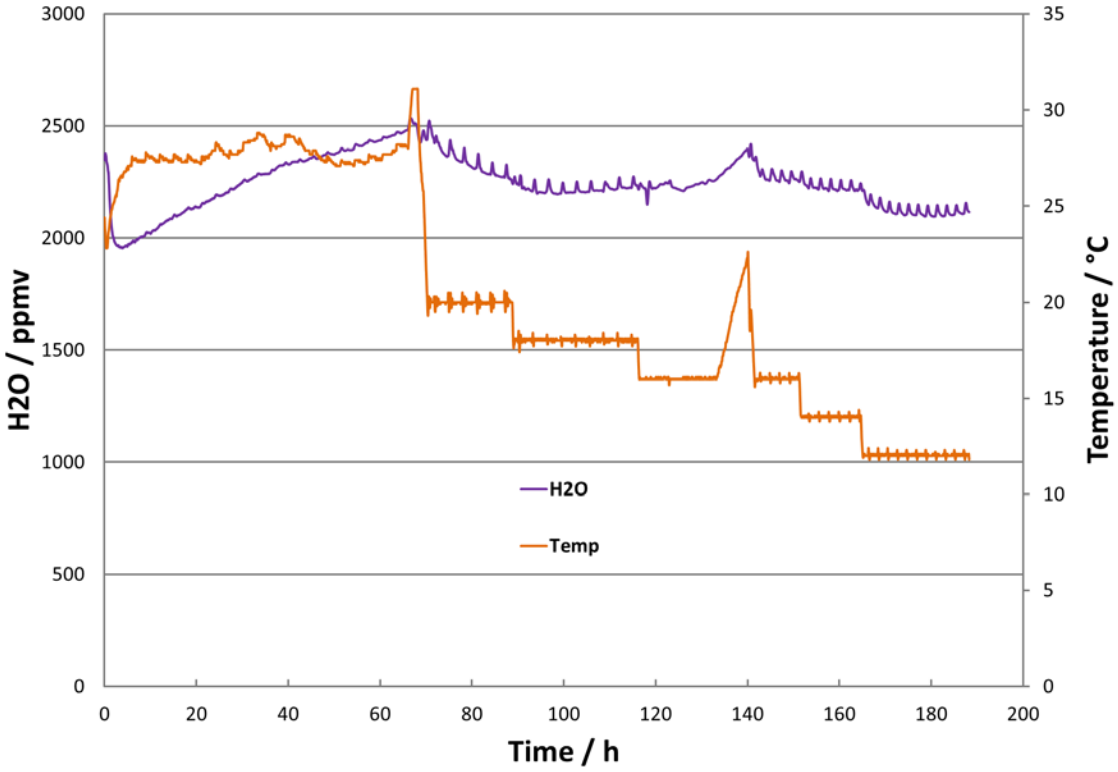

Figure 41 *The Solu 04 experiment was performed at the temperature 25°C, 95 bars of pressure, and a flow of 0.4 m/s. The measured water level (purple line) and the temperature (orange line) are plotted as a function of time.*

As seen from the figure, the temperature settles quickly on the new set points. Six different levels were tested from 27°C to 12°C. Small changes in measured water occurred when changing the temperature. Whether this is related to corrosion or an experimental artifact is uncertain.

Visual examination and SEM analysis of the sample surface

The carbon steel sample had some grey/black discoloration when they were removed from the loop. The color later changed to a weak rusty one after some days when stored in a heated sample chamber. SEM analysis showed that the surface was almost fully covered by corrosion products, see Figure 42.

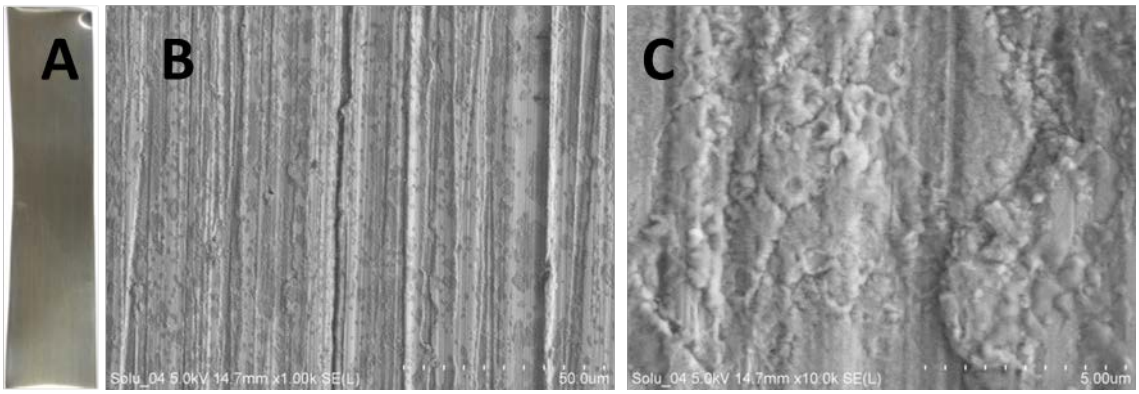

Figure 42 *SEM(B&C) and optical camera picture(A) of carbon steel sample exposed in experiment Solu 04 at two different magnifications, 1000 (B) and 10000 times(C). The SEM was set to 5 KeV and the working distance was 14.7 mm, the scale bar is on the lower right.*

The stripes seen in the background of the sample comes from sample preparation with grinding paper, they might look more corroded that the reference picture in Figure 51. There are uniformly distributed products at the surface, seen as slightly darker areas in picture B.

EDS analysis of the corrosion product

The EDS scan (Figure 43) verified Fe, C, and O presence in a ratio which indicate formation of $FeCO_3$, but there is large variation.

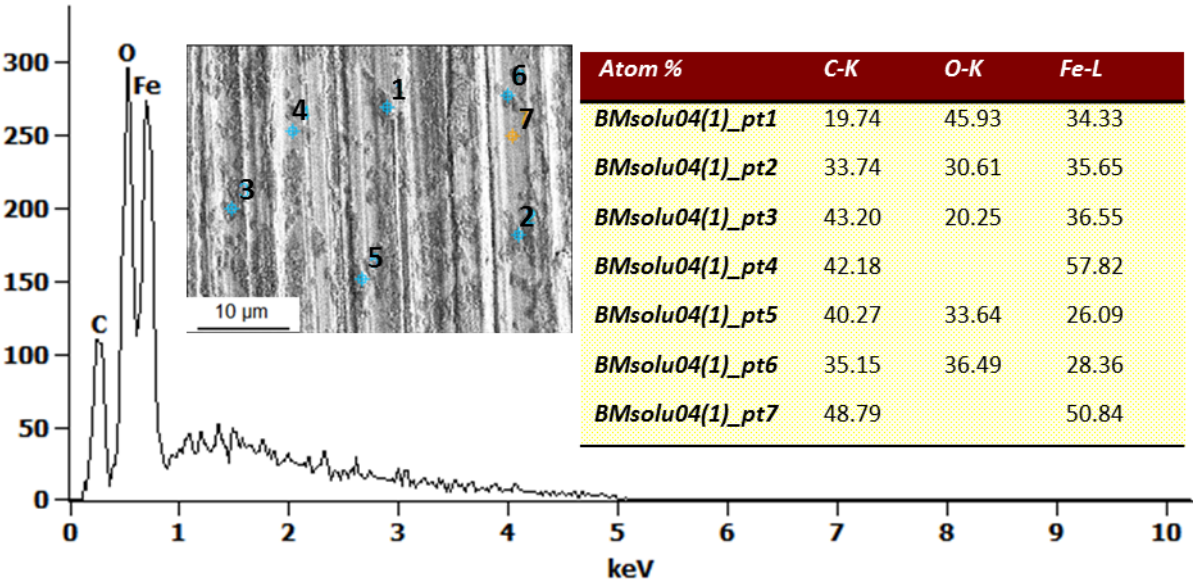

Atom %	C-K	O-K	Fe-L
BMsolu04(1)_pt1	19.74	45.93	34.33
BMsolu04(1)_pt2	33.74	30.61	35.65
BMsolu04(1)_pt3	43.20	20.25	36.55
BMsolu04(1)_pt4	42.18		57.82
BMsolu04(1)_pt5	40.27	33.64	26.09
BMsolu04(1)_pt6	35.15	36.49	28.36
BMsolu04(1)_pt7	48.79		50.84

Figure 43 *An EDS analysis taken at 5.0 KeV on the surface of a carbon steel sample exposed in the loop experiment, Solu 04. The table shows an seven point analysis place on the surface and are given in atomic percent.*

Weight loss

The weight loss of the sample was measured to be 23 ± 13 μg/cm^2 and film weight was 19 ± 13 μg/cm^2 (average ± SD; n = 5 samples) after the reference weight loss is withdrawn (the raw data for all experiments is summarized in Table 15). This equals an average corrosion rate of 1.4 μm/y and an average film thickness of 60 nm.

4.1.5 Experiment Solu 05 - low temperature and constant water level

Water measurements

As evident from Figure 44 the measured water are influenced by temperature changes, which could indicate that the water concentration exceeds the solubility limit in CO_2 and water accumulates in the loop. This is also supported by the observation from dry up period in the end of the experiment where first the measured water concentration deviates from the calculated water concentration and after water is dried up both curves overlap, further discussed in chapter 5.2.2.2 and Figure 79.

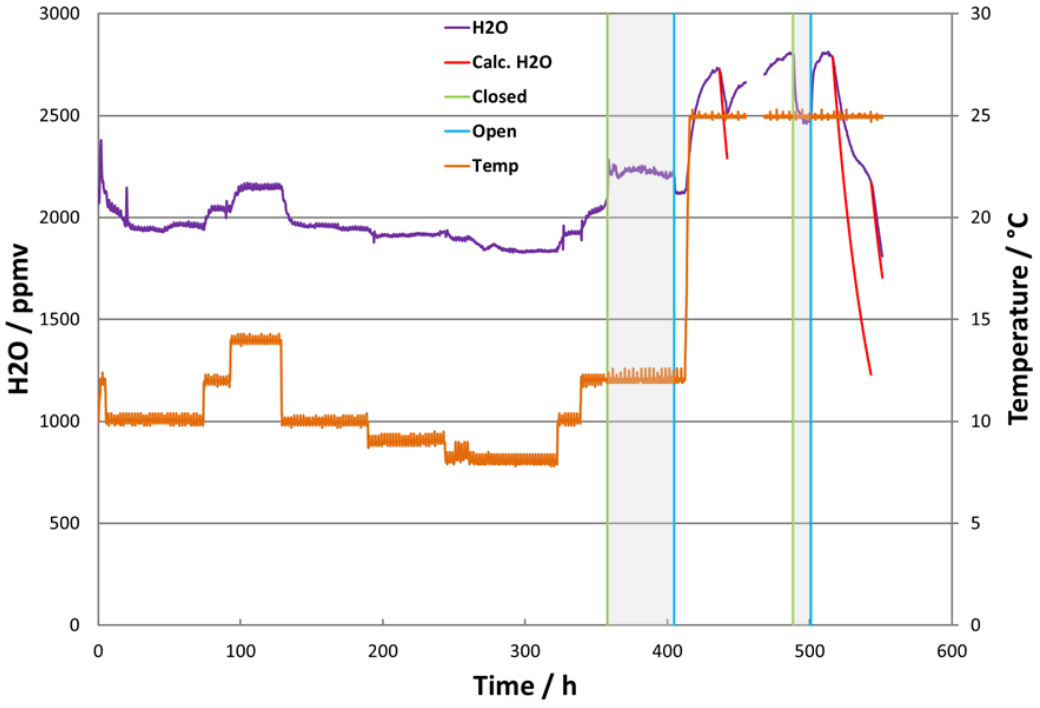

Figure 44 *The Solu 05 experiment was performed at the temperature 25°C, 95 bars of pressure, and a flow of 0.4 m/s. The measured water level (purple line) and the temperature (orange line) are plotted as a function of time. Grey area indicate closed periods.*

The CO_2 feed to the loop was closed at two different conditions. During the first closed period, the water measurements showed that the concentration in the bypassed CO_2 was higher than the level measured in the loop, which may indicated precipitation of water when loop is open. The first dry CO_2 period was short (red calculated line at 432 hours), but still the difference between measured water and calculated water was 320 ppmv (calculated H_2O stopped at 2290 ppmv, while measured H2O ended at 2510 ppmv). During second dry CO_2 period (starts red line at 513 hours) the deviation became 946 ppmv between calculated and measured value until curve makes a bend, and after that both lines follow the same trend.

Visual examination and SEM analysis of the sample surface

The sample was not as dark as Solu 04, but still darker than the other samples. The visual inspection gave no impression of corrosion. The SEM characterization (see Figure 45) however revealed that the surface was covered by corrosion products. At higher magnification it looks like the surface has been hit with small droplets and that the corrosion film growth to some extent starts from these points.

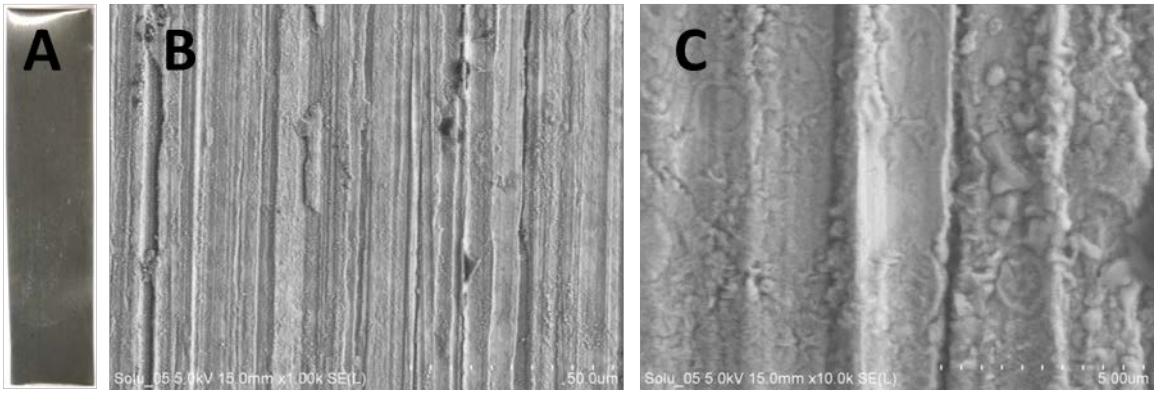

Figure 45 *SEM(B&C) and optical camera picture(A) of carbon steel sample exposed in experiment Solu 05 at 1000 times(B) and 10000 times(C) magnification. The SEM was set to 5 KeV and the working distance was 15.0 mm, the scale bar is on the lower right.*

The strips from sample preparation with grinding paper are not as clear as on the reference sample (see Figure 51). It looks like almost the whole surface is covered by products. There are some round growth areas which can be seen in picture C.

EDS analysis of the corrosion product

The EDS analysis (see Figure 46) found Fe, C, and O. The atomic percent indicates $FeCO_3$.

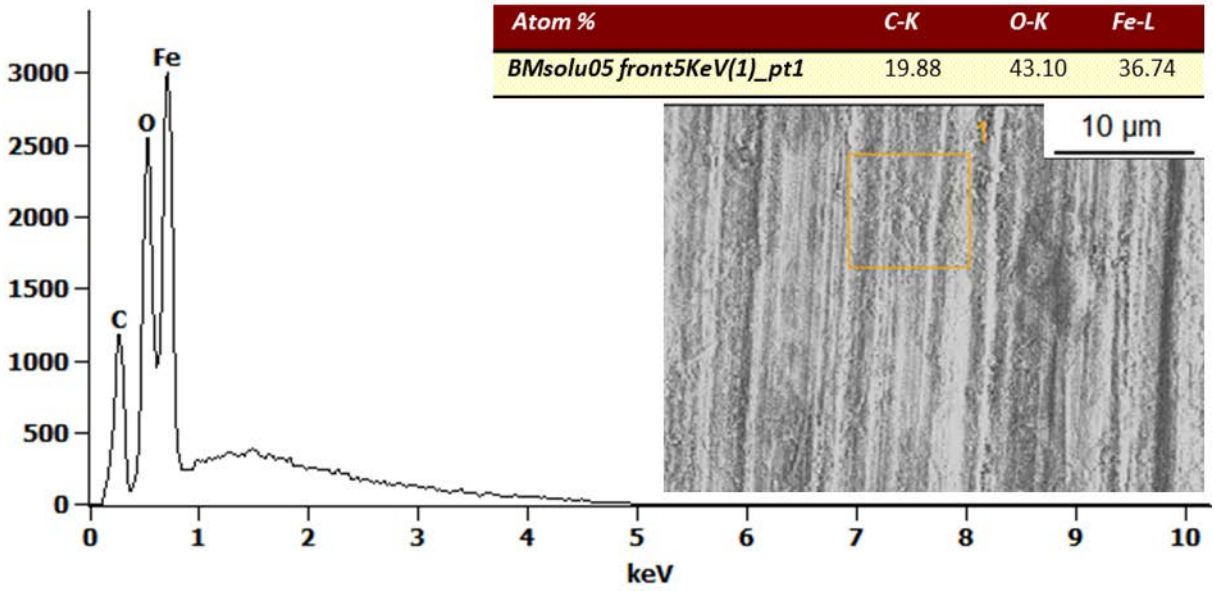

Figure 46 *An EDS analysis taken at 5.0 KeV on the surface of a carbon steel sample exposed in the loop experiment, solu 05. The table shows a line analysis done as a square place on the surface and are given in atomic percent.*

Weight loss

The weight loss of the sample was measured to be 48 ± 3 μg/cm^2 and film weight was 36 ± 3 μg/cm^2 (average ± SD; n = 5 samples) after the reference weight loss is withdrawn (the raw data for all experiments is summarized in Table 16). This equals an average corrosion rate of 1.0 mm/y and an average film thickness of about 120 nm.

4.1.6 Experiment Solu 06 - supercritical conditions

Water measurements

Experiment Solu 06 was performed at 35°C and in the supercritical region of the phase diagram of CO_2 to see if higher temperature affects the corrosion of carbon steel. The CO_2 feed to the loop was closed for certain periods of time and the plotted measurements in these closed periods (grey area between green and blue line) are from the CO_2 that was routed directly to the analyzer. The measured water concentration follows the calculated concentration until it stabilizes after 100 hours at about 2430 ppmv, ca. 100 ppmv lower than the calculated value. A power failure occurred after 190 hours that is the reason for the missing part of the curve. After 253 hours the CO_2 feed to the loop was resumed (after being stopped for 25 hours) and the

water concentration decreased by 105 ppmv. This corresponds to a corrosion rate of 0.059 mm/year if the drop is caused by corrosion.

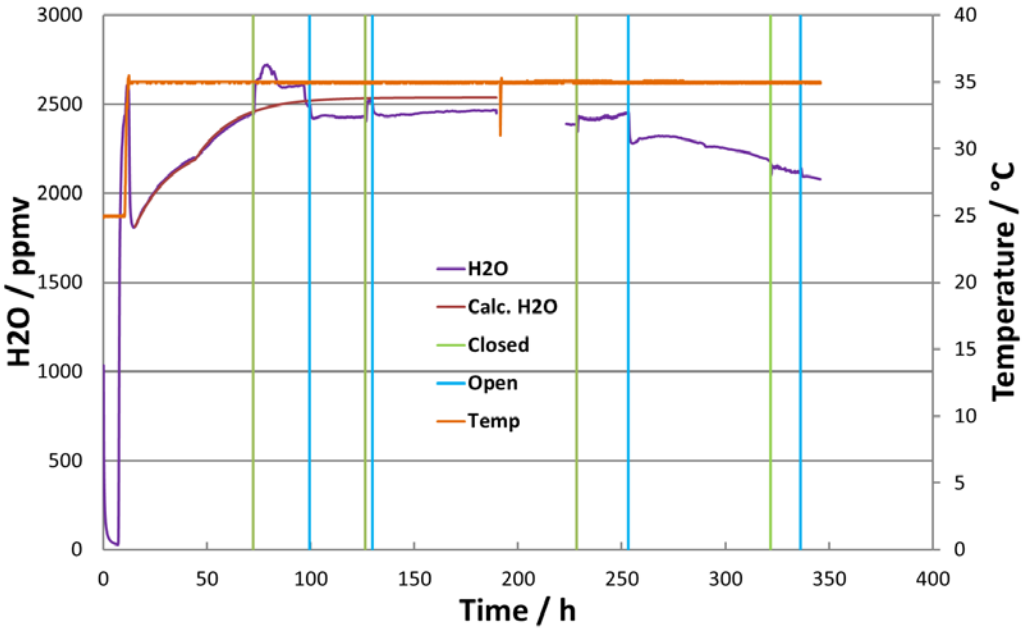

Figure 47 *The Solu 06 experiment was performed at the temperature 35°C, 95 bars of pressure, and a flow of 0.4 m/s. The measured water level (purple line) and the temperature (orange line) are plotted as a function of time.*

Visual examination and SEM analysis of the sample surface

After the experiment the sample looked almost as the reference sample and the visual inspection gave no impression of corrosion. The SEM inspection (see Figure 48) however revealed that the surface was covered by some product.

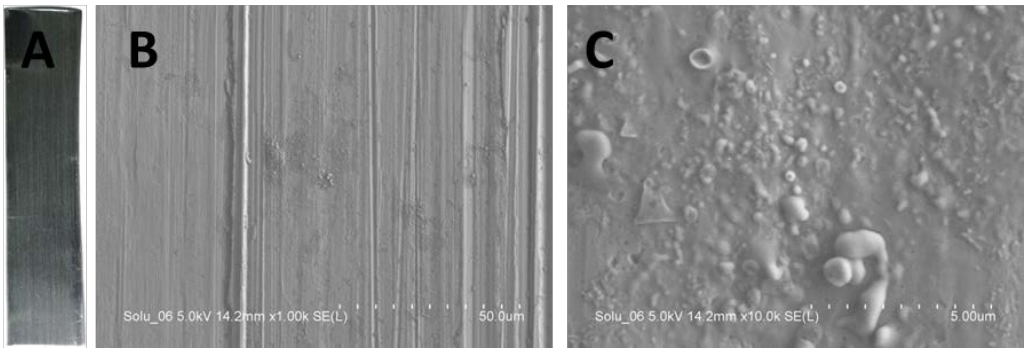

Figure 48 *SEM(B&C) and optical camera picture(A) of carbon steel sample exposed in experiment Solu 06 at 1000 times(B) and 10000 times(C) magnification. The SEM was set to 5 KeV and the working distance was 14.2 mm, the scale bar is on the lower right.*

The grinding stripes look similar to those in the reference in Figure 51. Picture B shows some growth area representative for the whole sample and picture C shows a typical growth area.

EDS analysis of the corrosion product

The EDS analysis (see Figure 49) indicated presence of Fe, C, and O on the surface. The atomic percent indicates $FeCO_3$ formation.

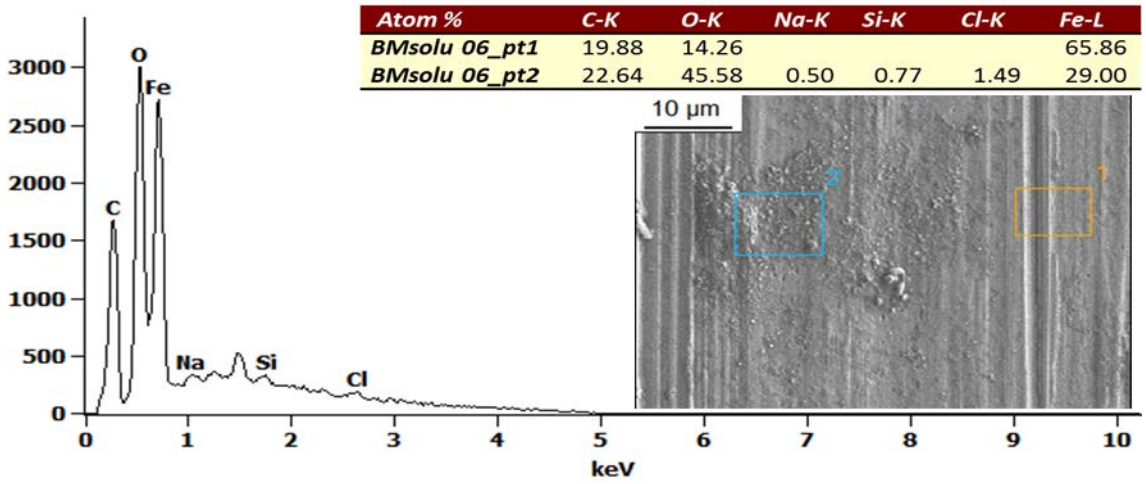

Figure 49 *An EDS analysis taken at 5.0 KeV on the surface of a carbon steel sample exposed in the loop experiment, Solu 06. The table shows a line analysis done as a square randomly place on the surface and are given in atomic percent.*

Weight loss

The weight of the sample had increased and the film weight was less than the reference weight loss during stripping of the film (the raw data for all experiments is summarized in Table 17). So no number on weight loss and film weight can be given.

Surface profile

The profile picture (Figure 50) was taken for analysis of localized attacks after the corrosion products was removed from the surface by stripping. An Alicona camera on an Axioskop 2, the picture was analyzed with Nanovea software was used for this propose. The picture and profile shows strips from the grinding paper and no clear signs of pits or localized attacks.

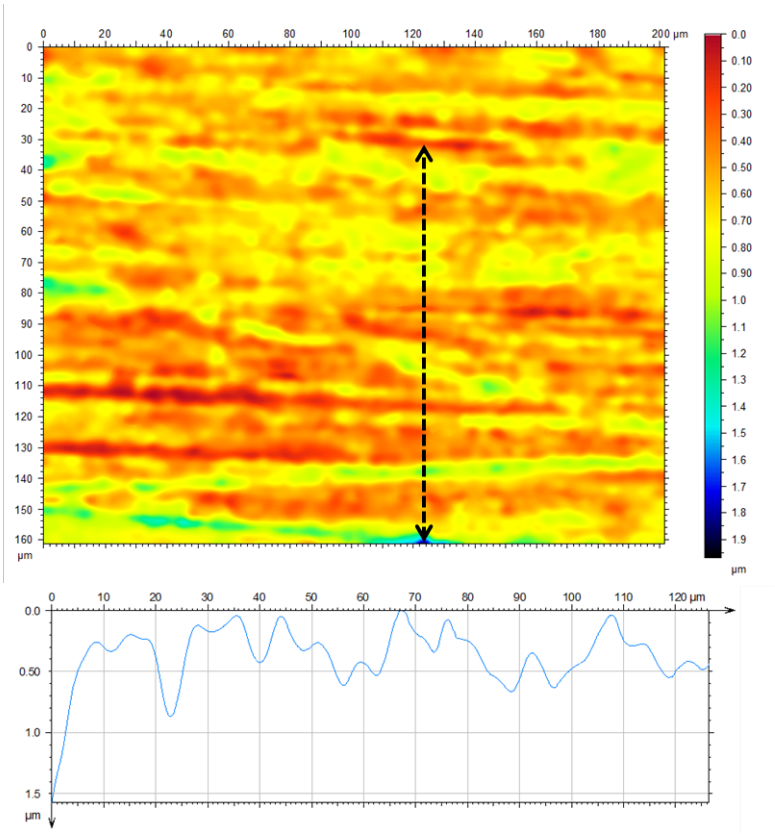

Figure 50 *A profile picture with extracted profile curve taken of Solu 06.*

4.1.7 Reference sample

The reference sample has not been used in any experiment, but prepared in the same manner as the other samples. Optical and SEM picture are shown in Figure 51 below and results of EDS analysis in Figure 52.

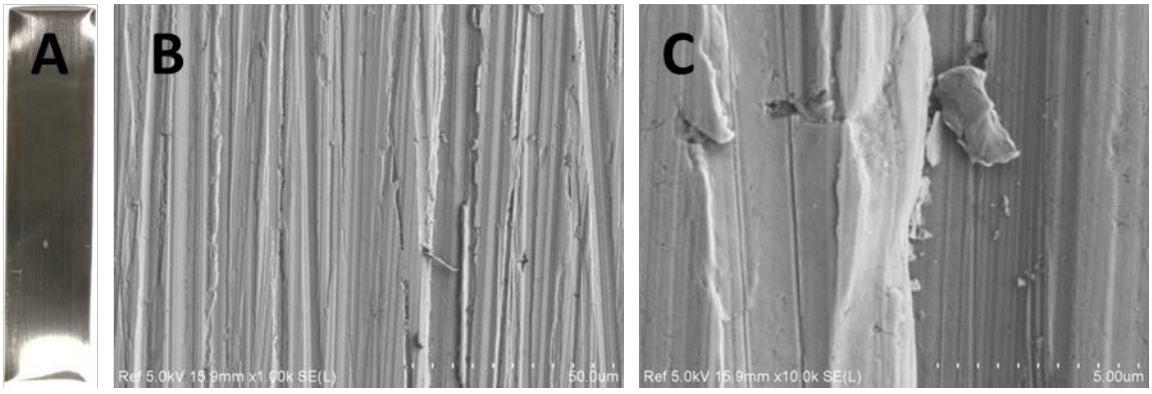

Figure 51 *SEM(B&C) and optical camera picture(A) of reference carbon steel sample at 1000 times(B) and 10000 times(C) magnification. The SEM was set to 5 KeV and the working distance was 15.9 mm, the scale bar is on the lower right.*

These pictures are used for comparison with pictures of samples that has been exposed. No products were found and grinding lines are clear.

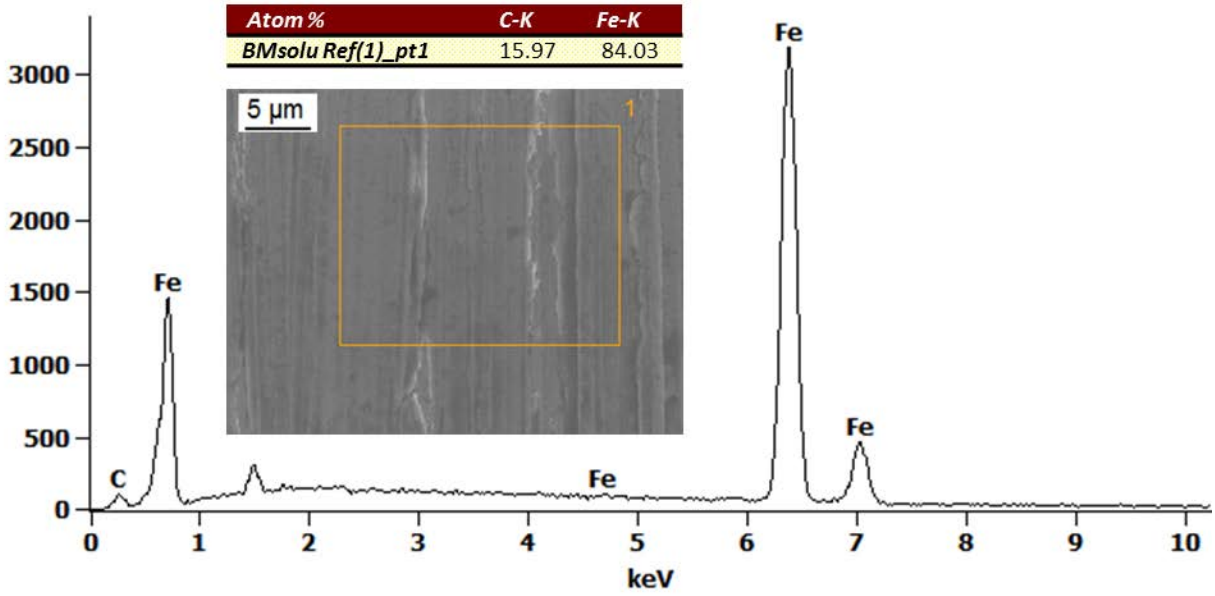

Figure 52 *An EDS analysis taken at 5.0 KeV on the surface of a reference sample. The table shows a line analysis done as a square place on the surface and are given in atomic percent. The EDS shows a high carbon content which can be related to the analysis method.*

The reference sample was also stripped so it can be withdrawn from the other samples. The weight loss from the stripping was 35.3 ± 5 μg/cm^2 (average ± SD; n = 5 samples) see Table 12 for rawdata.

Surface profile

The picture and profile (Figure 53) taken of the reference sample shows strips from the grinding paper and no signs of pits or localized attacks.

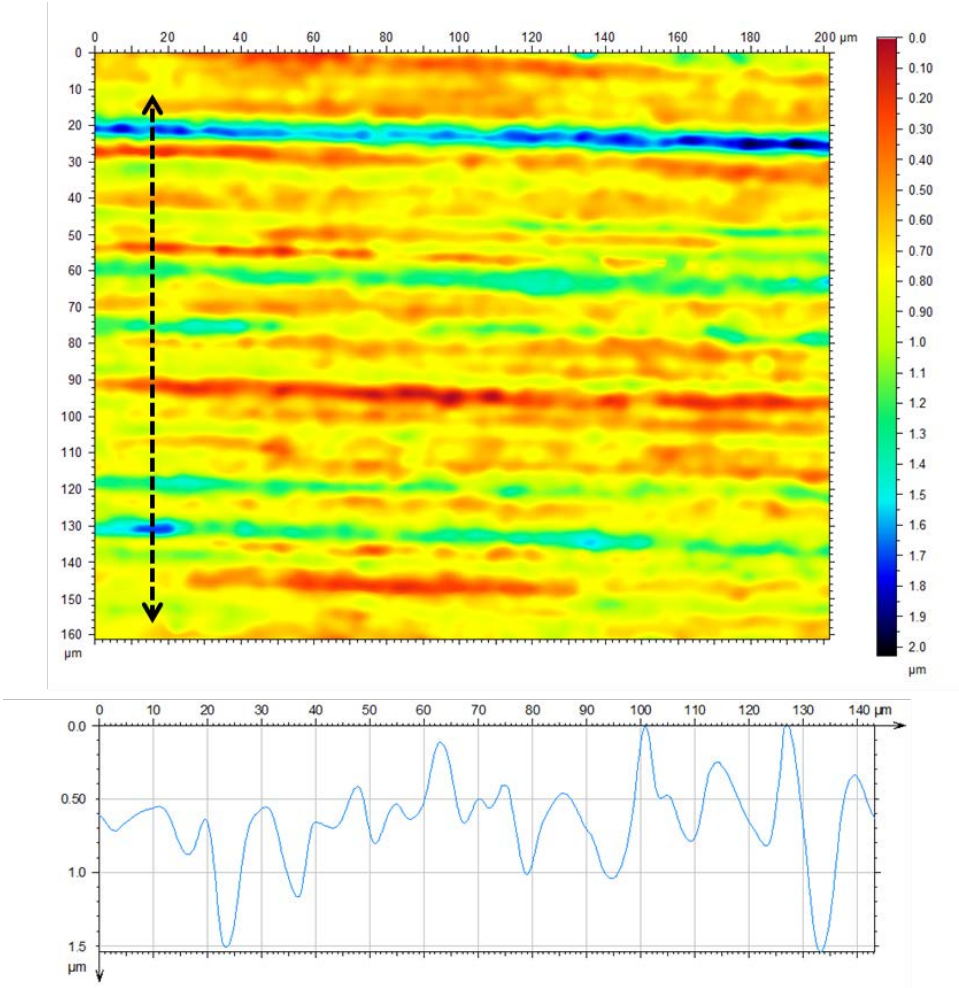

Figure 53 *A profile picture with extracted profile curve taken of the reference.*

4.1.8 Sample data

This chapter sums up all the data needed to calculate the average corrosion rates and film weight for the different experiments. To find the average corrosion rate and film weight the sample had to be stripped by dipping in a stripping solution (see experimental part). To find how much of the metal is removed in this process a reference sample was also stripped. The tables under shows the weight and area measured after the sample was stripped. A reference sample was cut in 5 pieces and the same was done with the samples from all experiments after weighing it.

Table 13 *Weight and area of the reference samples before and after stripping.*

Reference sample							
	Width cm	**Length cm**	**Area cm2**	**Weight before g**	**Weight after g**	**Film weight mg**	**Weight per area mg/cm2**
front oi1	1.323	5.677	15.02	1.2190	1.2185	0.5	0.033
mid oi1	1.239	5.679	14.07	1.1361	1.1356	0.5	0.036
mid ii1	1.240	5.979	14.82	1.1897	1.1893	0.4	0.027
mid ii2	1.231	5.556	13.68	1.0925	1.0919	0.6	0.044
mid oi2	1.253	5.433	13.61	1.0893	1.0888	0.5	0.037
						Average	0.035
						SD	0.005

Table 14 *Weight and area of the Solu 02 sample before and after stripping.*

Solu 02							
	Width cm	**Length cm**	**Area cm2**	**Weight before g**	**Weight after g**	**Film weight mg**	**Weight per area mg/cm2**
front oi1	1.186	5.258	12.47	0.9997	0.9990	0.7	0.056
mid oi1	1.164	5.279	12.29	0.9956	0.9951	0.5	0.041
mid ii1	1.189	5.219	12.41	0.9887	0.9878	0.9	0.072
mid ii2	1.181	5.256	12.42	0.9991	0.9983	0.8	0.064
mid oi2	1.264	5.493	13.89	1.1271	1.1262	0.9	0.065
						Average	0.060
						SD	0.011

Table 15 *Weight and area of the Solu 03 sample before and after stripping.*

Solu 03							
	Width cm	**Length cm**	**Area cm2**	**Weight before g**	**Weight after g**	**Film weight mg**	**Weight per area mg/cm2**
front oi1	1.259	5.493	13.83	1.1126	1.1121	0.5	0.036
mid oi1	1.252	5.563	13.93	1.1289	1.1284	0.5	0.036
mid ii1	1.221	5.505	13.44	1.0633	1.0631	0.2	0.015
mid ii2	1.225	5.568	13.64	1.0860	1.0857	0.3	0.022
mid oi2	1.228	5.423	13.32	1.0733	1.0729	0.4	0.030
						Average	0.028
						SD	0.008

Table 16 *Weight and area of the Solu 04 samples before and after stripping.*

Solu 04							
	Width cm	**Length cm**	**Area cm2**	**Weight before g**	**Weight after g**	**Film weight mg**	**Weight per area mg/cm2**
front oi1	1.191	5.336	12.71	1.0213	1.0206	0.7	0.055
mid oi1	1.190	5.163	12.29	0.9854	0.9849	0.5	0.041
mid ii1	1.199	5.411	12.97	1.0447	1.0442	0.5	0.039
mid ii2	1.235	4.998	12.35	0.9795	0.9786	0.9	0.073
mid oi2	1.314	5.676	14.92	1.1880	1.1871	0.9	0.060
						Average	0.054
						SD	0.013

Table 17 *Weight and area of the Solu 05 samples before and after stripping.*

Solu 05							
	Width cm	**Length cm**	**Area cm2**	**Weight before g**	**Weight after g**	**Film weight mg**	**Weight per area mg/cm2**
front oi1	1.216	5.601	13.62	1.0885	1.0875	1	0.073
mid oi1	1.260	5.536	13.95	1.1368	1.1358	1	0.072
mid ii1	1.216	5.3	12.89	1.0309	1.0300	0.9	0.070
mid ii2	1.189	5.534	13.16	1.0349	1.0339	1	0.076
mid oi2	1.174	5.155	12.10	0.9785	0.9777	0.8	0.066
						Average	0.071
						SD	0.003

Table 18 *Weight and area of the Solu 06 samples before and after stripping.*

Solu 06							
	Width cm	**Length cm**	**Area cm2**	**Weight before g**	**Weight after g**	**Film weight mg**	**Weight per area mg/cm2**
front oi1	1.213	5.325	12.92	1.0423	1.042	0.3	0.023
mid oi1	1.208	5.296	12.79	1.035	1.0346	0.4	0.031
mid ii1	1.198	5.398	12.96	1.0328	1.0327	0.1	0.008
mid ii2	1.249	5.294	13.15	1.0532	1.0529	0.3	0.023
mid oi2	1.223	5.55	13.58	1.0779	1.0777	0.2	0.015
						Average	0.020
						SD	0.008

Table 19 *Sample exposure time in the experiments and comments.*

Experiment name	Time h	Visual inspection after experiment
Solu 02	399.5	Weak light greyish color, no stains
Solu 03	263.7	Weak faint metallic, no stains
Solu 04	188.4	Dark grey/black color, rustic color after some days, no stains
Solu 05	550.1	Dark grey color, no stains
Solu 06	345.1	No visual change or stains

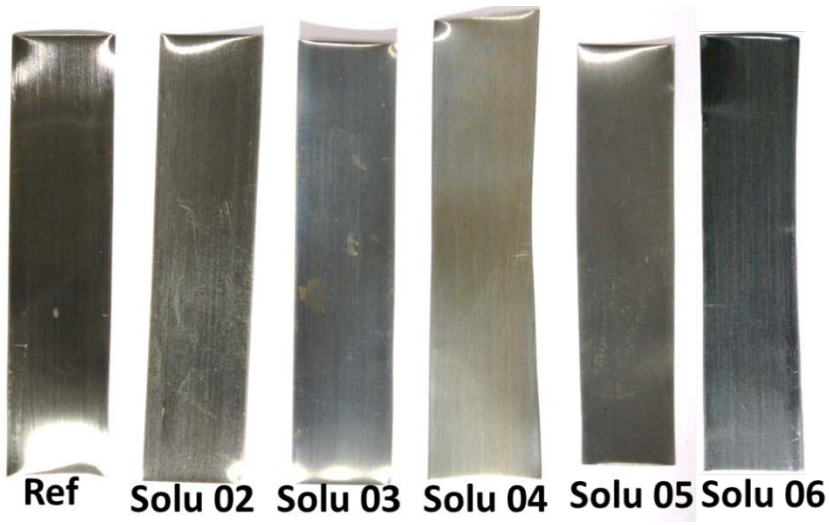

Figure 54 *Comparison of carbon steel sample exposed in different experiments.*

4.1.9 Film thickness estimation by Monte-Carlo method

The electron voltages are important when analyzing a sample in the SEM, too high voltage will make the electron beam penetrate a thin layer. Monte-Carlo simulation was performed to determine how deep into the iron carbonate film the electron beam reaches (Figure 55). It was further compared with EDS measurements with different acceleration voltages. This is not an accurate method to determine the film thickness, but should be looked at as a rough estimate. Five EDS scans at different acceleration voltages were performed on sample Solu 05 and the results are given in Table 20.

Table 20 *EDS analysis at three different electron voltages on Solu_05, concentration given in atomic percent.*

Atom %	C-K	O-K	Fe-L
solu05 1KeV	41.62	35.90	22.48
solu05 2KeV	28.77	46.65	24.58
solu05 3KeV	22.08	48.45	29.47
solu05 4KeV	18.72	44.23	37.05
solu05 5KeV	19.88	43.10	36.74

The figure below shows the Monte-Carlo simulation done by a program called Casino [68].

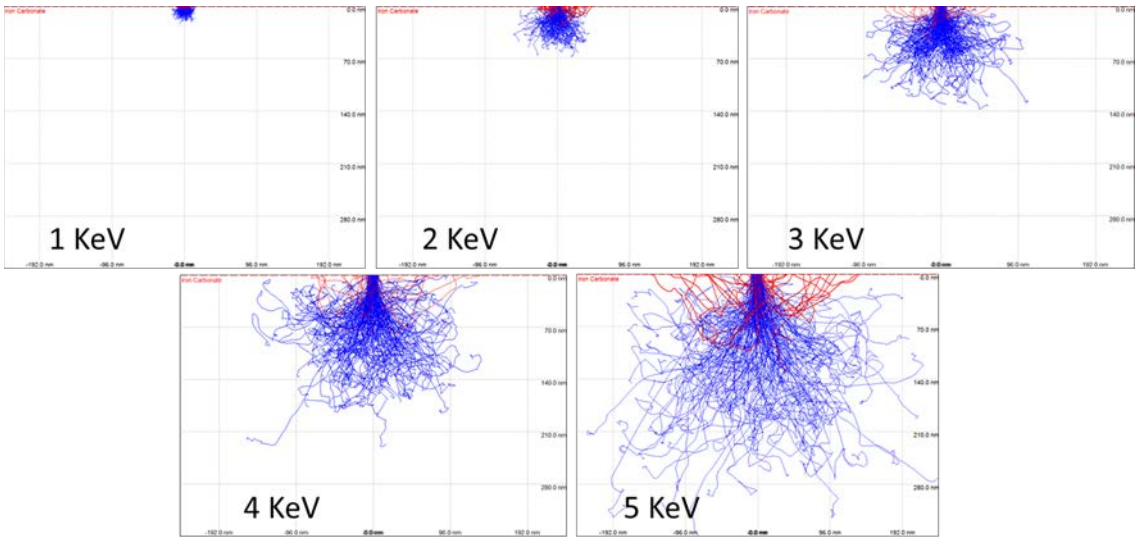

Figure 55 *Five different Monte-Carlo simulations with 1, 2, 3, 4 and 5 KeV for iron carbonate as the substrate.*

The blue lines show penetration depths of the electron trajectories and the red lines shows the penetration depths in the sample of electron trajectories that will escape the sample surface, back scattered electrons. The vertical scale shows the depth of the electrons trajectories in nm and the horizontal scale is the width of the electrons trajectories. The depth of the 1, 2, 3, 4 and 5 KeV simulation was 20, 60, 100, 170 and 250 nm, respectively.

4.2 Dense Phase Loop and free water saturated with CO_2

The experiments presented in this chapter were performed in a free water phase saturated with CO_2.

4.2.1 Iron count versus weight loss

The measurements of the iron concentration are important in these experiments, since they are used to determine the corrosion rate during the experiment. To determine how exact they are, iron measurement in all the experiments are compared with the weight loss in the end of experiment. Table 21 below shows the concentration of iron as measured in the liquid and the weight loss from the samples.

Table 21 *Comparing iron concentration (Fe^{2+}) in the liquid and the weight loss after the experiment.*

Experiment	Iron in liquid ppmv	Total Iron mg	Weight loss mg	Deviation* %
Geo 01	445	1977	1952	-1.3
Geo 02	730	3175	3220	1.4
Geo 04**	670	3045	3170	3.9
Geo 05**	628	2429	2545	4.6

*Deviation from the weight loss.

**Anodic and cathodic sweep preformed during experiment.

The weight loss and measurements of iron shows good similarities, and it can be concluded that the measured iron concentration in liquid reflects well the corrosion process occurring in the loop. Since we can measure the iron at any time during the experiment this method can be used to make a trend of the corrosion rates.

4.2.2 Dense phase loop and the first version test section

4.2.2.1 Experiment Geo 01 - corrosion test at 100 bar CO_2

The LPR measurement run in the loop with the first version of test section is shown in Figure 56 (Experiment Geo 01) together with corrosion rates estimated from the iron counts.

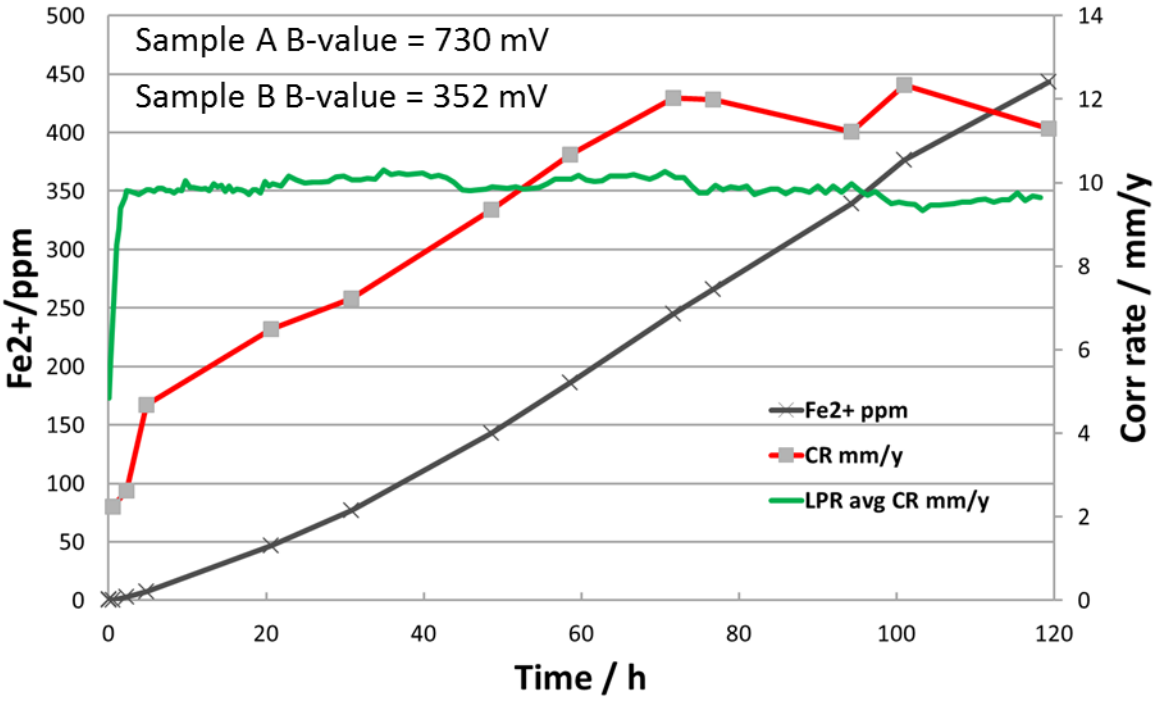

Figure 56 *The diagram shows the concentration of Fe^{2+} in the liquid (left axis) and corrosion rate (right axis) either based on LPR measurement or calculated from the iron count in the liquid. The experimental parameters for Geo 01 were 25°C, 100 bar and 0.65 m/s flow. The LPR measurements are adjusted with a B-*value (Equation 22) to *have a good agreement with the iron count values.*

The B-value (calculated by Equation 22) for sample A had to be 730 mV and for sample B 352 mV to get the LPR curve to fit with the measured iron concentration, as indicated in Figure 56. The average corrosion rate measured by weight loss was 9.9 mm/year and the iron count in the liquid had an average corrosion rate of 10.1 mm/year. The adjusted corrosion rate for LPR measurement was about 10 mm/year with the indicated B-values. The iron count indicates, as shown in Figure 56, that the corrosion rate was lower in the beginning and stabilized at 11.7 mm/year (average of the last 4 measurements) in the end.

The sample after the experiment was black with some gold color layer on top (see Figure 57A&D). The corrosion film did not stick well to the metal sample, some of the film fell off during sample handling. The SEM picture (see Figure 57B, C, E&F under) shows corrosion product on the surface. It looks porous and does accordingly not offer much protection.

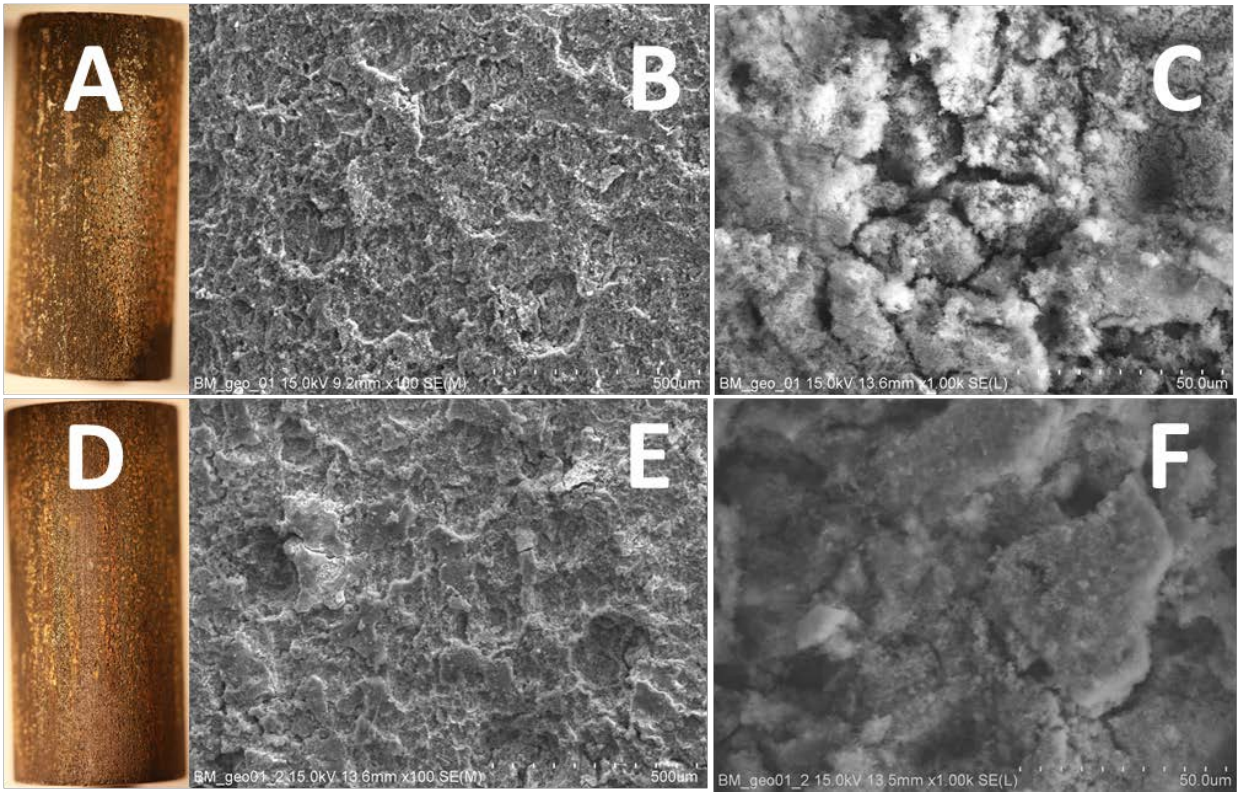

Figure 57 *SEM(B,C, D&F) and optical camera picture(A&D) of carbon steel samples exposed in experiment Geo 01 at 100 times(B&E) and 1000 times(C&F) magnification. The SEM was set to 15 KeV . The scale bar is in the lower right corner. The optical picture shows a gold color layer on top of black powder film.*

The EDS analysis is shown in Figure 58. Several elements are observed in the scan. If we look at the C, O, and Fe ratio it is close to what are expected for $FeCO_3$. The Na and Cl could be an impurity left in the loop after the salt solution experiments, while Al signal comes from the sample holder and Si from the detector. The copper concentration in the EDS analysis was as high as 6.5 atomic percent in some measurements and can indicate copper contamination of the loop.

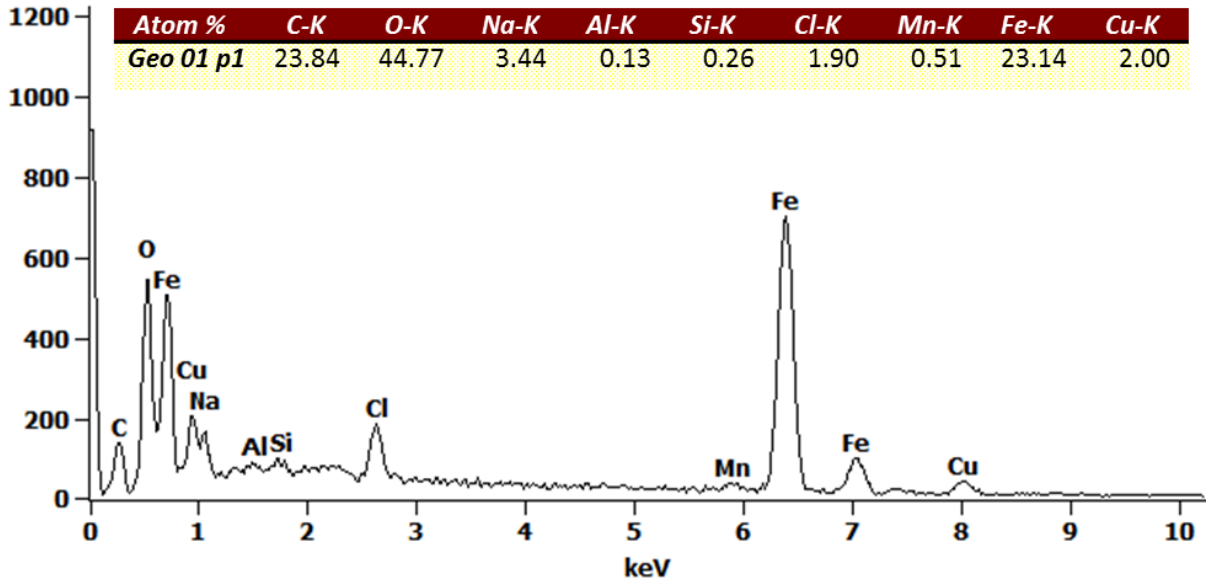

Figure 58 *A spot EDS analysis from the surface of sample A.*

The weight loss of sample A was found to be 111 mg/cm^2 and sample B 101 mg/cm^2. The film weight of sample A and B was 1.5 mg/cm^2 and 0.9 mg/cm^2, respectively. This equals to an average corrosion rate of 10.4 mm/y for sample A and 9.4 mm/y for sample B.

4.2.2.2 Experiment Geo 02 - corrosion test with ramping pressure

The temperature was 25°C and flow was 0.65 m/s throughout the experiment. The iron count at different pressure made it possible to fit the linear polarization resistant measurements. The B-values is presented in Figure 59. The experimental parameters for Geo 02 were 25°C and 0.65 m/s flow. Four different pressure levels with CO_2 were tested and gave three levels off corrosion. The LPR measurements are adjusted with a B-value (Equation 22) to have a good corresponds with the iron count values.

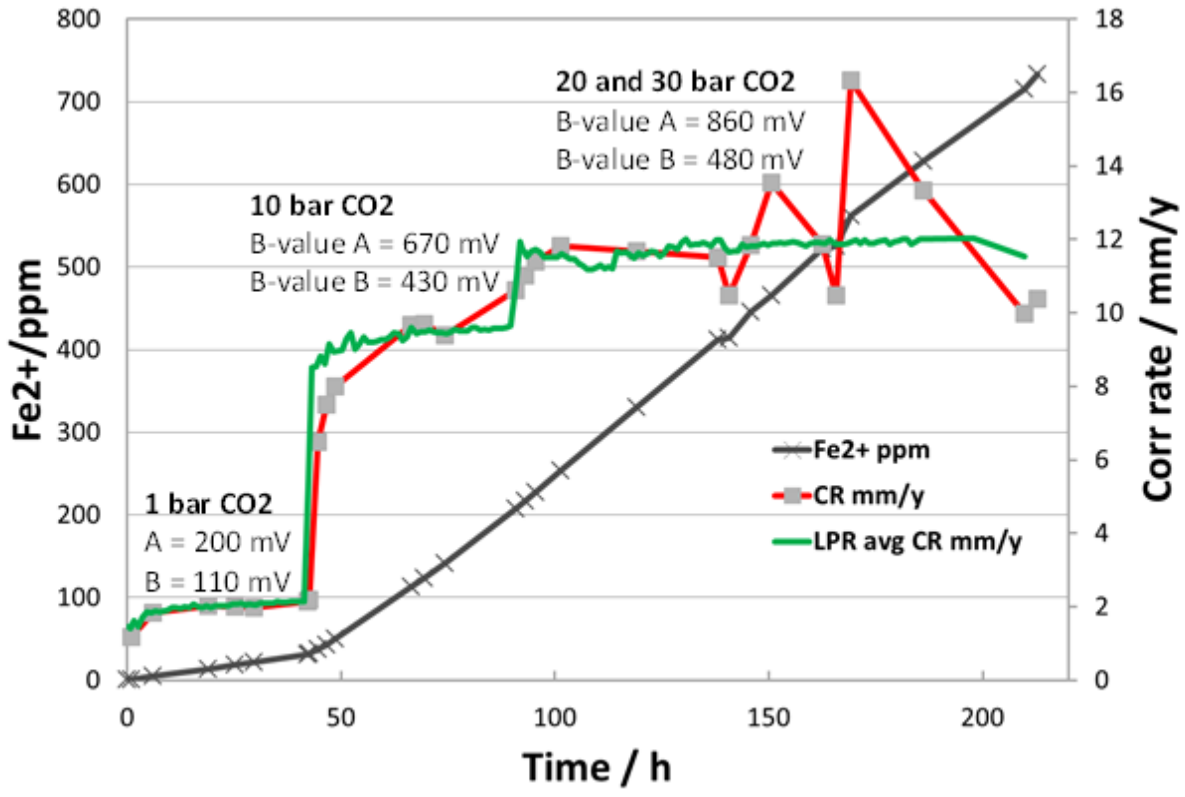

Figure 59 *The diagram shows the dissolved iron in the liquid on the left axis and corrosion rate on the right axis either based on LPR measurement or calculated from the iron count in the liquid.*

The change in CO_2 pressure results in a steep change in LPR value since the new B-value is put in the equation at the time the pressure was changed while the Iron count is measured with different time intervals. The B-values at 1 bar CO_2 was 200 and 110 mV for sample A and B, and at 10 bar CO_2 it was necessary to increase the B-value to 670 and 430 mV for sample A and B, respectively. At 20 bar the B-value had to be raised again to 860 and 480 mV for sample A and B. The change from 20 to 30 bar of CO_2 was done at 138.5 hours, the change gave unstable iron count and for that reason the same B-value were kept.

The sample appearance after the exposure was similar to Geo 01; it was black with some gold color layer on top (see Figure 60A&D). The corrosion film did not stick well to the sample, so that some of the film fell off during sample handling. The SEM picture (see Figure 60B, C, E&F) shows corrosion product on the surface but it looks very cracked and not so protective for the metal surface.

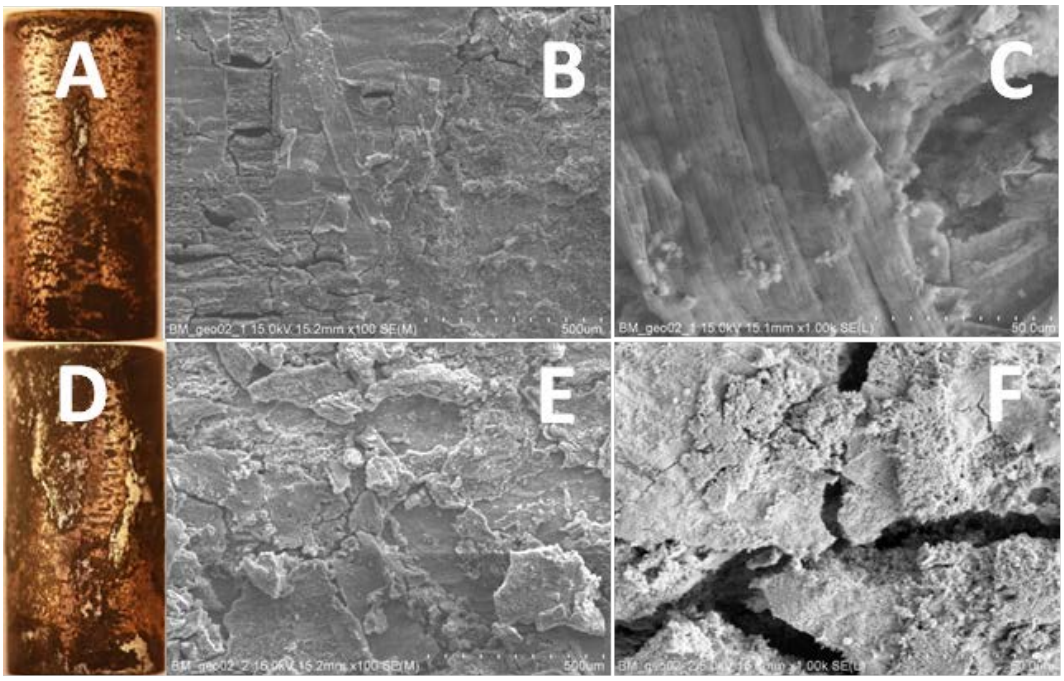

Figure 60 *Optical images (A,D) and SEM (B,C,D,F) images of carbon steel samples exposed in experiment Geo 02 100 times(B&E) and 1000 times(C&F) magnification. The scale bar is in the lower right corner. The optical picture shows a gold color layer on top of black powder film, can also see the bare metal were the film fell off.*

The EDS analysis is shown in Figure 61. When the beam voltage was lowered the scan showed a ratio similar to $FeCO_3$ if we look at the C, O, and Fe. High concentration of copper was detected in the EDS analyses even up to 14 atomic percent in some measurements.

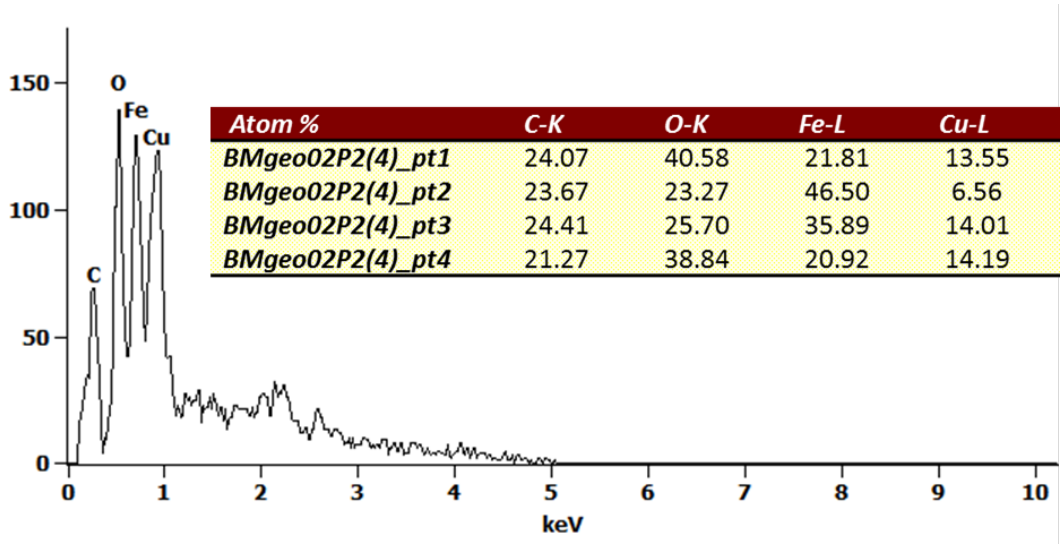

Atom %	C-K	O-K	Fe-L	Cu-L
BMgeo02P2(4)_pt1	24.07	40.58	21.81	13.55
BMgeo02P2(4)_pt2	23.67	23.27	46.50	6.56
BMgeo02P2(4)_pt3	24.41	25.70	35.89	14.01
BMgeo02P2(4)_pt4	21.27	38.84	20.92	14.19

Figure 61 *A spot EDS analysis from the surface of sample B in Geo 02.*

The weight loss of sample A was found to be 180.3 mg/cm^2 and sample B 176 mg/cm^2. The film weight of sample A and B was 3.3 mg/cm^2 and 3.1 mg/cm^2, respectively. This corresponds to an average corrosion rate of 9.3 mm/y for sample A and 9.1 mm/y for sample B.

4.2.2.3 Glass cell test at 1 bar, Geo 03

The high and varying B-values required to fit the LPR data in the loop experiments were surprising. It was therefore decided to perform a glass cell experiment in order to test if similar B-values as in the loop tests were obtained. The temperature during the experiment was 25°C and the system was continuously purged with CO_2 at atmospheric pressure. The iron count and LPR data are shown in Figure 62.

In the beginning of the test (1)(numbers are related to Figure 62) the samples was mounted as in the loop with one sample as reference. No corrosion was detected with either LPR or iron count. After 40 hours a separate reference electrode was installed in the glass cell, but still the LPR did not show a good signal. Then after 42 hours (2 starts) both samples were changed and a new sample C with a new sample holder was installed, and corrosion rate was measured to about 0.7 mm/y. At 74 hours (3 starts) the old sample A replaced sample C, on the new sample holder, then the corrosion rate dropped again to zero. Around 116 hours (4 starts), sample A was dipped in hydrochloric acid and mounted on the loop sample holder. The corrosion rate was measured to 1.0 mm/y. At about 190 hours (5 starts) the separate reference electrode was removed and replaced with sample B as a reference on the loop sample holder, corrosion rate kept at it level. In the end of the test (6), sample B change place with sample A, which now function as a reference for B. The corrosion rate increased slowly to 1.7 mm/y. During these different actions the B-value was kept at 15 mV. Since the samples were put in and out of the system, and dipped in acid, no analyses were done on them after the test. The sample holder had a defective contact on one of the connection places due to this treatment and had to be replaced.

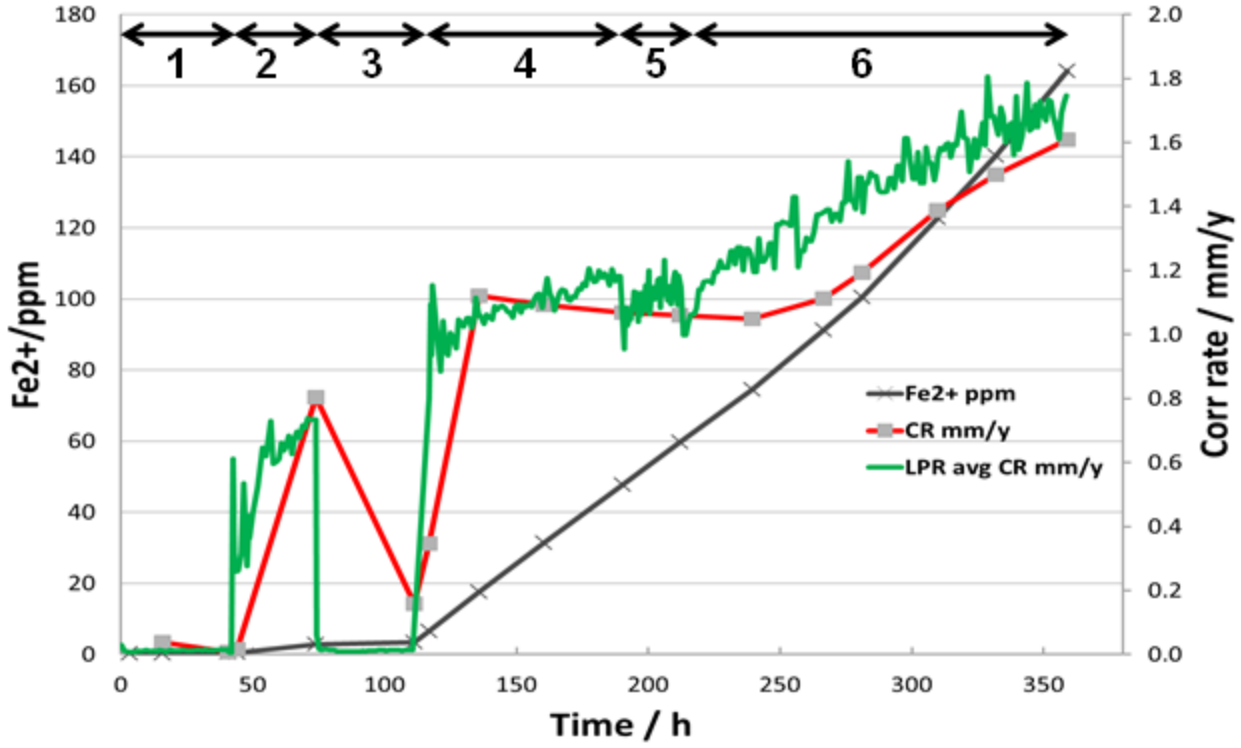

Figure 62 *The diagram shows the dissolved iron in the liquid on the left axis and corrosion rate on the right axis either based on LPR measurement or calculated from the iron count in the liquid.*

4.2.3 Dense phase loop and the second version test section

4.2.3.1 Experiment Geo 04 - corrosion test with ramping pressure

The sample connection point and the sealing between the samples were improved, so the connection point was more stable and dry. The measured iron and LPR from experiment Geo 04 are presented in Figure 63. Four different CO_2 pressure levels were tested and gave distinct levels off corrosion. The LPR measurements are adjusted with a B-value (Equation 22) to have a good corresponds with the iron count values. The sample was change after 88 hours to inspect the sample holder and new samples were mounted, but the iron count measurement was very unstable after this and it was not possible to make a good fit for the LPR measurements.

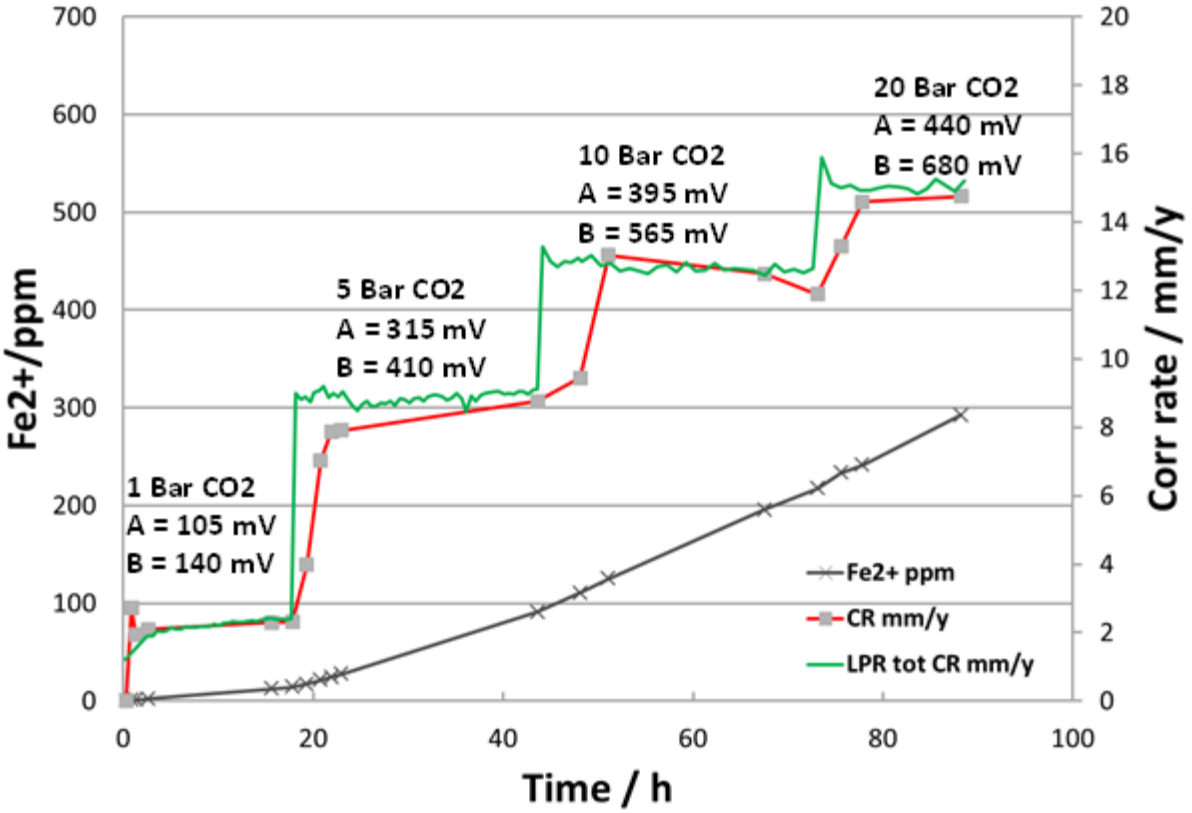

Figure 63 *The diagram shows the dissolved iron in the liquid on the left axis and corrosion rate on the right axis either based on LPR measurement or calculated from the iron count in the liquid. The experimental parameters for Geo 04 were 25°C and 0.65 m/s flow.*

The sample was black with some orange area on top of the surface (see Figure 64A&D). The corrosion film did not stick well to the metal sample and just as for the previous Geo experiments some of the corrosion film fell off during handling of the samples. The SEM picture (see Figure 64B, C, E&F under) shows corrosion product on the surface. The film has a lot of cracks and is not so protective for the metal surface.

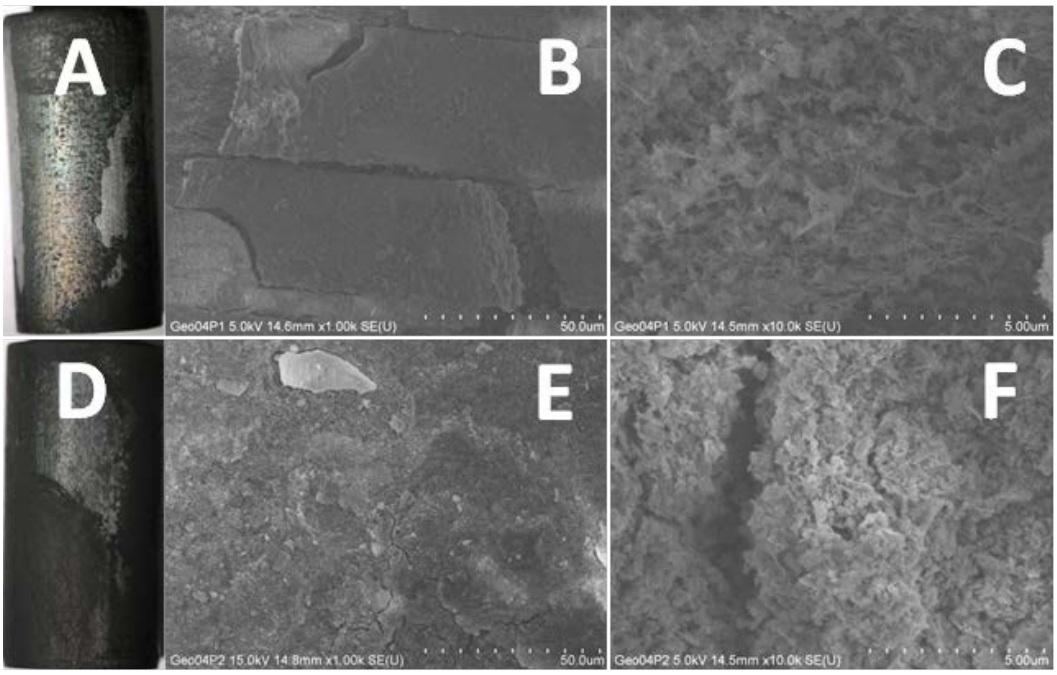

Figure 64 *SEM(B,C, D&F) and optical camera picture(A&D) of carbon steel samples exposed in experiment Geo 04 at 100 times(B&E) and 1000 times(C&F) magnification. The scale bar is in the lower right corner. The optical pictures show a colored layer on top of black powder film. Bare metal can be seen were the film fell off.*

The EDS analysis is shown in Figure 65. When the beam voltage was lowered to 5 KeV the ratio between C, O, and Fe was corresponding to $FeCO_3$. Also in this experiment copper contamination occurred.

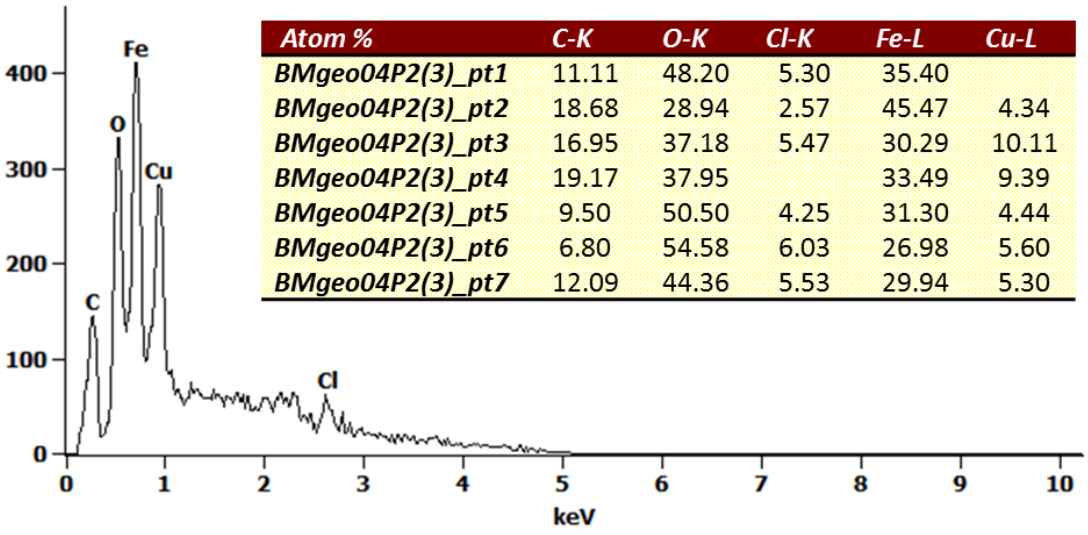

Atom %	C-K	O-K	Cl-K	Fe-L	Cu-L
BMgeo04P2(3)_pt1	11.11	48.20	5.30	35.40	
BMgeo04P2(3)_pt2	18.68	28.94	2.57	45.47	4.34
BMgeo04P2(3)_pt3	16.95	37.18	5.47	30.29	10.11
BMgeo04P2(3)_pt4	19.17	37.95		33.49	9.39
BMgeo04P2(3)_pt5	9.50	50.50	4.25	31.30	4.44
BMgeo04P2(3)_pt6	6.80	54.58	6.03	26.98	5.60
BMgeo04P2(3)_pt7	12.09	44.36	5.53	29.94	5.30

Figure 65 *A spot EDS analysis from the surface of sample B in Geo 04.*

The weight loss of sample A was found to be 87 mg/cm^2 and sample B 71 mg/cm^2. The film weight of sample A and B was 1.1 mg/cm^2 and 1.1 mg/cm^2, respectively. This corresponds to a corrosion rate of 10.6 mm/y for sample A and 8.7 mm/y for sample B.

A sample was molded in epoxy and cut so the cross section could be studied in the SEM to determine the film thickness (Figure 66). The film looks fluffy and the thickness vary a lot, but the average thickness was about 5 µm and this is also confirmed by the weighing of film (see Table 22) which gave a thickness of 3.6 µm.

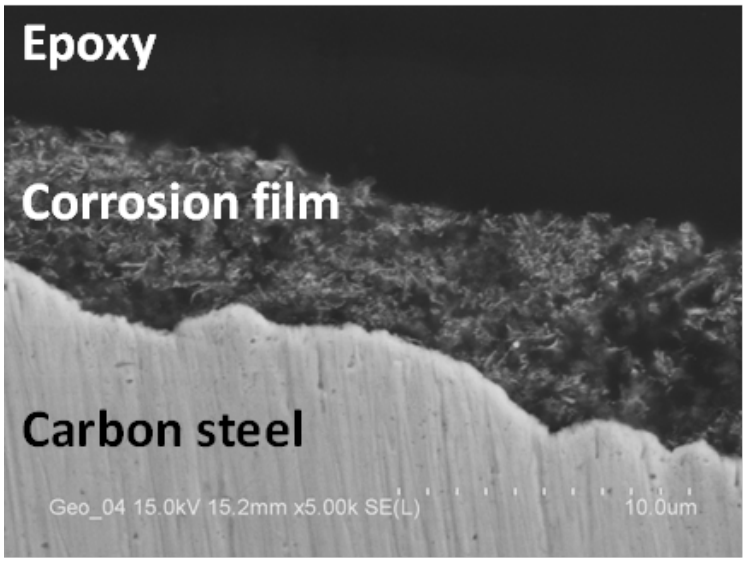

Figure 66 *The cross section of a molded sample Geo 04. The dark area is epoxy, the white area is carbon steel, while the area in the middle is the corrosion film.*

4.2.4 Dense phase loop and the third version

4.2.4.1 Experiment Geo 05- corrosion test with ramping pressure

The previous test sections used the metal casing of the test section as counter electrode, but in the new version a PEEK cylinder covers the samples. The measured of iron and LPR are presented in Figure 67. In this experiment there was only LPR measurements on one sample, the second sample was dedicated as a reference electrode.

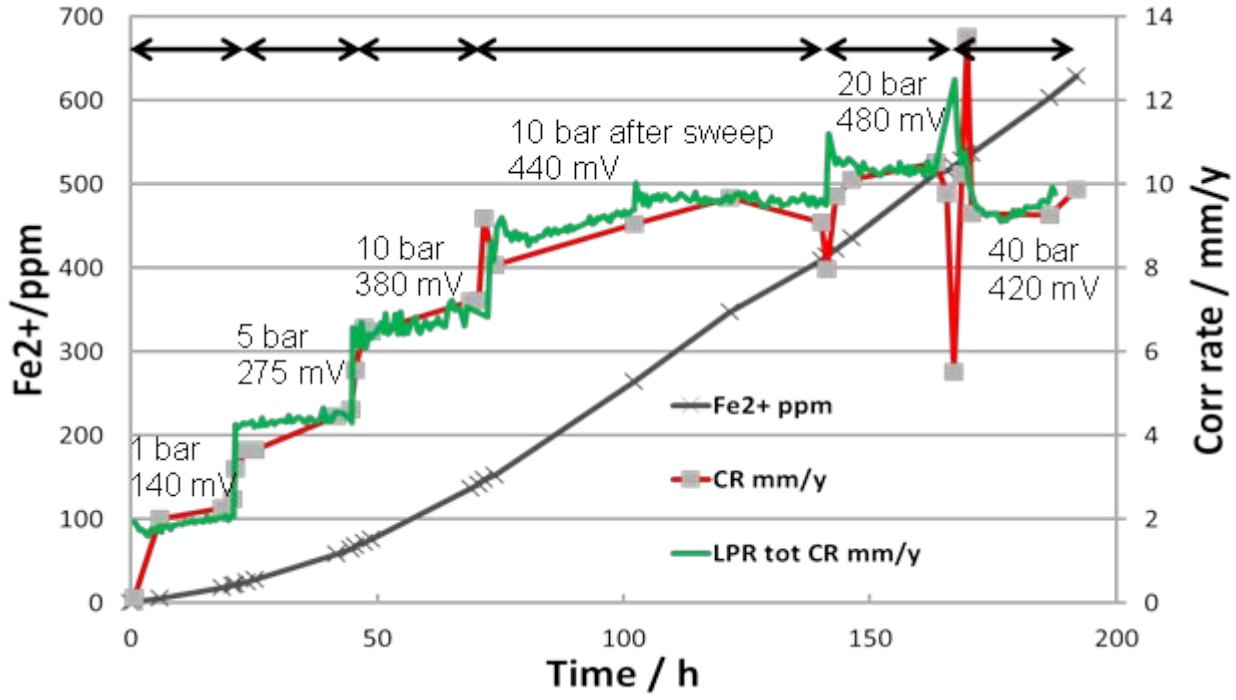

Figure 67 *The diagram shows the dissolved iron in the liquid on the left axis and corrosion rate on the right axis either based on LPR measurement or calculated from the iron count in the liquid. The experimental parameters for Geo 05 were 25°C and 0.65 m/s flow.*

Five different CO_2 pressure levels were tested and they gave distinct levels off corrosion. The LPR measurements are adjusted with a B-value (Equation 22) to have a good correspondence with the iron count values. Two sweeps (cathodic-anodic) were performed, the first sweep was done after 69 hours at 10 bars and the second after 164 hours. Both sweeps influenced the iron measurement, the most evident change was after 69 hours where the corrosion rate increased from 7 mm/y to 9 mm/y after the sweep. There were also some irregularities in the measurement after the second sweep. However, there the pressure was also change shortly after the sweep and this makes it difficult to decide which one of the changes to the system influenced the corrosion most.

After the experiment the sample was black (see Figure 68A&D) and the corrosion film did not stick well to the metal sample, some of the film fell off during sample handling. The SEM picture (see Figure 68B, C, E&F) shows corrosion products on the surface but it looks very cracked up and not so protective for the metal surface.

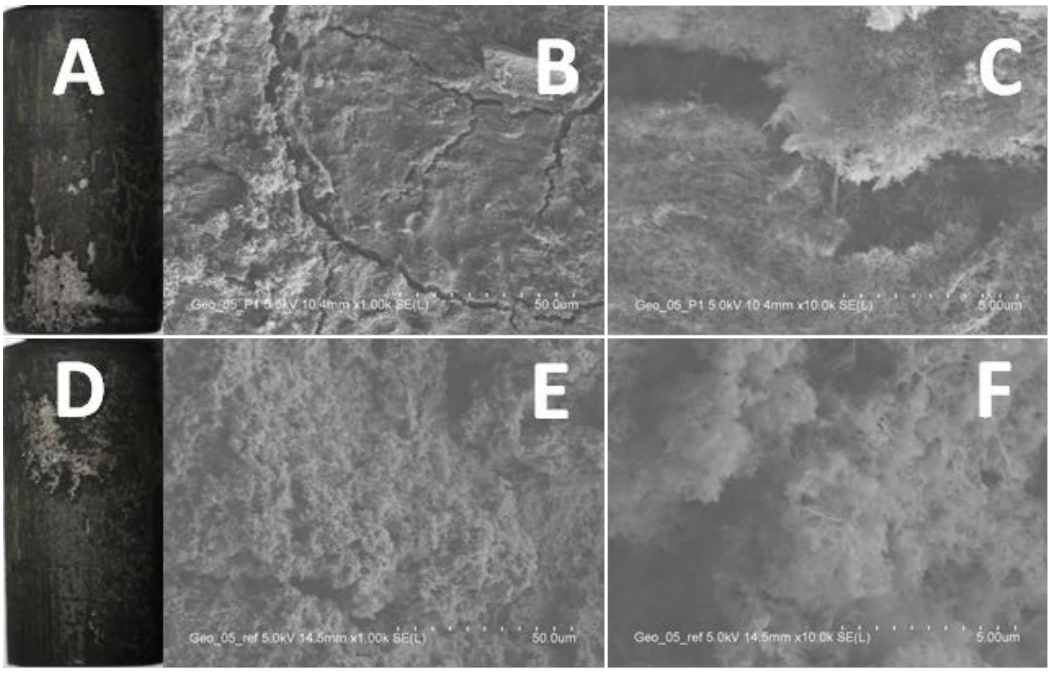

Figure 68 *SEM(B,C, D&F) and optical camera picture(A&D) of carbon steel samples exposed in experiment Geo 05 at 100 times(B&E) and 1000 times(C&F) magnification. The scale bar is in the lower right corner. The optical picture shows some rust color in the cracks of the film which occurred after the experiment while waiting for analysis, can also see the metal were the film fell off.*

The ratio of C, O, and Fe from the EDS analysis is shown in Figure 69 corresponds to $FeCO_3$. There was found a high copper concentration in the EDS analysis up to 9 atomic percent in some measurements and some chloride was also so found.

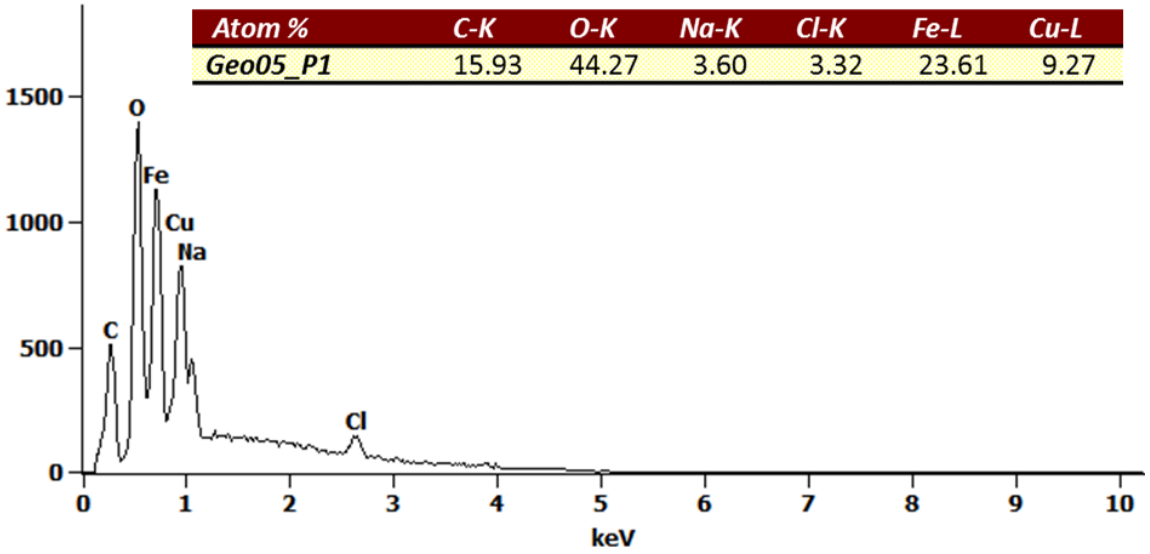

Figure 69 *A spot EDS analysis from the surface of sample X in Geo 05.*

The weight loss of sample A was found to be 133 mg/cm^2 and sample B 146 mg/cm^2. The film weight of sample A and B was 1.2 mg/cm^2 and 1.4 mg/cm^2, respectively. This corresponds to an average corrosion rate of 7.7 mm/y for sample A and 8.4 mm/y for sample B.

4.2.5 B-values from sweep

This chapter will show two anodic/cathodic sweeps performed during the experiments. The B-values are calculated by fitting the sweep curve to Equation 20 and they all are lower than those calculated from the LPR fitting.

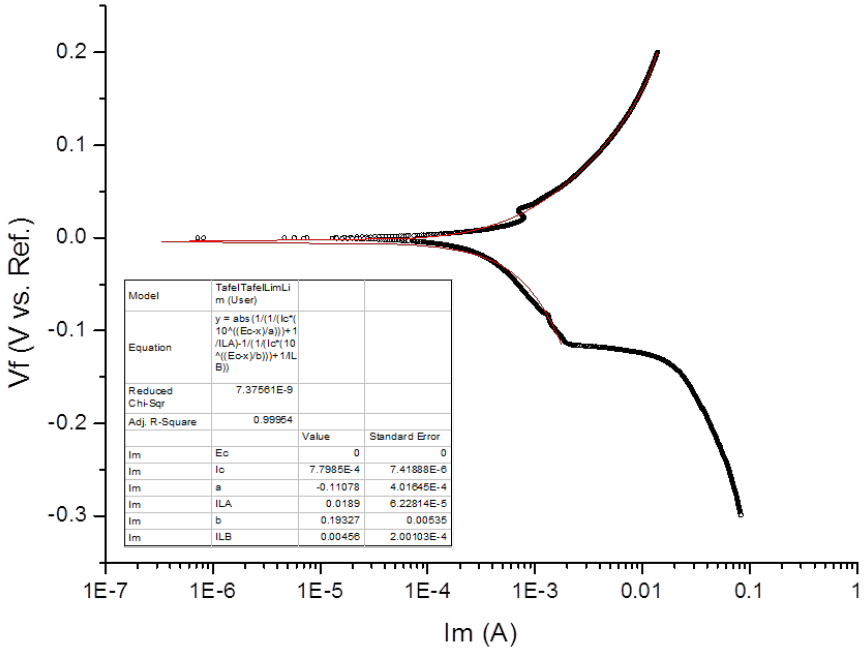

Figure 70 *A anodic and cathodic sweep during experiment Geo 04 at 95 bar of pressure. The B-value found from the fitting was 30.4 mV and corrosion rate 1 mm/y.*

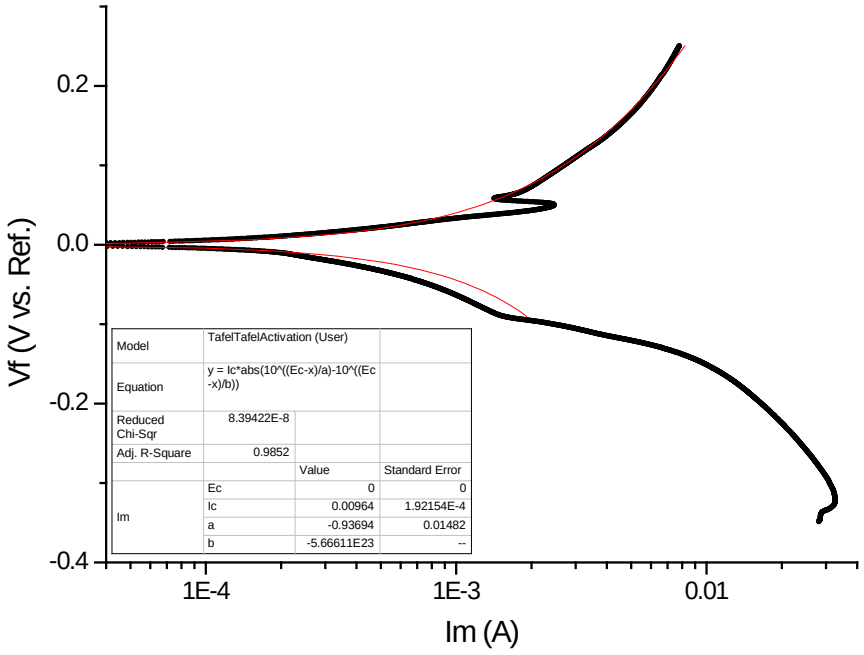

Figure 71 *A anodic and cathodic sweep during experiment Geo 02 at 30 bar of pressure. The B-value found from the fitting was 65.7 mV and corrosion rate equal 1.7 mm/y.*

4.2.6 Summary of data, corrosion rates and B-values

Table 22 *The sample weights before experiments, weight before and after stripping, surface area of the samples, the calculated average film thickness, and average corrosion rate.*

	Geo 01		Geo 02		Geo 04		Geo 05	
	A	**B**	**A**	**B**	**A**	**B**	**A**	**B**
Start mass, g	14.3288	13.6405	14.0252	13.4929	14.3033	13.7895	13.8836	14.0123
After exp. mass, g	13.3016	12.7372	12.3972	11.9598	13.5038	13.1534	12.6838	12.6904
After strip mass, g	13.288	12.7292	12.3665	11.9319	13.4938	13.1437	12.6733	12.6777
Film mass, g	0.0136	0.008	0.0307	0.0279	0.01	0.0097	0.0105	0.0127
film thickness, um	4.9	3.0	11.1	10.5	3.6	3.6	3.9	4.6
Total mass loss, g	1.0408	0.9113	1.6587	1.561	0.8095	0.6458	1.2103	1.3346
Surface area, cm^2	9.349	9.01	9.199	8.859	9.312	9.048	9.085	9.161
CR, mass, mm/y	10.4	9.4	9.4	9.2	10.8	8.8	7.7	8.5

The corrosion rates and B-values found in the experiments by either weight loss or iron count measurements are summed up in Table 23.

Table 23 *Corrosion rates and B-values (Stearn-Geary constant) determined from iron measurement in the water phase. The LPR measurements are forced to fit the iron measurements and then the B-value is read out.*

Trykk bar	CR, Iron mm/y	Stearn-Geary B-value, mV	Exp. name
1	2.2	200	geo02_P1
1	2.1	110	geo02_P2
1	1.1	15	geo03_P1-P3
1	2.6	105	geo04_P1
1	2.1	140	geo04_P2
1	2.0	140	geo05_P1
1	2.2		geo05_P2
5	9.6	315	geo04_P1
5	7.9	410	geo04_P2
5	4.4	275	geo05_P1
5	4.8		geo05_P2

Trykk bar	CR, Iron mm/y	Stearn-Geary B-value, mV	Exp. name
10	9.6	670	geo02_P1
10	9.4	430	geo02_P2
10	13.6	395	geo04_P1
10	11.1	565	geo04_P2
10	6.7	380	geo05_P1
10	7.3		geo05_P2
10S	9.0	440	geo05_P1
10S	9.8		geo05_P2
20	12.0	860	geo02_P1
20	11.7	480	geo02_P2
20	16.2	440	geo04_P1
20	13.3	680	geo04_P2
20	9.9	480	geo05_P1
20	10.9		geo05_P2
40	9.0	420	geo05_P1
40	9.8		geo05_P2
100	11.8	730	geo01_P1
100	10.8	350	geo01_P2

The corrosion rate and B-values in table above are shown in Figure 72 and Figure 73.

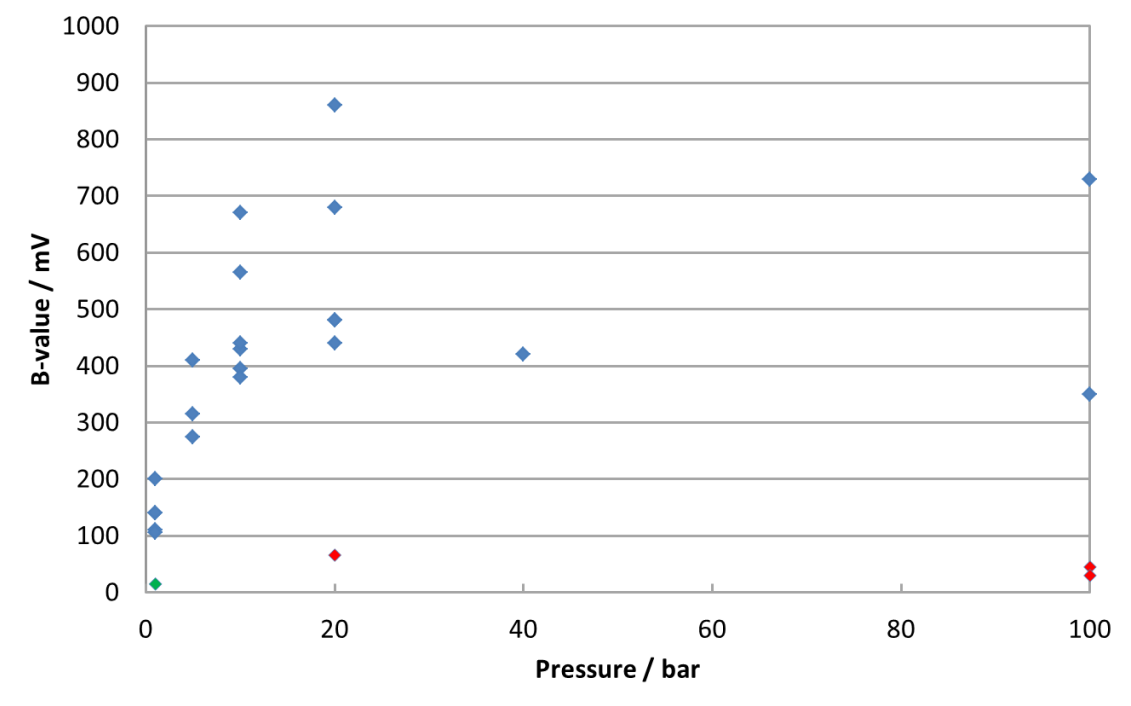

Figure 72 *The B-values plotted as a function of pressure, from Table 23. Red markers indicates B-values found by sweeps and the green marker indicates B-value found in the glass cell experiment.*

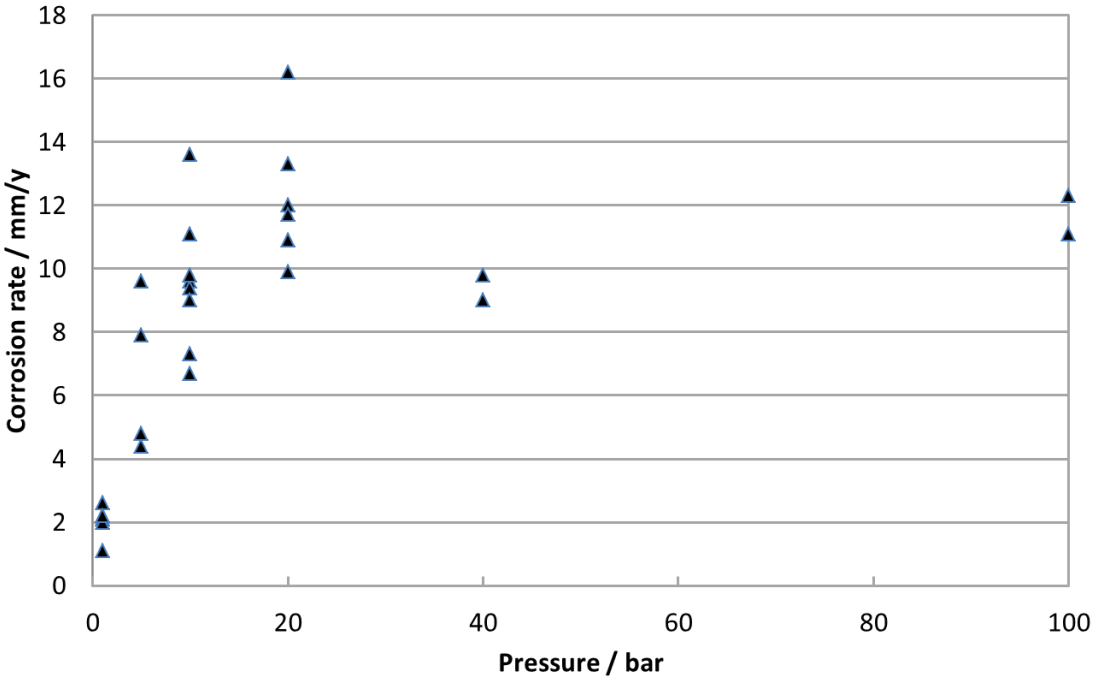

Figure 73 *The corrosion rates plotted as a function of pressure, from Table 23.*

5. Discussion

Two essentially different approaches were used to test corrosion of carbon steel with high pressures of CO_2. The first approach was corrosion in dense phase CO_2 with small amounts of water dissolved and the second one was corrosion in water equilibrated with dense phase CO_2. It is important to distinguish between these two situations because the corrosion behavior is fundamentally different.

One of the main aims of the thesis was to develop experimental equipment which could perform experiments in dense phase CO_2 containing water levels up to the solubility limit. This has been accomplished and for the first time experiments have been performed with full control of the dosed water concentration in the test loop. The experiments showed good stability on both the measurements and the dosing.

The corrosion rates determined in these experiments was very low. While the corrosion rates found in the free water phase experiments was very high and pressure depended up to 20 bars of CO_2, and then they stabilized for further increase of pressure.

5.1 Equipment and analyzing techniques

5.1.1 Controlling the amount of dissolved water in dense phase CO_2

The flow of the fluid over the samples creates a share stress to mimic the real situation in transport pipelines. There is a difference for the corrosion rates between static experiments and experiments with stirring for free aqueous phase [8, 32]. The fluid flow transports the corrosion products away from the surface and corrosive phase forms continuously on the metallic surface.

Most of the published papers on corrosion in dense phase CO_2 with dissolved water are based on injection of liquid water in an autoclave before adding CO_2. Very few actually analyzed the CO_2 to check the resulting water content. Thus it is possible that the water was unevenly distributed inside the test equipment and consequently the reported experimental conditions can be incorrect.

An important part of this project was to build a system with accurate water dosing and an accurate analyzer for monitoring the levels of water. The results showed that it was possible to have good control of the water content (Figure 34) and there was good agreement between the measured and theoretical concentrations. The water dosing could maintain a stable concentration of 500 ppmv for over 11 months without any refill, which makes it possible to perform long term experiments.

However, some limitations of the system were also observed and they will be discussed in the following chapters.

5.1.1.1 Pressure oscillation in the water dosing unit

The dosing unit was based on the dilution of wet CO_2 with dry CO_2 and therefore temperature and pressure was important. The water content in dense phase CO_2 is highly dependent on both temperature and pressure (Figure 5). The temperature of the humidifier tank (Figure 12) was controlled by a thermostat and the pressure was controlled by a piston pump. When the piston retracted for refill there was temporarily a pressure drop of about 1 bar in the system. The pressure drop reduced the solubility of water in CO_2 and could therefore result a small variations of the water content in the final mixed CO_2. Two heated expansion tanks were included in the system to lower this pressure drop and minimize the effect on the experiments. The temperature in these tanks was around 40°C and the CO_2 was super critical. Super critical CO_2 is more compressible than liquid CO_2 and this allowed small volume changes to pass without giving a large pressure drop, as would be the case in liquid CO_2. Another challenge was connected with the liquid pressure regulator which was mechanical and controlled the pressure for the dosing line and the loop. The regulator had a loading spring which let in more liquid when the pressure was low. There were some delays in this spring load system and when it first opened the set pressure could be temporarily exceed which resulted in a pressure oscillation. When more liquid CO_2 is let in by the regulator, the water concentration will be lowered, but since it is oscillating and the loop volume (2160 ml) is large compared to the dosing rate (1.2 ml/min), it will not significantly affect the water concentration in the loop.

5.1.1.2 Temperature fluctuation

The system was rather sensitive to variations in the temperature, but changes were relative small. An example from the Solu 04 experiment is shown in Figure 74. The loop-room, the dosing unit, transport lines, and the cabin that surrounds the loop were all temperature regulated, but each with a different control system.

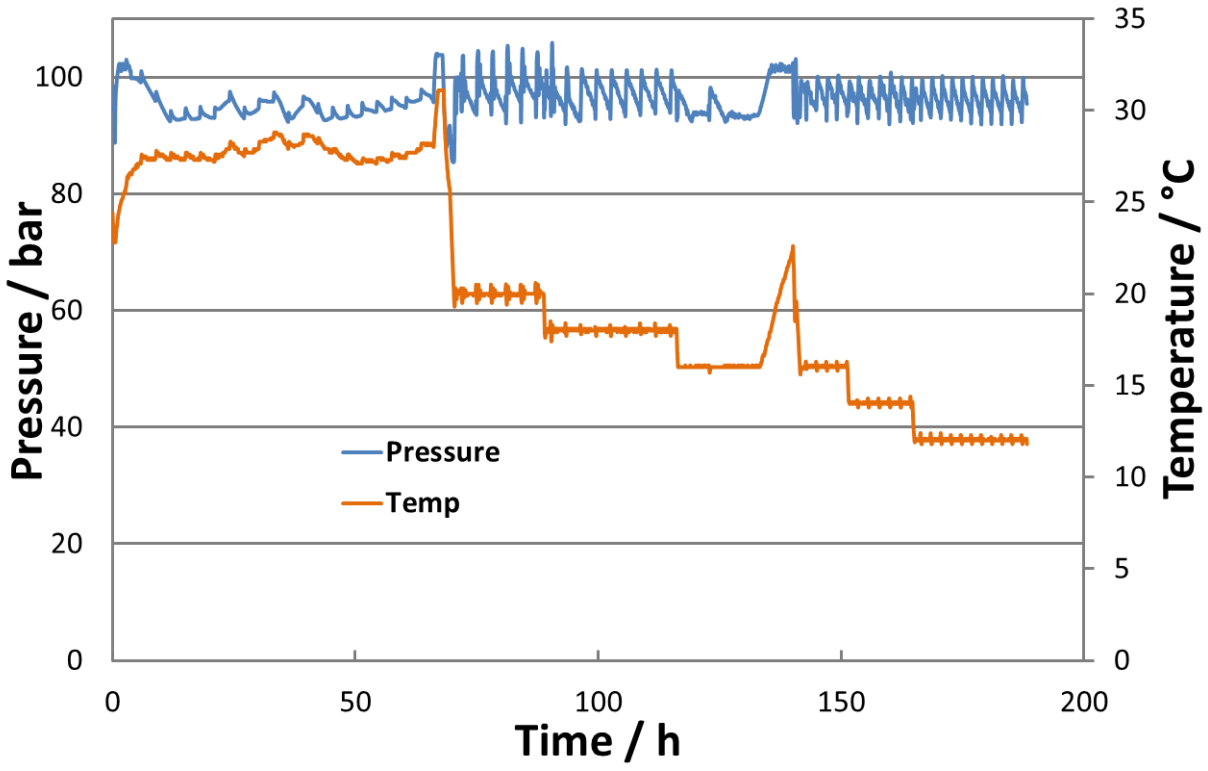

Figure 74 *The temperature and the pressure of experiment Solu 04.*

Figure 74 shows the temperature (orange line) at the right axis and the pressure at the left axis (blue line). In the beginning (the first 60 hours) the temperature difference between the loop cabin and the room was small, both were set to 20°C (room temperature held at 20°C at all time). This gave small changes in temperature and pressure when the defrost function of the cooling unit on the cabin started (3 hours cycle). Then the temperature decreased which affected both the density of the CO_2 and the temperature difference between the room and the cabin (cabin temperature was 12°C below the wanted set point). This makes the pressure inside the loop even more sensitive and this we can observe in the diagram above starting from 60 hours. The temperature fluctuated ±0.5°C from the set point at the defrost periods. But the pressure was fluctuating around ±6.5 bars in the same periods. By minimizing the temperature difference between the temperature set point and the cabin, the temperature and pressure fluctuation became ±0.3°C and ±3.5 bars. An attempt to extend the period between the defrost function was done at 116 hour. It worked for 17 hours before the cooling unit was clogged with ice, but the pressure was not fluctuating during this period. Nitrogen flushing of the cabin was also tried but without any success. These fluctuations give the water measurements the saw tooth shape and the water concentration increases with about 20 ppmv before it decreases

again. Since the temperature variations, this would probably not influence the results from the experiments.

5.1.1.3 Heated pressure regulator

The measured water concentration was affected by the temperature inside the gas regulator. Although the average measured concentration was the same it was fluctuating if the temperature was too low. The fluctuation stopped if the temperature was increased, as shown in (Figure 14, Solu Blank). The pressure regulator could be filled with products from the experiment and this could influence the performance in two important ways. First, if the regulator was partly blocked it would give a pulsating flow through the regulator and the low pressure side will fluctuate, leading to a fluctuating and wrong water measurements. Secondly, if the products were situated in-between the poppet valves it would gradually open for more media to go through and the pressure on the low pressure side would increase, causing erroneous water measurements. Figure 34 shows an example of this; after 215 hours the pressure fluctuated until the pressure was too high for the massflow controller and the system was shut down (open area in the diagram). This happens more frequently in experiments with several impurities reacting and creating products.

5.1.1.4 Massflow controllers

Two massflow controllers were used. The one controlling the ventilation rate to the analyzer was set to 1.1 g per minute in all experiment. According to the producer the mass flow controllers had an accuracy of ±0.5 percent of the value and a control stability of ±0.1 percent of the full scale, which equals to about ±0.004 g per minute. It was very important for the water dosing that the ventilation rate was stable, since all changes will affect the amount of dry CO_2 into the loop. If the dry CO_2 rate changed, the water level would change. Normally this sudden change of the ventilation rate should not happen. It has been observed when the heated pressure regulator failed and the low pressure (2-3 bar) side increases to higher pressures (30-60 bar), that the massflow controller get a sudden change in the calibrated value. This is very hard to notice since the set point at the massflow controller is the same, while the amount going through changes. All changes in the ventilation rate will only affects the amount of dry CO_2, since wet CO_2 is controlled by set point of flow rate and not pressure as dry CO_2, therefore the dosed water concentration (dry CO_2 + wet CO_2) in the end be affected.

The wet massflow controller worked fine during all experiments. It is important that the pressure drop over the controller is not too high since this will lead to lower water solubility and the water could accumulate inside the controller and eventually block the valve. The

temperature should be the same or higher for the controller than for the humidifier. When maximum water level is required, the wet massflow controller is set to 1 g/h under the ventilation rate. This was necessary because of the pressure fluctuation of the liquid pressure regulator and to avoid pressure build up in the system. During the maximum water level the CO_2 has the shortest retention time in the humidifier and could for this reason hold lower water concentration.

5.1.2 Water measurements

The TDLS worked excellent for the continuous water measurements. The results were stable and accurate as long as the sampling was good. Pressure had the largest influences on the measurements as shown in Figure 34. After 286 hours an increase of the pressure in the TDLS sample chamber is observed as a rapid increase in the water concentration. This shows the importance of holding the pressure stable inside the analyzing tube at all time. The calibration was valid only for a given pressure, and if the pressure changed a new calibration should be made. The measured water concentration was almost proportional to the pressure in the laser tube up to about 10 bar. At higher pressure the proportionality was lost, most likely because CO_2 behaved more and more different from an ideal gas for increasingly higher pressures. The TDLS was not affected by contamination or corrosion products since the laser was locked on a wave length unique for water. Even when the sapphire windows separating the laser from the analyzing tube were smudged the laser worked fine. The transmission rate of the laser was logged to be able to detect this. If the transmission rate had become as low as 10 percent, some maintenance should have been performed. That was, however, not necessary during this work.

A weakness of the analyzer was that it would always give a signal and if there was not control of all the parameters, as mention above, the value could be completely wrong. Thus, keeping track of the sampling parameters was very important to get reliable measurements.

5.1.2.1 Leakage

The high pressure impurities loop for dissolved water was mainly built of Hastelloy C 276, a material which is considered hard to machine and has a tendency to be smeared due to the metal friction when fittings are mounted. The loop had over 40 Hastelloy fittings and over 80 stainless steel (SS316) fittings, all of them could be considered as a potential leaking point. Soft material is often used in valves as packing. There are 6 Hastelloy valves with Teflon as packing material and the control valve for wet-dosing had Kalrez© as packing material. Dense phase CO_2 has a tendency to be adsorbed by soft material and even material that are considered as CO_2

resistant may swell if the material goes through a rapid depressurization. Cycling of pressure and temperature for soft material can eventually lead to a leakage.

Normally a leakage would not affect the experiment unless a high water concentration is required. The effect will be the same as for the change in ventilation rate, since the wet dosing unit delivers a fixed flow all leakage will be compensated by an increased flow of dry CO_2 which tries to hold the pressure constant. An example; the wet CO_2 has a concentration of 3000 ppmv of water, the wet dosing rate is 54 gram per hours, and the total ventilation flow is 65 gram CO_2 per hours (using dilution calculating), the concentration going in the loop will then be 2500 ppmv. If all fittings have together a leak of about 5 gram per hours which increases the total ventilation flow to 70 gram CO_2 per hours, the concentration now going to the loop is 2300 ppmv of water.

We did not manage to get up to the solubility limits of water in CO_2, the reason might be caused by small leakage in our system or because of the retention time in the humidifier, we cannot rule out one or the other.

5.1.3 Flow loop with free water phase

5.1.3.1 Iron measurement

The Dense Phase flow loop had a reservoir tank of 6 liters. The tank was essential when varying the liquid volume and gas volume in the system. The large liquid volume allowed large amounts of iron to dissolve before saturation of iron carbonate was reached. The solubility is strongly temperature dependent, but the composition of the aqueous phase is also important. If iron precipitates the Fe^{2+} measurements can no longer be used for calculating the corrosion rate. The most common technique for measuring corrosion rate is weight loss. The weight loss gives the average corrosion rate through-out the whole experiment. To reduce the number of experiments it was decided to alter the CO_2 pressure several times during one experiment, doing this the average corrosion rate based on the weight loss cannot be used to determine the in-situ corrosion rates needed do calculate the Stern-Geary constant, B-value.

The iron measurement was therefore used to estimate the in-situ corrosion rate by calculating the difference in iron concentrations over a known period of time. Very accurate values for the corrosion rate can be obtained as long as insignificant precipitation of iron containing products takes place. The total amount of iron (including the iron taken out for analyzing) measured was compared with the weight loss after the experiment (Table 21). For the two experiments without anodic and cathodic sweep the results were similar, but there was some deviation for

the other two experiments. If the deviation was caused by the sweeps, precipitation or other reasons are not known, still the method proves to be within acceptable accuracy.

The iron method is well known and often used in many laboratories and our method was based on the Norwegian standard, NS 4741.

5.1.3.2 Electrochemical setup

Measuring corrosion rates with LPR is quite common and the ASTM G102 standard explains how to relate electrochemical measurements to mass loss rates. The Stern-Geary constant, B-value, must be calculated and there are several ways do this. In the present work, the B-value was calculated from mass loss and polarization resistance. The mass losses were calculated from the iron concentration in the liquid. Some Tafel plots were made by plotting the cathodic and anodic sweeps and the B-value was calculated from them. The results indicated good contact between the connecting cables and the samples throughout all experiments. The electrodes (samples and test section wall) seemed to have good contact in all tests. The cable and the potentiostat were tested with a dummy cell and performed as expected.

5.1.3.3 Test section and sample holder

The difference between the first and the second sample holder was the electrode connection point; the second version had a larger contact area between the sample and the wire, and the contact area was dry during the experiment. It could mean that the corrosion of the wire was more likely in the first version, the wire was also damage and the inner copper core was visible. This probably happened when the sample was mounted and it scratched the wire as it was slide onto the holder.

The last sample holder had a dedicated counter electrode made of platinum and the whole measuring area was isolated from the rest of the test section. The motivation was to see if another type of counter electrode material gave different results. Turned out not to be the case. The mounting and disassembling was by fare improved with these three sample holders compared with older versions from IFE and experiments with weight loss and iron measurements were easier to conduct.

5.2 Discussion of results

5.2.1 Free water phase with dissolved CO_2

5.2.1.1 Corrosion rates

Figure 75 shows the average corrosion rate obtained from iron measurements (Table 23) for different pressures tested in the experiments. The corrosion rate increased with increasing CO_2 pressure until it reached 20 bar, above which rate stabilized at a slightly lower level.

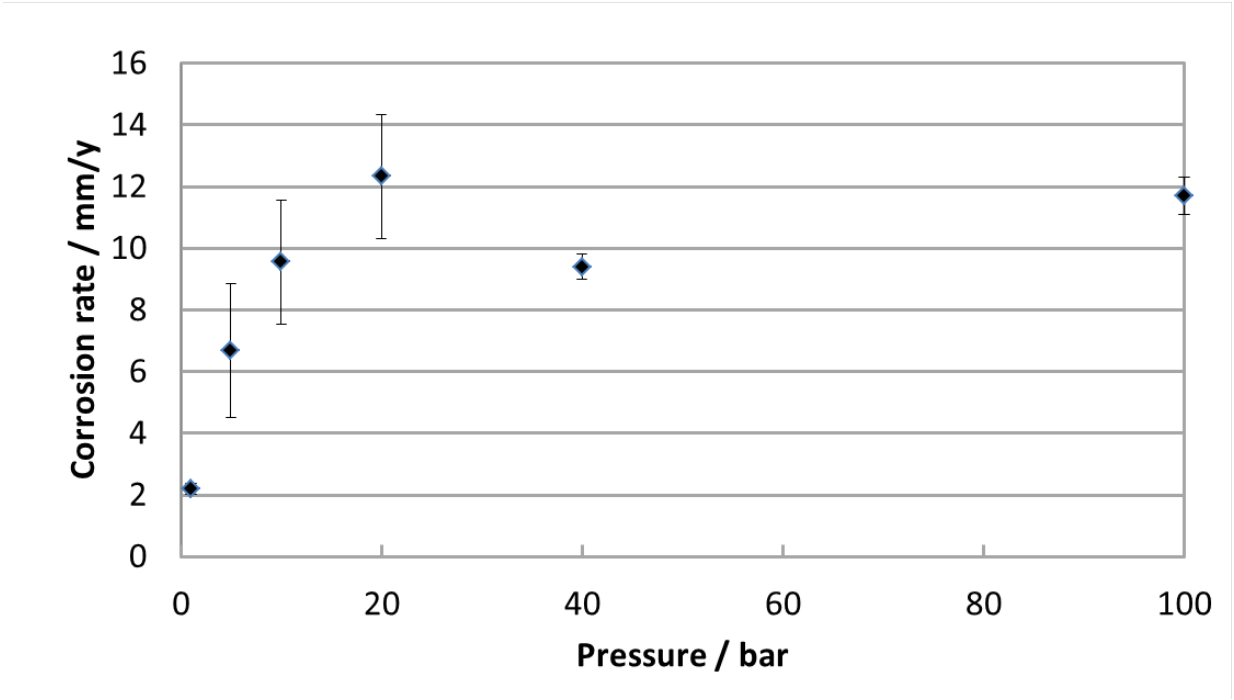

Figure 75 *Average corrosion rates as a function of CO_2 pressure. The corrosion rates were obtained by iron measurements. The error-bars represent ± one standard deviation.*

The present results are in good agreement with previously published data for corrosion at low CO_2 pressure (Table 4). Declining corrosion rates with increasing CO_2 pressures has been observed before [70] and it was indicated that another corrosion mechanism occurs at high pressures. Seiersten et al. reported a corrosion rate of 5.6 mm/year under stagnant conditions with 10 bar CO_2 (40 °C) whereas it decreased to below 1 mm/year at 95 bar CO_2 with the same temperature. The low corrosion rate at the highest CO_2 pressures is different from the present results, and it can be explained by the flow effect. Firstly the flow will enhance the transport of corrosive species toward and away from the metallic surface. Secondly the flow can remove protective film/product from the surface as they are formed. The SEM investigation of exposed

samples showed a porous nonprotective film with a thickness of 3-11 µm, which could indicate that the corrosion rate is higher than the precipitation rate at the steel surface. At 25°C the precipitation rates can be very slow, but the increase of pH due to the corrosion process will increase the precipitation rates due to lower solubility of iron carbonate with increasing pH [52]. Figure 76 shows the correlation between the pressures, solubility of CO_2 in the aqueous phase, and the pH.

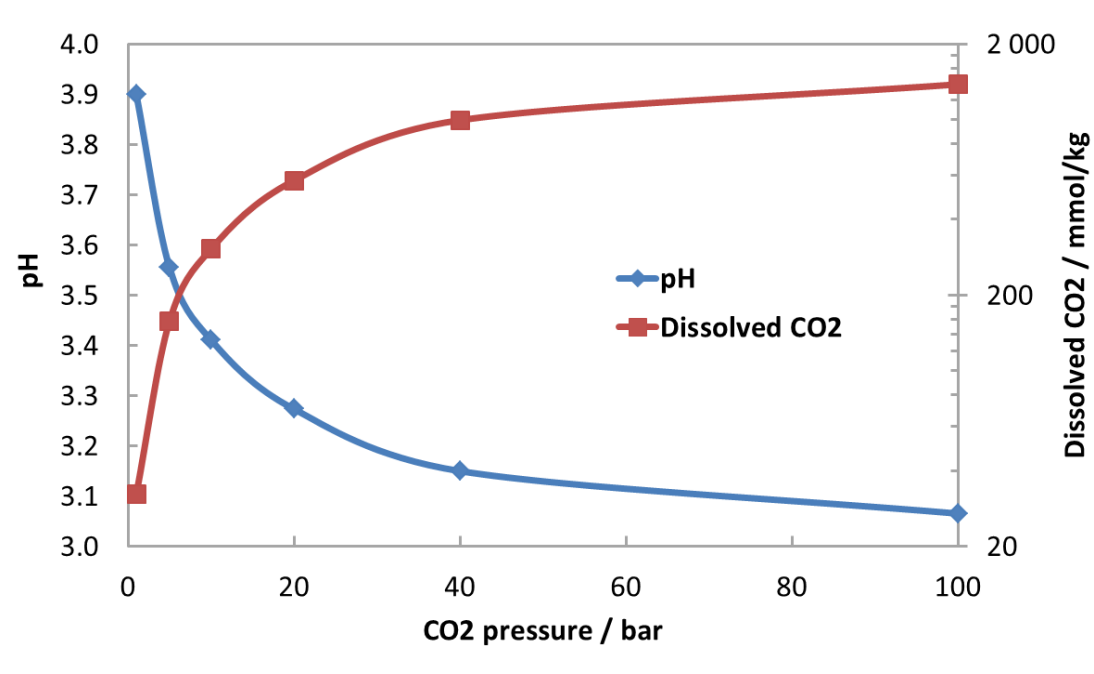

Figure 76 *Dissolved CO_2 (sum of CO_2, H_2CO_3, HCO_3^- and CO_3^{2-}) and pH as a function of pressure. The calculation was carried out with MultiScale.*

The experiments up to 40 bar CO_2 were carried out as experiment in series without changing the loop liquid. This means that a lot of corrosion products already were present in the loop liquid. The increase of Fe^{2+} in the aqueous phase will increase the pH due to formation of bicarbonate when steel corrodes. This increase in pH will lead to increased likelihood for precipitation of iron carbonate which might explain the drop of corrosion rate at 40 bar, since the accumulated iron concentration in the liquid was high at this measurement (measured in the end of Geo 05, Figure 67, 600 ppm of Fe^{2+} in the liquid).

5.2.1.2 B-value

The Stern-Geary constant was calculated from the iron measurement and it shows the same trend as the corrosion rates, compare Figure 77 and Figure 75. The B-values have a large spread

and changes a lot when the pressure is changed. There are also large differences in the B-values calculated from the iron measurements and those determined from anodic/cathodic sweeps. The sweep values give corrosion rates which are one order of magnitude lower than the iron measured corrosion rate. Their error is consistent and this leads to believe that there is something wrong with the setup in the loop.

The glass cell experiment with 1 bar CO_2 was carried out to elucidate this discrepancy. The resulting B-value was 15 mV and the corrosion rate was the same for both LPR and iron measurements. A B-value of 15-20 mV been used at IFE for the electrochemical measurements found through many years and thousands of experiments. The loop experiment at 1 bar CO_2 gives one order magnitude higher B-values but only twice the corrosion rate. The doubling in corrosion rate can be explained by flow effects but the increase in B-value is not yet understood.

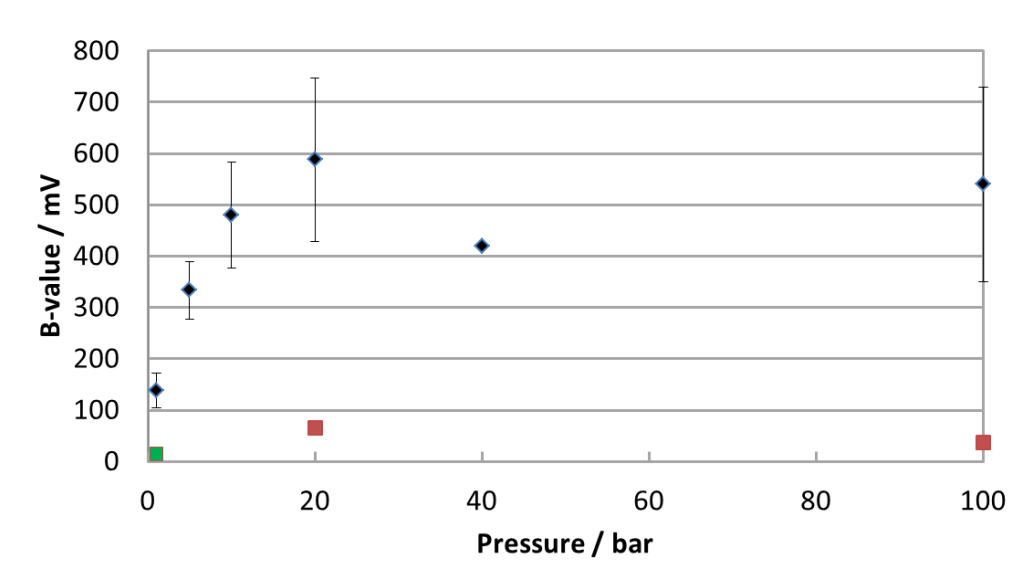

Figure 77 *Calculated B-values (blue) from iron measurement versus pressure, compared to B-values obtained from anodic/cathodic sweep (red) and the B-value from glass cell (green).*

The glass cell and loop experiments were carried out under, as much as possible, similar conditions. The electrolyte was the same, the IR compensation measured during loop experiment was 1.2 ohm, and the distance between counter electrode and working electrode was short. The wire had contact with both electrodes before and after experiments, and the geometry of the test section was good with the cylindrical arrangements. The cables used in the LPR measurements were original Gamry cable with shield and the test of cable on a dummy cell showed no deviation. The reference electrode could be questioned since there are some distance (6 mm) between the reference and the working electrode, and it can be argued that it

was not close enough to the surface of the sample. The reference was identical to the sample coupon and they corrode in the same manner during the experiment. The loop has many different electrical instruments connected and they could potentially interfere with the LPR measurements as they are not on the same grounding point as the potentiostat. It still remains to identify why there are so large deviations between the loop and the glass cell and the literature which normally operates with a B-value between 15 to 60 mV [59].

5.2.1.3 Possible copper contamination

Only general corrosion was observed on the corrosion coupon surface, which is expected since the corrosion rate is high and no protective film formed on top. The porous film had a copper containing top layer with a golden appearance in all experiments. It was more pronounced with the first version of the sample holder. It was not possible to measure the thickness of this thin copper-rich layer. The layer frequently fell off during sample handling, exposing a completely black film underneath. The copper layer appears as thin "sheets" in SEM images (Figure 61). The presence of the copper enriched layer might have introduce galvanic effects if the layer is conducting (metallic Cu or CuS) that affected the corrosion rate. It was probably not much since the corrosion rates were so high, but it might have an influence on the LPR measurements and the B-value. It was not possible to establish if the source of the copper was the copper wire used to connect the corrosion coupon to the potentiostat, or if the copper came from the steel itself. When the sample was mounted on the sample holder, some force was needed to slide it over the wire, and this likely damaged the silver plating and the copper was exposed. The connection point with the sample and the wire was not dry in the first version of the sample holder, which might lead to copper corrosion. If copper ions leaked out to the solution they could in principle plate out (accumulate) on the less nobble iron (carbon steel) samples. The carbon steel grade that was used for corrosion coupons could contain up to 0.2 weight % of copper and the high corrosion rates removed about 100 – 230 µm thickness of each sample. If one assumes that all copper from the corroded steel accumulated on the surface it would result in about 0.2-0.5 µm thick film, calculated by Equation 40. Considering the mass loss of the corrosion samples (Table 22) each sample would provide 3 to 6.5 mg Cu if one assumes the maximum Cu content of 0.2 weight %. If we assume that all the copper is accumulated on the surface of the porous film, we can calculate the average copper film thickness with the following equation:

$$\text{Thickness Cu} = \text{Corroded steel thickness} \cdot X_{Cu} \frac{\rho_{Cu}}{\rho_{Fe}} \qquad \textbf{Eq 40}$$

where X is mass fraction of copper in the steel, ρ_{Cu} is the density of copper and ρ_{Fe} is the density of iron (carbon steel).

The calculated copper thickness is given in Table 24. Copper enrichment was also measured in the SEM/EDS analysis. The SEM investigation showed that copper was not evenly spread out over the surface, but present as sheets in certain locations. Geo 02 had the highest copper weight loss and the sample from those experiments had the most golden appearance.

Table 24 *Theoretical copper film thickness if all copper in the corroded carbon steel would accumulate on the sample surface.*

Experiment	**Theoretical thickness of Cu film ** (μm)**
Geo 01	0.3
Geo 02	0.5
Geo 04A*	0.2
Geo 04B*	0.3
Geo 05	0.4

*Changed samples during the experiment.

** Assuming all copper in the corroded layer stays on the surface film.

These high copper values give support for that the copper contamination comes from the sample itself. Why it preferably stays at the outer surface of the corrosion products as “sheets” and if the copper will influence the LPR measurements is not clear for the author. The analyses of the cross section sample (Geo 04) did not give a conclusive answer on whereas the copper only was at the other surface or evenly distributed throughout the whole film.

5.2.2 Water dissolved in CO_2

As discussed in the literature review, most previous experiments that tried to simulate corrosion under dense phase CO_2 transportation conditions did not have good control of the water content. The present work was carried out in an advanced loop system with good control of the water content in the dense phase CO_2 and will therefore give corrosion rates for highly realistic transport conditions. The present loop system has four important advantages which separates our investigation form previously published experiments: accurate control of water dosing and replenishment of reacted water, measurement of the actual water level in the reaction chamber, no uncontrolled droplets formation of water, and no overdosing in the beginning of the experiment. All these advantages make it possible to run long term experiments and get corrosion rates that can be trusted.

5.2.2.1 Comparison of water measurements and corrosion rates (Solu 02)

Five experiments were carried out to study corrosion of carbon steel in dense phase CO_2.

In the first experiment (Solu 02) the water concentration was ramped from 540 ppmv and up to 2400 ppmv with a huge surface area of carbon steel inside the loop which could react with water. The deviation between the dosed and measured water concentration was recorded. The difference became noticeable at a water content of 1500 ppmv and higher. It is believed that this deviation might be a result of shorter retention time in the humidifier. Thus, less water had time to dissolve in the CO_2.

If the consumption rate of water is known it is possible to calculate a theoretical corrosion rate. Figure 78 below shows the water consumption versus the corrosion rate calculated by Equation 26 which is built on one mole water for one mole of iron. To get a deviation of 80 ppmv as observed at the 1500 ppmv level, the corrosion rate needs to be 0.3 mm/year to consume the water. The deviation in the end of Solu 02 is about 350 ppmv between the measured and the calculated water. This equals 0.3 mm/year of corrosion but it is far from the weight loss corrosion even though this deviation period is only 25 percent of the total exposure time. Absorption of water on the internal surfaces in the loop likely contributed to the differences in water content. But equilibrium should be reached with time meaning that the contribution for absorption is only temporarily, therefore experimental limitations due to wetting of CO_2 could be the main reason. The calculated water (Equation 31) assumes ideal condition and does not account for adsorption of water to surfaces. When we get close to the maximum water level the retention time of CO_2 in the humidifier becomes shorter and this can affect the moisture level in the wetted CO_2, maybe the CO_2 does not have time to reach the saturated level.

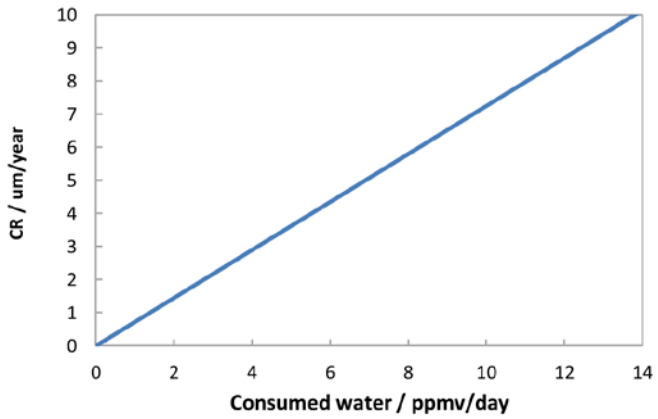

Figure 78 *Corrosion rates calculated from the consumption of water, based on 25°C, 95 bar, loop volume of 1.883 liter, and a metal surface area of 1245 cm^2 (Eq 26).*

The low corrosion rates calculated by mass loss (1 µm/y) would theoretically equal the consumption of 1.4 ppmv of water per day, a difference which is not possible to detect with the current setup. It would require a long closed periods (no injection or release of dense phase CO_2 to the loop) to be able to detect such a small water consumption rate, typically 100 or 200 days. To measure corrosion rates by water measurements some parameters need to be changed, e.g. the volume of the reaction chamber, increase the temperature to lower the density, or increase the carbon steel surface area. If the volume was decreased to 0.1 liter the water consumption would theoretically increase from 1.4 to 26 ppmv per day. In addition, increasing the temperature (this would of course change the experimental conditions) to 50° C would lower the density and the water consumption would then increase from 26 to 85 ppmv of water per day. If the carbon steel surface area was doubled, the water consumption would be 170 ppmv per day (assuming a corrosion rate of 0.001 mm/year). It might not be possible to measure the water consumption continuously, but it should be possible after closing the loop for a few days and then measure how much water was consumed during this period.

5.2.2.2 Water precipitation and adsorption

Figure 41, Solu 04, shows the changes in water concentration when the temperature was stepwise reduced. There was only small change in water concentration when the solubility limit for water in CO_2 was reached by decreasing the temperature, indicating that there was no significant change in corrosion rate. In Solu 05 the water measurements followed the temperature change which indicates that the water content is above the solubility limit and thus water should accumulate in the loop. This is confirmed in the end of Solu 05 where dry CO_2 is dosed in and the water concentration should decrease fast. This was done twice, the first was only a short period. The second period was compared with the water concentrations from Solu Blank, and the calculated water concentration, shown in Figure 79. The deviation is clear and show that Solu 05 dries up slower than Solu Blank, indicating that free water was present in the loop.

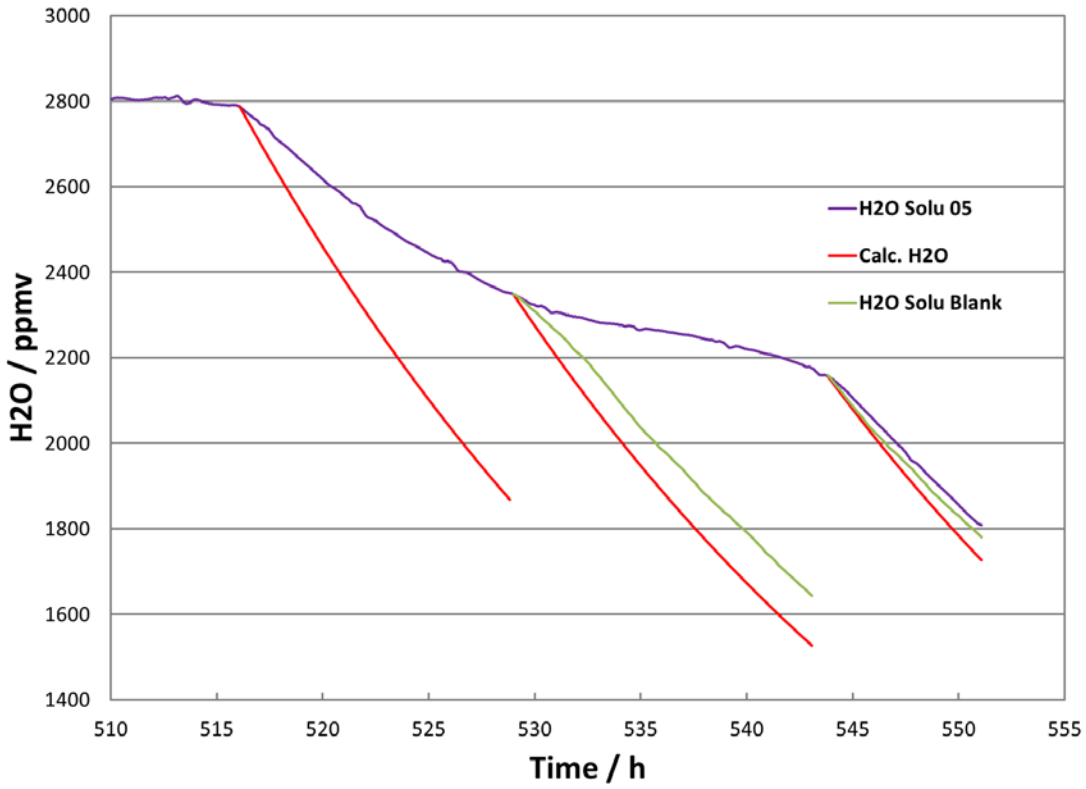

Figure 79 *Water concentration from Solu 05, compared with Solu Blank and calculated water at 25 °C and 95 bar. The dry CO_2 dosing rate is the same for both Solu experiment during the dry up period.*

The concentration of water in Solu Blank before dry up was lower than Solu 05, so we compared them from the equal concentration. The fact that Solu Blank did not reach the same water concentration with the same dosing indicates that water has precipitated during the Solu 05 at low temperature and when the temperature increased in the end of the experiment, the precipitated water starts dissolving to establish the new equilibrium. The first comparison between Solu 05 and calculated water at the start of dry up, shows a large difference which ends at ΔC_{H2O} = 480 ppmv at 528 hours. The Solu blank dry up deviates also from the calculated water but this is significantly less, and the deviation is probably due to adsorption/desorption of water on the internal surfaces (this effect is not included in the calculated water). The deviation between Solu 05 and Solu Blank is significant (ΔC_{H2O} = 530 ppmv at 543 hours), and supports that water has precipitated in Solu 05 and this water needs time to dry up. At 545 hours the free water was likely gone since the Solu 05 and Solu Blank followed the same trend and the deviation from the theoretical curve was small. The shape of the dry up curve shows that the flux of water to the dense phase (dissolution of free water) and changed with time. There is continuous surface of bulk water at the loop wall in the beginning (lower mass flux of water) and the mid part of the diagram this surface has broken up in smaller droplets until the bulk water is dried up and only dilution of the dense phase CO_2 remains Figure 80 shows how

the mass flux differs across a liquid surface. Edges, which would dominate on small droplets, can provide higher fluxes than the "bulk" surfaces. Since many small droplets have relatively more edges than fewer larger droplets, the droplet size could have a significant effect on the mass flux of water to the dense phase CO_2.

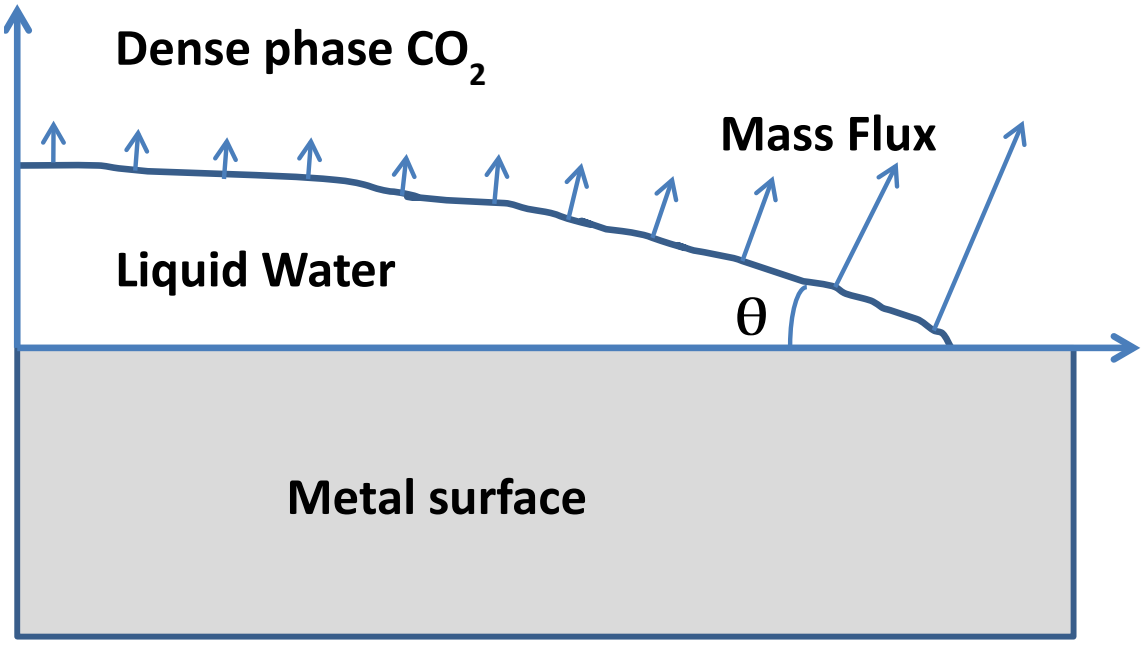

Figure 80 *Evaporation of water, mass flux is higher at the edge (modified from [71]).*

Another reason for increased mass flux of water could be increased concentration difference between the CO_2 and wall. The wall represents pores and crevices which holds water. When the water concentration in CO_2 decreases, the diffusion of water from the wall might increase and at some point the diffusion rate is almost equal the dilution rate (dry CO_2 dilute the wet CO_2 in the loop) until liquid water is used up.

It is possible by integration of the concentration difference to determine how much water that precipitated, but the important point is that the solubility limit was exceeded and a free water phase was present without significantly increased corrosion rates. The behavior of the free water when the solubility limit is crossed is important. In principle the water could circulate in the loop as a type of mist, it could accumulate on a surface or a combination of both. It was not possible to find any literature on this subject for CO_2, but the mist and dew in the nature has been extensively studied. For example if the temperature decreases, the water in moist air will precipitate as a mist or it can form droplets on surfaces. In our loop the walls were cooled (always 8 °C lower on the outside when we lowered the temperature inside) and were therefor

slightly colder than the dense phase CO_2, so it is likely that the water precipitation occurred there. This is supported by the water measurements (Figure 44, Solu 05) which are relatively stable when the solubility limit was exceeded, one would expect an increase in measured water if small droplets of water enters the sampling line and the heated gas regulator. These droplets would be regarded as liquid water and when they are vaporized in the heated gas regulator, the water gas volume would increase thereby increasing the measured water value, which we did not observe in our experiments.

For a CCS pipeline this could be an important observation since the CO_2 that enters the transport pipeline is most likely warm (due to compression) and as the CO_2 travels through the pipeline, e.g. on the bottom of the North Sea, the outer pipeline walls will be colder than the CO_2 inside the pipeline. Not avoid precipitation on the walls, the water concentration of the CO_2 that enters the pipeline has to be lower than the solubility limit for water at the coldest point on the route for the CO_2.

5.2.2.3 Corrosion rates

The corrosion rates measured in the experiments are very low (Table 19) and close to the detection limit. All of our experiments should be regarded as high water level to saturated condition, since we always did end up at 2400 ppmv or a relative humidity from 75 percent to more than 100 percent depended on the temperature. Even for water concentration from 500 ppmv to above the solubility limit the corrosion rates were not higher than 1.4 μm/y, which is negligible from a pipeline engineering point of view. A wide range of corrosion rates in dense phase CO_2 has been reported, from no corrosion [8, 29, 37, 42, 44-49] to 3.5 mm/y [38], depending on the water levels and the temperature. The large spread in published corrosion rates indicate the technical difficulties of carrying out corrosion experiments under such conditions. Thodla and Ayello [38, 40] claimed to have a water concentration of 100 to 4880 ppmv, but the water was injected as droplet over the corrosion coupons, and most likely present as a free water phase around the corrosion coupons. The water droplet did not fully dissolve during the stagnant experiment, not even for the 100 ppmv concentration. The duration of the experiments was around 6-7 hours and still some of the water was not dissolve. Thus the condition was water with dissolved CO_2, not CO_2 with dissolved water and it can be questioned whether the reported corrosion rates are at all representative for dense phase CO_2 transport in pipelines.

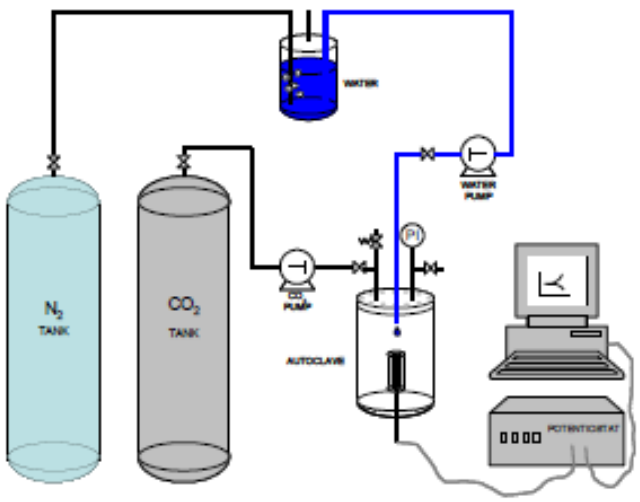

Figure 81 *The experimental setup with droplet of water on the electrodes [38].*

Most of the experiments that are published on this topic in the literature are of stagnant nature and in all of them water was injected as a liquid to be dissolved in the experimental chamber. This raises the question if the concentration reported in the experiment could be wrong, at least locally around the corrosion coupon. There are two possible scenarios, the first is that the reported corrosion rates are conservative since the water levels are lower than expected due to the fact that some of the water is not completely dissolved and the water level was low in the beginning of the experiment until all the water dissolves. The second possibility is when filling the experimental chamber with CO_2, the water is spread around in the chamber as small droplets and even hitting the sample. This can give high localized attacks due to corrosion under the droplet until all water is consumed [72]. The possibility to replenish the water is an important benefit with the test system developed at IFE, particularly for low concentration experiment since a corrosion rate of 0.1 mm/y in 50 °C with 25 cm^2 sample surface will consume 135 ppmv of water in a week.

Sim et al. [39] reported corrosion rates around 0.1 mm/y at 40 °C for water concentrations ranging from 240 ppmv to saturated condition. Hua et al [41] reported corrosion rates around 0.01 to 0.1 mm/y for 35 °C and 50 °C, respectively. Both of them reported deep localized attacks, from 0.2 mm/y up to 1.4 mm/y after 7 days of exposure. No sign of localized attacks were observed in our experiments. The Solu 06 experiment at 35 °C had an exposure time of two weeks and there were some products on the surface, but the corrosion rate could not be calculated since the weight loss was too small. Figure 82 show a comparison of the exposed samples from the literature [39, 41] and from experiment (Solu 06) in the present work.

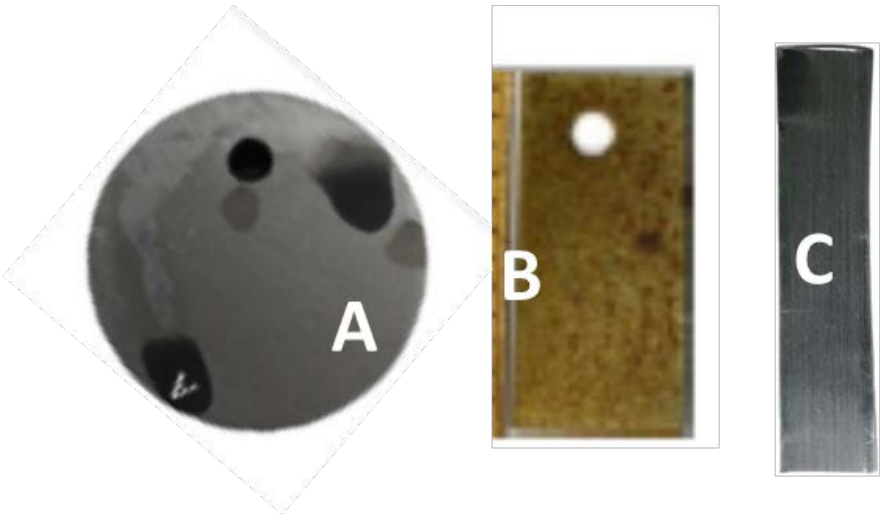

Figure 82 *Carbon steel samples exposed to water dissolved in dense phase CO_2, Sample A from Hua et al. [41] 2800 ppmv at 35 °C, Sample B from Sim et al. [39] at 40 °C, and Sample C from Morland at 35 °C (present work).*

The samples look quite different. It seems like free water droplets were present on coupon A and B where corrosion occurred underneath. The small *A* (down to the left) in coupon A shows where the authors have found the highest localized corrosion. Sample B was exposed to 50000 ppmw (122000 ppmv) which was over the saturation level, since the solubility at the exposed temperature and pressure was about 1500 ppmw. This means that there was a lot of excess water available and it was present as a free water phase in the bottom of the reaction chamber. Furthermore there were several ways the free water could hit the sample. Water could splash when the chamber was filled with CO_2. Since the autoclave was heated from the outside the corrosion coupon was initially colder than the bulk phase and some condensation could therefore occur in the initial startup phase. The heat comes from the outside and the samples are suspended in the middle of the chamber. The heated CO_2 saturated with water hits the colder samples and condenses, the condensed water will stay there because of zero mass flux from the water to the water saturated CO_2. The water will disappear by corrosion consumption.

In the present work the water was already dissolved in the CO_2 before the CO_2 was injected into the loop, effectively preventing droplet formation for conditions below the solubility limit. Droplets could form when the temperature was reduced, as in Solu 05. The SEM pictures (Figure 45) from this experiments show indications of iron carbonate in the shape of micro droplets on the sample surface, but it is not possible to conclude for sure since it could also be the growth mechanism of the iron carbonate that gives this morphology.

5.2.2.4 Corrosion products

Since the corrosion rate was low there was only limited amounts of corrosion products on the sample surfaces, but it was present on all samples. The average film thickness was ranging from 60 to 120 nm calculated from the weight loss measurements. Since the film was so thin it was hard to confirm that it consisted of iron carbonate from the EDS analysis, but it is well known that this is the expected product when carbon steel is exposed to water with CO_2 (no O_2 and H_2S present) [52, 56]. A Monte Carlo Simulation was performed to estimate the film thickness, assuming the substrate was only iron carbonate. These simulations were compared with EDS analysis at different accelerating voltage as shown in Table 20 and Figure 83. Although EDS results at so low acceleration voltages have relatively large uncertainty the results indicate a constant iron content for 4 keV and higher. According to the Monte Carlo simulations this would indicate that the surface layer was less than 100-150 nm thick. This supports the finding from the average film thickness.

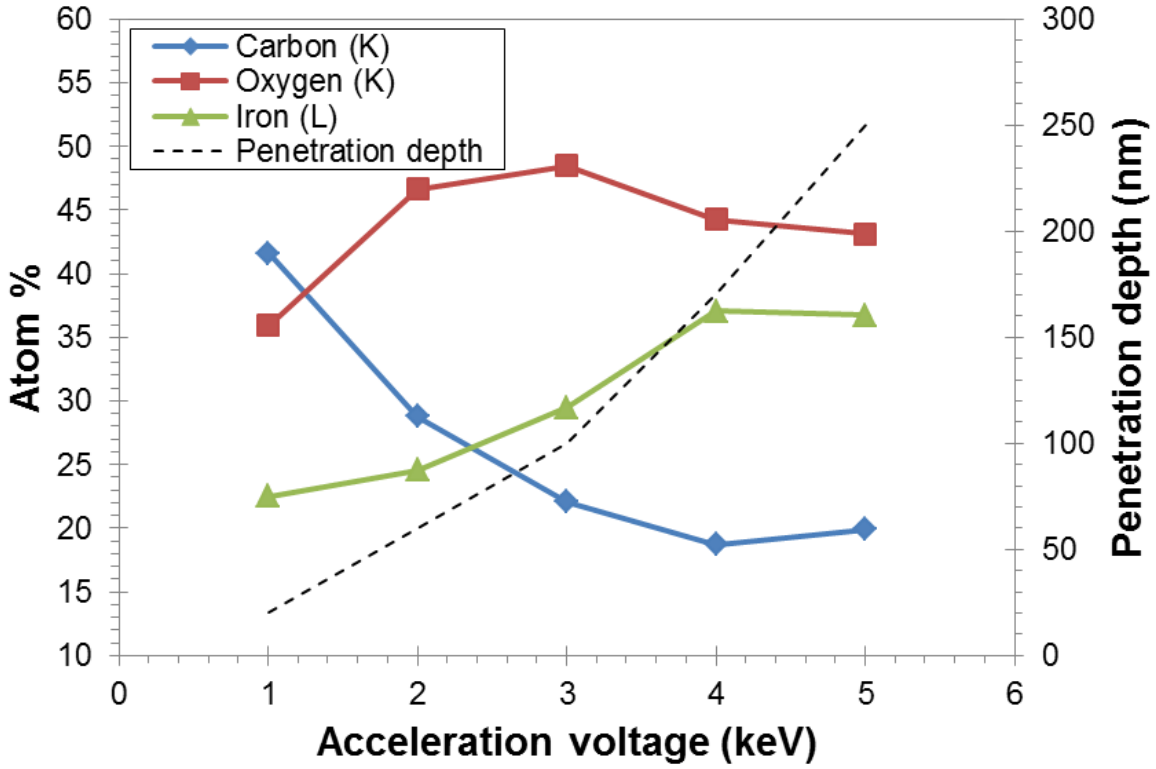

Figure 83 *The measured element concentration (atomic percent) and the simulated penetration depth versus acceleration voltage of the electron beam.*

The SEM investigation showed more corrosion products on samples from Solu 04 and Solu 05 experiments where the temperature was adjusted so the water content was close to the

solubility limit, even though the measured film by weight on Solu 04 was lower than Solu 02. The statistical analysis (one-way ANOVA, Tukey pairwise comparison) conclude that Solu 02, Solu 04, and Solu 05 are significant different from Solu 03, Solu 06, and reference. There is no difference between Solu 02, Solu 04, and Solu 05. And there are no differences between Solu 03, Solu 04, and the reference. P values less than 0.05 were regarded. This was most likely related to uneven distribution of corrosion products on the sample surface, but it could also be attributed to very small mass losses, which were at the detecting limit for the scales.

The surface was not fully covered by the corrosion film and would therefore not be in a state to give full corrosion protection yet, how thick or how long this will take is difficult to ascertain. For corrosion with free water phase protective scales of iron carbonate could be as thin as ~1 µm [52]. If this is representative for the dissolved water corrosion it could take over half a year to produce this thickness of the film if the growth rate is linear.

A film thickness of 100 nm of iron carbonate in a 20-inch pipeline equals 0.6 kg per km of pipeline. About 0.1 ton of product is produced on the wall if the pipeline is 200 km long, this will not affect the pipeline much but it could matter for a the CO_2 storage reservoir if this product stay at the wall or falls of.

5.2.2.5 Effects of O_2

We measured oxygen in our experiments and the concentration was kept around 2-4 ppmv. The literature reports few experiment with O_2 in combination with water. In general a moderate increase in corrosion rate has been observed compared to similar conditions without O_2 [22, 27, 29, 50, 73, 74]. The oxygen level in our experiment should according to the literature not influence the corrosion rates.

6. Conclusion

Previous studies in the literature have reported highly different corrosion rates in systems where water below the solubility limit was dissolved in CO_2. This discrepancy was, in some of the studies, most likely related to short-comings in methodology, where the presence of free water was responsible for the high corrosion rates. In the present work, an experimental setup that allowed complete control of the water concentration in CO_2, without the risk of droplet formation was used.

It was shown that the corrosion rates were below 1.5 µm/y and without localized attacks as long as the water content was below the solubility limit. This corrosion rate is so low that it is without practical significance. However, with water content above the solubility limit, i.e. in the present of a free water phase, the corrosion rate increased by several orders of magnitude to 8 - 17 mm/y, depending on the CO_2 partial pressure. The corrosion rate increased with increasing CO_2 pressure up to 20 bar (17 mm/y), at higher pressures the corrosion rate was slightly lower (9-12 mm/y) and independent of CO_2 pressure. No protective film was formed under these conditions.

This work has shown that corrosion will not be problem for a CO_2 transport pipelines as long as the water is kept below the solubility limit to prevent formation of a free water phase. Furthermore, this work has shown the detrimental effect of free water, which would result in unacceptably high corrosion rates that would dramatically reduce the lifetime of the pipeline.

Water control and water analysis must be an important part of a CCS pipeline integrity system.

7. Further work

The correlation between the B-values and change of CO_2 pressure was not completely understood in this study, further experiments and modification of the test approach are needed to identify the mechanisms and correlations.

The present study investigated corrosion in pure CO_2/water systems. However, other impurities are likely to be present, and the concentration of these will vary depending on the CO_2 source and capture process. The type and concentration of impurities in the captured CO_2 may have important effects on the CCS pipelines, like corrosion or particle formation. The impurities that are most likely to have a corrosive effect include hydrogen sulfide, oxygen, sulfur dioxide, and nitrogen dioxide. Several single impurity system show great effects on the rate of corrosion and solid formation [21, 22, 27, 36, 50, 74, 75]. In addition to the impurities originating from the captured gas, there might be some carry over from the capture plant. Presently, amines are most frequently used in the CO_2 capture process, and glycol can be used for dehydration of the CO_2 before compression. These compounds, although at trace levels, will end up in the CO_2. There is limited data available on the effect of amines and glycols in CCS transport systems, but if they form a separate phase containing water the corrosion rate might be high.

Furthermore, few relevant data on the combined effect of all impurities in dense phase CO_2 exist. Data from our lab suggest that impurities, when present in the CO_2, can react or catalyze the formation of corrosive compounds [12, 76]. It is also likely that solids can be formed under these conditions, but there are few published studies to support it.

A natural follow up of the present study would be to investigate CO_2 with mixtures of impurities. In such a system the corrosion rates can be high, and solid formation could be an equally important contributor to pipeline instability. The experimental setup used in this study can, with just minor modifications, be used to examine effects of combined impurities on corrosion and solid formation. Such data would be important for the CCS industry since they would more realistically resemble the conditions in an actual CO_2 pipeline. Such results would contribute to defining a correct CO_2 transport specification with respect to corrosion and solids formation.

References

[1] IPCC, "Summary for Policymakers. In: Climate Change 2013: The Physical Science Basis. Contribution of Working Group I to the Fifth Assessment Report of the Intergovermmental Panel on Climate Change [Stocker,T.F., D. Qin, G.-K. Plattner, M. Tignor, S.K. Allen, J. Boschung, A. Nauels, Y. Xia, V. Bex and P.M. Midgley (eds.)]. ," IPCC, Cambridge University Press, Cambridge, United Kingdom and New York, NY, USA.2013.

[2] J. Hansen, R. Ruedy, M. Sato, M. Imhoff, W. Lawrence, D. Easterling, T. Peterson, and T. Karl, "A closer look at United States and global surface temperature change," *Journal of Geophysical Research: Atmospheres,* vol. 106, pp. 23947-23963, 2001.

[3] UNFCCC. (2013). *Decision on greenhouse gas concentration*. Available: http://unfccc.int/documentation/decisions/items/3597.php

[4] IEA, "Technology Roadmaps Technology Roadmap: Carbon Capture and Storage: Complete Edition," IEA, SourceOECD Energy 1608-019X, 2010.

[5] A. Oosterkamp and J. Ramsen, "State-of-the-Art Overview of CO2 Pipeline Transport with relevance to offshore pipelines," 2008.

[6] E. Visser de, C. Hendriks, M. Barrio, M. J. Moelnvik, K. G. de, S. Liljemark, and G. Y. Le, "Dynamics CO2 quality recommendations," *Int. J. Greenhouse Gas Control,* vol. 2, pp. 478-484, // 2008.

[7] CCP. (2013). *CO2 Capture Project, CO2 transport.* Available: http://www.co2captureproject.org/co2_transport.html

[8] A. Dugstad, B. Morland, and S. Clausen, "Corrosion of transport pipelines for CO2 - effect of water ingress," *Energy Procedia,* vol. 4, pp. 3063-3070, // 2011.

[9] M. Mohitpour, P. Seevam, K. Botros, B. Rothwell, and C. Ennis, *Pipeline Transportation of Carbon Dioxide Containing Impurities*, 2012.

[10] G. de Koeijer, Y. Enge, K. Sanden, O. F. Graff, O. Falk-Pedersen, T. Amundsen, and S. Overå, "CO2 Technology Centre Mongstad–Design, functionality and emissions of the amine plant," *Energy Procedia,* vol. 4, pp. 1207-1213, // 2011.

[11] TCM. (2013). *Technology Centre Mongstad*. Available: http://www.tcmda.com/no/

[12] A. Dugstad, M. Halseid, and B. Morland, "Effect of SO2 and NO2 on Corrosion and Solid Formation in Dense Phase CO2 Pipelines," *Energy Procedia,* p. Ahead of Print, 2013.

[13] S. Jäger, C. Bosch, A. Meyer, and A. Lucci, "Requirements for safe and reliable CO2 transportation pipeline," presented at the Pipeline technology conference, 2013.

[14] G. Nahas and M. Mohitpour, "Engineering pipelines for transportation of CO2 with impurities," 2010, pp. 165-177.

[15] K. D. Watson and D. G. Siekkinen, "Sheep Mountain CO2 project development and operation," *Energy Prog.,* vol. 6, pp. 155-64, // 1986.

[16] B. A. George and M. S. Heiman, "Design and operating experience of Amoco's Bravo Dome facility," *Energy Prog.,* vol. 6, pp. 219-21, // 1986.

[17] D. Huxley, B. Feldman, and D. Peightal, "Dakota Gasification Company CO2 sequestration verification project," presented at the Prepr. Symp. - Am. Chem. Soc., Div. Fuel Chem., 2004.

[18] Worldsteel. (2013). *About steel*. Available: http://www.worldsteel.org/faq/about-steel.html

[19] Worldsteel, "Steel`s contribution to a low carbon future," Position paper, 2013.
[20] Y. Zhang, K. Gao, and G. Schmitt, "Inhibition of steel corrosion under aqueous supercritical CO2 conditions," *CORROSION 2011,* 2011.
[21] A. Dugstad, M. Halseid, B. Morland, and S. Clausen, "Dense phase CO2 transport – when is corrosion a threat?," presented at the NACE 2011, 2011.
[22] A. Dugstad, M. Halseid, and B. Morland, "Corrosion in Dense Phase CO2 Pipelines State of the Art," presented at the Eurocorr2011, 2011.
[23] M. Seiersten, "Materials Selection for Separation, Transportation and Disposal of CO2," *CORROSION 2001,* 2001.
[24] S. M. Hesjevik, S. M. Olsen, and M. M. Seiersten, "Corrosion at high CO2 pressure," *CORROSION 2003,* 2003.
[25] M. Seiersten and K. O. Kongshaug, "Materials selection for capture, compression, transport and injection of CO2," 2005, pp. 937-953.
[26] Y.-S. Choi and S. Nešić, "Corrosion behavior of carbon steel in supercritical CO2-water environments," *CORROSION 2009,* 2009.
[27] Y.-S. Choi and S. Nešić, "Effect of Impurities on the Corrosion Behavior of Carbon Steel in Supercritical CO2-Water Environments," *CORROSION 2010,* 2010.
[28] Y.-S. Choi and S. Nešić, "Determining the corrosive potential of CO2 transport pipeline in high pCO2–water environments," *International Journal of Greenhouse Gas Control,* vol. 5, pp. 788-797, 2011.
[29] A. Dugstad, S. Clausen, and B. Morland, "Transport of Dense Phase CO2 In C-steel Pipelines-When is Corrosion an Issue?," *CORROSION 2011,* 2011.
[30] Y. Zhang, X. Pang, S. Qu, X. Li, and K. Gao, "The relationship between fracture toughness of CO2 corrosion scale and corrosion rate of X65 pipeline steel under supercritical CO2 condition," *International Journal of Greenhouse Gas Control,* vol. 5, pp. 1643-1650, 2011.
[31] Y. Zhang, X. Pang, S. Qu, X. Li, and K. Gao, "Discussion of the CO2 corrosion mechanism between low partial pressure and supercritical condition," *Corrosion Science,* vol. 59, pp. 186-197, 2012.
[32] A. Nor, M. Suhor, M. Mohamed, M. Singer, and S. Nesic, "Corrosion of Carbon Steel in High CO2 Containing Environments - the Effect of High Flow Rate," presented at the Corrosion 2012, 2012.
[33] M. Halseid and A. Dugstad, "State of the Art 2014 Corrosion in Dense Phase CO2 Transportation," Institute for Energy Technology, KDC JIP, Report2014.
[34] M. Seiersten, "Corrosion of pipeline steel in supercritical CO2/water mixtures," presented at the Eurocorr 2000, 2000.
[35] Y. Zhang, K. Gao, and G. Schmitt, "Inhibiting steel corrosion in aqueous supercritical CO 2 conditions," *Materials Performance,* vol. 50, pp. 54-59, 2011.
[36] A. Dugstad, M. Halseid, B. Morland, and A. O. Sivertsen, "Corrosion in dense phase CO2 with small amounts of SO2, NO2 and water.," presented at the Eurocorr2012, 2012.
[37] J. Collier, S. Papavinasam, J. Li, C. Shi, P. Liu, and J. Gravel, "Effect of Impurities on the Corrosion Performance of Steels in Supercritical Carbon Dioxide: Optimization of Experimental Procedure," presented at the Corrosion 2013, 2013.

[38] R. Thodla, A. Francois, and N. Sridhar, "Materials performance in supercritical CO2 environments," *CORROSION 2009,* 2009.
[39] S. Sim, F. Bocher, I. S. Cole, X.-B. Chen, and N. Birbilis, "Investigating the Effect of Water Content in Supercritical CO2 as Relevant to the Corrosion of Carbon Capture and Storage Pipelines," *Corrosion,* vol. 70, pp. 185-195, 2014.
[40] F. Ayello, K. Evans, R. Thodla, and N. Sridhar, "Effect of Impurities on Corrosion of Steel in Supercritical CO2," *CORROSION 2010,* 2010.
[41] Y. Hua, R. Barker, and A. Neville, "Effect of temperature on the critical water content for general and localised corrosion of X65 carbon steel in the transport of supercritical CO2," *International Journal of Greenhouse Gas Control,* vol. 31, pp. 48-60, 12// 2014.
[42] B. P. McGrail, H. T. Schaef, V.-A. Glezakou, L. X. Dang, and A. T. Owen, "Water reactivity in the liquid and supercritical CO2 phase: Has half the story been neglected?," *Energy Procedia,* vol. 1, pp. 3415-3419, 2009.
[43] H. El Alami, C. Augustin, B. Orlans, and J. Servier, "Carbon Capture and Storage projects: material integrity for CO2 injection and storage," presented at the Eurocorr2011, Stockholm, Sweden, 2011.
[44] F. Schremp and G. Roberson, "Effect of supercritical carbon dioxide (CO2) on construction materials," *Old SPE Journal,* vol. 15, pp. 227-233, 1975.
[45] F. Schremp and G. Roberson, "Effect of Supercritical co 2 on Materials of Construction," in *meeting of Society of Petroleum Engineers of AIME in Las Vegas, Nevada*, 1973.
[46] J. West, "Design and Operation of a Supercritical CO2 Pipeline-Compression System Sacroc Unit, Scurry County, Texas," in *SPE Permian Basin Oil Recovery Conference*, 1974.
[47] W. Newton, "SACROC CO2 project--corrosion problems and solutions," *Mater. Performance;(United States),* vol. 23, 1984.
[48] T. Gill, "Canyon Reef Carriers Inc. CO2 pipeline: Description of 12 years of operation," presented at the ASME Pipeline Engineering Symposium, 1985.
[49] W. Propp, T. Carleson, C. M. Wai, P. Taylor, K. Daehling, S. Huang, and M. Abdel-Latif, "Corrosion in supercritical fluids," Lockheed Idaho Technologies Co., Idaho Falls, ID (United States)1996.
[50] Y.-S. Choi, S. Nesic, and D. Young, "Effect of Impurities on the Corrosion Behavior of CO2 Transmission Pipeline Steel in Supercritical CO2− Water Environments," *Environmental science & technology,* vol. 44, pp. 9233-9238, 2010.
[51] S. Sim, F. Bocher, I. S. Cole, X. B. Chen, and N. Birbilis, "Investigating the effect of water content in supercritical CO2 as relevant to the corrosion of carbon capture and storage pipelines," *Corrosion,* 2013.
[52] S. Nešić, "Key issues related to modelling of internal corrosion of oil and gas pipelines – A review," *Corrosion Science,* vol. 49, pp. 4308-4338, 12// 2007.
[53] S. Nesic, "A Critical Review of CO2 Corrosion Modelling in the Oil and GAS Industry," presented at the 10th Middle East Corrosion Conference 7-10 March 2004, 2004.
[54] S. Nesic, J. Postlethwaite, and S. Olsen, "An electrochemical model for prediction of corrosion of mild steel in aqueous carbon dioxide solutions," *Corrosion,* vol. 52, 1996.
[55] A. Dugstad, "Fundamental Aspects of CO2 Metal Loss Corrosion - Part 1: Mechanism," presented at the NACE International, Houston, 2006.

[56] A. Dugstad, "Fundamental Aspects of CO2 Metal Loss Corrosion, Part I: Mechanism revisited," presented at the NACE International, 2015.
[57] J. O. M. Bockris, D. Drazic, and A. R. Despic, "The electrode kinetics of the deposition and dissolution of iron," *Electrochimica Acta,* vol. 4, pp. 325-361, 8// 1961.
[58] C. D. Waard and D. E. Milliams, "Carbonic Acid Corrosion of Steel," *Corrosion,* vol. 31, pp. 177-181, 1975.
[59] Gamry. (2015). *Basics of Electrochemical Corrosion Measurements*. Available: http://www.gamry.com/application-notes/basics-of-electrochemical-corrosion-measurements/
[60] P. A. Thiel and T. E. Madey, "The interaction of water with solid surfaces: Fundamental aspects," *Surface Science Reports,* vol. 7, pp. 211-385, 10// 1987.
[61] C. Leygraf, *P. Marcus, J. Oudar (Eds.), Corrosion Mechanisms in Theory and Practice*. New York, 1995.
[62] Y. Ben-Da, S. Meilink, G. W. Warren, and P. Wynblatt, "Water Adsorption and Surface Conductivity Measurements on Alumina Substrates," *Components, Hybrids, and Manufacturing Technology, IEEE Transactions on,* vol. 10, pp. 247-251, 1987.
[63] D. Persson and C. Leygraf, "Analysis of Atmospheric Corrosion Products of Field Exposed Nickel," *Journal of The Electrochemical Society,* vol. 139, pp. 2243-2249, August 1, 1992 1992.
[64] Yokogawa. (2012). *TDLS200, Tunable Diode Laser Spectroscopy Analyzer*. Available: http://www.yokogawa.com/
[65] Michell. (2014). *XZR400 Series, Oxygen Analyzers*. Available: www.michell.com
[66] T. Waters, *Industrial Sampling Systems*: Swagelok Company, 2013.
[67] Kaya&Laby. (2015). *X-ray absorption edges, characteristic X-ray lines and fluorescence yields*. Available: http://www.kayelaby.npl.co.uk/atomic_and_nuclear_physics/
[68] P. Hovington, D. Drouin, and R. Gauvin, "CASINO: A new monte carlo code in C language for electron beam interaction —part I: Description of the program," *Scanning,* vol. 19, pp. 1-14, 1997.
[69] MultiScale, 4 ed. http://exprogroup.com/wp-content/uploads/MultiScale4.pdf.
[70] M. Seiersten, "Corrosion at high CO2 pressures," 2001.
[71] K. Sefiane, S. K. Wilson, S. David, G. J. Dunn, and B. R. Duffy, "On the effect of the atmosphere on the evaporation of sessile droplets of water," *Physics of Fluids (1994-present),* vol. 21, p. 062101, 2009.
[72] A. Dugstad, M. Halseid, and B. Morland, "Corrosion and solid formation in pipelines transporting dense phase CO2 with impurities - what do we know and what do we need to know," presented at the International Forum on the Transportation of CO2 by Pipeline, 2012.
[73] Y.-S. Choi and S. Nešić, "Effect of Water Content on the Corrosion Behavior of Carbon Steel in Supercritical CO2 Phase with Impurities," *CORROSION 2011,* 2011.
[74] Y. Xiang, Z. Wang, C. Xu, C. Zhou, Z. Li, and W. Ni, "Impact of SO2 concentration on the corrosion rate of X70 steel and iron in water-saturated supercritical CO2 mixed with SO2," *The Journal of Supercritical Fluids,* vol. 58, pp. 286-294, 9// 2011.
[75] F. Farelas, Y. Choi, and S. Nešic, "Effects of CO2 Phase Change, SO2 Content and Flow on the Corrosion of CO2 Transmission Pipeline Steel," presented at the NACE 2012, 2012.

[76] A. Dugstad and M. Halseid, "Internal corrosion in dense phase CO2 transport pipelines - state of the art and the need for further R&D," presented at the Corrosion 2012, 2012.

Appendix

Chemicals

Table 25 *Chemicals used for producing developer for iron measurements.*

Name	CAS-number	comment
1,10-phenanthroline mono hydrate	5144-89-8	Pro analysis
Acetic acid	64-19-7	Pro analysis
Hydroxylamine hydrochloride	547011-1	Pro analysis
Sodium acetate	127-09-3	Pro analysis
Distilled water	------	Lab produced

Table 26 *Chemicals used for producing the Clark solution for stripping.*

Name	CAS-number	comment
Hydrochloric acid	7647-01-0	37 percent
Tin(II)chloride	7772-99-8	Pro analysis
Antimony trichloride	10025-91-9	Pro analysis

Table 27 *Chemicals used when handling the samples.*

Name	CAS-number	comment
Acetone	67-64-1	Technical
Isopropanol	67-63-0	Technical
Struers epofix hardener	112-24-3	Kit for molding
Struers epofix resin	------	Kit for molding

Table 28 *Gas used in the experiments.*

Name	Quality	CAS-number	comment	Experiment
Carbon dioxide	5.0	124-38-9	With riser	Solu
Carbon dioxide	Mapcon	124-38-9	Normal	Geo ≤ 40 bar

Table 29 *Carbon steel grade used as specimen iron as balance.*

	C (wt%)	Mn (wt%)	Si (wt%)	P (wt%)	S (wt%)	Cr (wt%)	Cu (wt%)
S355J2	≤0.2	≤1.6	≤0.55	≤0.030	≤0.030	≤0.55	
X-65	≤0.16	≤1.6	≤0.50	≤0.015	≤0.005	≤0.50	≤0.20